Dissertation Advisor: Joan S. Brugge, Ph.D. Rachel Alexis Davidowitz

Mechanisms Governing Mesothelial Clearance by Ovarian Cancer Spheroids

ABSTRACT

Metastatic dissemination of ovarian tumors involves the invasion of multi-cellular tumor cell clusters into the mesothelial cell lining of organs in the peritoneal cavity. We developed an *in vitro* assay that models this initial step of ovarian cancer metastasis to investigate the mechanisms of invasion. Pre-clustered ovarian cancer multicellular spheroids are incubated with GFP-expressing mesothelial monolayers and the extent of mesothelial invasion is monitored by time-lapse video microscopy.

Time-lapse microscopy revealed that ovarian cancer spheroids intercalate into mesothelial monolayers, protrude under the mesothelial cells, trigger mesothelial cell matrix adhesion disassembly, and ultimately, mesothelial cell migration away from the intercalating spheroid. Mechanistic studies demonstrated that actomyosin-generated contractile force exerted by the ovarian cancer spheroid, via α5β1 integrin, myosin II, and Talin I, on the fibronectin matrix surrounding the mesothelial cells is required for clearance of the mesothelial monolayer.

To more comprehensively investigate the mechanisms regulating mesothelial clearance, we examined the clearance ability of a large panel of established ovarian cancer cell lines. Approximately two-thirds of the cells lines produced spheroids that were clearance-competent, while one-third of the cell

lines produced spheroids that were clearance-incompetent. Microarray analysis revealed that genes in an Epithelial to Mesenchymal (EMT) core signature were enriched in clearance-competent cell lines, while epithelial genes were enriched in clearance-incompetent cell lines. The importance of this signature was supported experimentally; over-expression or knockdown of EMT-inducing transcription factors promoted or attenuated clearance, respectively. The role of EMT in mesothelial clearance was further supported in a more clinically relevant panel of primary cell samples; clearance-competent primary cell spheroids were enriched for the mesenchymal marker, vimentin, while clearance-incompetent primary cell spheroid were enriched for the epithelial marker, E-cadherin.

The studies in this dissertation revealed that cellular components implicated in the regulation of cell adhesion and migration -- namely integrin matrix receptor complexes and actomyosin contractility -- drive mesothelial clearance by ovarian cancer spheroids. In addition, our data strongly suggest that tumor cells that display a mesenchymal phenotype play a more significant role in mesothelial clearance. These findings provide a framework for future studies on the mechanisms of clearance by ovarian cancer spheroids.

To

Grandpa Phil

Acknowledgements

First and foremost I would like to thank my thesis advisor, Dr. Joan Brugge. She provided me with the opportunity and resources to pursue a research project that was tailored to my interests. No matter how busy she was she always had time to provide the mentorship that I needed. I am grateful for her guidance, support, and dedication through out my time as a graduate student.

I would also like to thank Dr. Marcin Iwanicki. Marcin developed the mesothelial clearance assay that I used in all of the studies in this dissertation. We worked together during my rotation in the Brugge lab, and he has been a great mentor and friend ever since.

Next, I would like to thank Dr. Ronny Drapkin. Not only was he a collaborator and member of my dissertation advisory committee (DAC), he has been a second advisor to me. His guidance, encouragement, and primary cells have allowed me to successfully complete my research.

I would also like to thank the other members of my DAC, Dr. Alex Toker and Dr. Gaudenz Danuser for their feedback during the progression of my project. I am especially grateful to Alex for driving the progress of my DAC meetings and for agreeing to serve as the chair of my defense committee. In addition, I would like to thank the members of my defense committee, Dr. David Frank, Dr. Karl Munger and Dr. Robert Weinberg for taking time out of their busy

schedules to read my dissertation, attend my defense and discuss my research with me.

I would like to thank all of the lab members who have been so supportive through out my time at the Brugge lab, including Dr. Laura Selfors, Dr. Ghassan Mouneimne, Dr. Cheuk Leung, Dr, Taru Muranen, Dr. Michelle Hickey, Dr. Jon Coloff, Dr. Rosa Ng, Amy Bui, Dr. Alex Grassian, and Sabin Dhakal. I'd especially like to thank Laura for help with statistical analyses and her encouragement, Ghassan, who has not only given me advice on my project and life as a graduate student, but has also spent many hours learning After Effects with me, Rosa, Amy and Alex who have provided advice on being a graduate student, and Sabin, Michelle and Jon for being my qPCR buddies.

I would also like to thank the Nikon imaging Center for training me on their microscopes and making the images in my dissertation possible. In addition I would like to thank Kate Hodgins, Maria Bollinger, Daniel Gonzalez and Stephen Obuchowski of the Harvard Biological and Biomedical Sciences program office who made sure that I was fulfilling my degree requirements.

I am truly fortunate to have had the opportunity to work with all of these wonderful people, without whom my dissertation would not have been possible.

Finally, I would like to thank my boyfriend, parents, brother and the rest of my family for all of their love, encouragement and support while I figure it all out.

Table of Contents

Chapter 1

Introduction

Ovarian cancer is the fifth leading cause of cancer mortality among women in the United States with over 22,000 new cases diagnosed each year (1, 2). Typically, ovarian cancer remains undetected until patients present with late stage metastatic disease (stage III/IV) (3), resulting in the highest death-to-incidence ratio of any cancer (1). Screening methods, including blood tests and ultrasounds, are ineffective, as they are unable to detect small tumor masses and often produce false positives (4, 5). The current treatment options for ovarian cancer involve cytoreductive surgery followed by platinum/taxane-based chemotherapy. Patients often respond well to these first-line treatments (6-8), however relapse is common. The mortality of ovarian cancer is a consequence of the excessive tumor bulk that results from peritoneal metastases. In fact, the volume of tumor bulk correlates with poor overall survival in ovarian cancer patients (9, 10). It is therefore, very important to understand the mechanisms by which ovarian cancer cells seed peritoneal metastases, in order to determine how seeding can be prevented, and develop treatments that target the cells are not effectively eradicated by current treatments.

Ovarian Cancer Subtypes:

Ovarian Cancer is classified into four major subtypes: Serous, Endometrioid, Clear Cell and Mucinous. Serous carcinomas are the most

common, accounting for 60-80% of all cases. Endometrioid carcinomas are the second most common accounting for 8-19%, while mucinous carcinomas account for 3-11% and clear cell carcinomas account for less that 5% of all ovarian carcinomas(11-13). While it was previously thought that all ovarian cancers developed in the tissues of the ovary, it is now becoming apparent that most ovarian cancers are derived from non-ovarian tissue and more closely resemble the mullerian-derived tissue of the reproductive tract (6, 14). Endometrioid and clear cell tumors resemble the endometrial lining of the uterus and are believed to develop when retrograde menstrual flow carries endometrial tissue from the uterus to the peritoneal cavity, causing endometriosis. This mislocalized endometrial tissue forms tumors in the ovary (14, 15). Tubal ligation has been shown to protect against endometrioid and clear cell ovarian cancer, presumably because retrograde endometrial flow is inhibited (16). Mucinous ovarian cancer, unlike the other three subtypes of ovarian cancer, does not resemble mullerian-derived tissues. Instead, mucinous cancers resemble the tissue of the gastrointestinal mucosa (14, 17).

High Grade Serious ovarian cancer is the most aggressive of all the ovarian cancer subtypes. While serous ovarian carcinomas were originally thought to be derived from the ovarian surface epithelium, there is increasing evidence that the fallopian tube fimbria is the site of origin of serous ovarian carcinoma (18-21). Serous ovarian carcinomas express PAX8, a mullerian marker, and their genetic profiles share more similarity with fallopian tube epithelial cells than ovarian surface epithelial cells (22-24). p53 mutations are

found in 96% of all high grade ovarian serous carcinomas (2, 25-27) and identical p53 mutations are often found in both serous tubal intraperitoneal carcinomas (STICS) [lesions in the fallopian tube that are though to be early occurrences of the disease] and concomitant high grade serous carcinomas (18, 19, 28, 29), further suggesting that the fallopian tube is the site of origin of serous ovarian cancer.

The different subtypes of ovarian cancer display varying degrees of metastatic aggressiveness. Clear cell, mucinous, low-grade endometrioid and low-grade serous carcinomas are generally confined to the ovary when they present, whereas high-grade serous and high-grade endometrioid carcinomas are highly metastatic. Therefore, the subtype of ovarian cancer should be taken into account when studying the mechanisms of ovarian cancer metastasis.

Ovarian Cancer Metastasis:

Typically, metastatic events occur when tumor cells separate from a primary tumor that is embedded deep within a tissue and migrate through collagen I rich connective tissue to blood or lymph vessels. Once in contact with a vessel, the cells intravasate and travel to new sites where they attach to the endothelium, extravasate, and invade surrounding tissues (30). Ovarian cancer metastasis proceeds differently, however. There is no anatomical barrier to peritoneal metastasis so intravasation and extravasation are not required for spread of the ovarian tumors. Rather, malignant cells are shed from the primary tumor and collect in the peritoneal cavity, where they are disseminated by the

physiological movement of the peritoneal fluid (3, 6). Malignant cells can be found as both single cells and cell aggregates (spheroids) within the peritoneal cavity and single cells can aggregate within the peritoneal cavity to form clusters (31-33). The aggregates then settle on the surface of peritoneal cavity organs where they attach and disaggregate (31, 34).

All of the surfaces within the peritoneal cavity, including the bowel serosa, omentum, diaphragm, and peritoneum, are lined with a single layer of mesothelial cells (3, 35). The mesothelial monolayer acts as a low friction surface that regulates the transport of fluid and solutes between the peritoneal cavity, interstitial space and circulation. Directly beneath the mesothelial layer is a basement membrane composed of collagen types I and IV, laminin and fibronectin; fibroblasts and macrophages are found dispersed within these extracellular matrix (ECM) molecules (36). Ultrastructural analyses of ovarian cancer nodules attached to peritoneal cavity organs using electron microscopy revealed that mesothelial cells are absent from underneath the attached tumor mass (37), suggesting that ovarian cancer cell aggregates invade into the mesothelial lining of the peritoneal cavity, displace the mesothelial cells and attach to the underlying basement membrane. The nodules rarely invade deeper into the basement membrane, however, or metastasize further via the vasculature (3, 32, 38). It is, therefore, very important to understand the mechanisms of ovarian cancer invasion through and displacement of the mesothelial monolayer (a process we refer to as “mesothelial clearance”) so that

better treatment options, which take these mechanisms into account, can be developed.

Mechanisms Governing Ovarian Cancer Spheroid Invasion into Mesothelial Monolayers:

Current Studies of Ovarian Cancer Cell Attachment and Spreading:

The goal of my dissertation research was to further understand the mechanisms that regulate mesothelial clearance by ovarian cancer spheroids. Previously published mechanistic studies focused predominantly on the cell adhesion molecules that mediate ovarian cancer spheroid attachment to mesothelial monolayers and ovarian cancer spheroid spreading on ECM-coated glass. Ovarian cancer cells from established cell lines and from the ascites fluid of ovarian cancer patients are able to attach to and spread on ECM components including, collagen I, collagen IV, laminin and fibronectin, as well as on cultured mesothelial cell monolayers (34, 39-42). Integrins are the major ECM receptors that mediate attachment to the ECM. Ovarian cancer cell adhesion and spreading on both ECM components and mesothelial monolayers has been shown to be inhibited by incubating the ovarian cancer cells with β1-integrin neutralizing antibodies (40, 43-45). α integrins, including α5, α6 and αV, have also been implicated in the adhesion of ovarian cancer cells to ECM and mesothelial monolayers, but the extent of the effects depend on the ovarian cancer cell line and ECM component studied (40, 41, 43, 46-49). In addition to

integrins, the cell adhesion molecule CD44 can promote ovarian cancer cell binding to mesothelial cell monolayers (45, 50, 51).

While ovarian cancer cell adhesion has been well studied, there has been much less focus on the mechanisms required for the ovarian cancer cells to invade into mesothelial monolayers or collagen rich basement membranes. Ahmed and colleagues found that α3, α6, and β1-integrin neutralizing antibodies significantly decreases the ability of HEY ovarian cancer cells to invade through Boyden chambers coated with Matrigel (43) and several groups have shown that inhibiting VCAM, a4-integrin, β1-integrin, MMP-2, or MMP-9 reduces the migration of single ovarian cancer cells through a mesothelial monolayer (46, 52, 53). Together, these studies suggest that cell adhesion molecules play a role in ovarian cancer cell adhesion and invasion, but they do not address the role of integrins in mesothelial clearance by ovarian cancer multicellular spheroids.

To characterize mesothelial invasion, Burleson and colleagues incubated OVCA5 ovarian cancer spheroids on a mesothelial monolayer and found that the spheroids adhered and disaggregated on top of the monolayer (34, 42). While the authors concluded that the spheroids had invaded into the mesothelial monolayer, neither the ovarian cancer cells nor the mesothelial cells were labeled in any way that would allow the two populations to be distinguished, so the extent of invasion and displacement of the mesothelial monolayer could not be measured with this model system. We have developed an *in vitro* model system that uses fluorescently-labeled mesothelial cells to distinguish the ovarian

cancer cells from the mesothelial monolayers, allowing for the measurement of mesothelial clearance (Chapter 2).

Cell Migration Machinery**:**

Cell migration plays an important role in many physiological processes: e.g. during development, large groups of cells migrate collectively to form the three germ layers of the embryo (54); during immune surveillance, leukocytes migrate from the circulation to surrounding tissues (55); and during renewal of the skin and intestinal tissue, new epithelial cells migrate up from the basal layer and crypts, respectively (56). It is likely that ovarian cancer cells use mechanisms involved in these normal migratory processes to invade into mesothelial monolayers.

Using confocal microscopy, we observed that ovarian cancer spheroids invade into the mesothelial monolayer by protruding between the mesothelial cells, adhere to the underlying surface, and translocating beneath the monolayer cells. These actions promote the mesothelial displacement as the spheroid continues to spread. Protrusion, adhesion and translocation are all steps of the cell migration cycle, so we initially chose to focus on the components of the cell migration machinery during our investigation of the mechanisms regulating mesothelial clearance. Furthermore, the increased migratory and invasive ability of cancer cells has been linked to increased contractile force produced by the cancer cell (57). We therefore, sought to determine if molecules involved in contractile force generation during migration could also regulate mesothelial

clearance.

Four components of the cell migration machinery that are important for force generation are actin, myosin, integrins, and talin (58, 59). Actin is one of the components of the cytoskeleton that is responsible for maintaining cell shape and remodeling of the actin cytoskeleton regulates migration and invasion (60). It is present in the cell in two forms, a monomeric G-actin and a filamentous F-actin. Actin filaments are polarized; the positive (barbed) end has a much higher monomer on-rate than off-rate, while the negative (pointed) end has a higher monomer off-rate than on-rate, which promotes growth of the actin filament from the positive end only (61). The actin cytoskeleton produces forces on the extracellular environment in two ways: through protrusions created when actin polymerizes against the cell membrane and through contractions produced with the help of the motor protein myosin (59, 62, 63).

Myosin is a plus end motor protein that contains a head, neck and tail domain. The head domain binds to actin, while the tail domain binds the tail domains of other myosin molecules, therefore, myosin strengthens the actin network by cross-linking actin fibers. When the heads of opposing myosin molecules retract, they pull actin filaments in opposite directions, causing the actin network to contract (64).

Integrins are transmembrane proteins that connect the cytoskeleton to the extracellular matrix (65, 66). The extracellular domain of an integrin binds with specificity to ECM molecules (67, 68), while the intracellular domain attaches to actin polymers via adaptor proteins, such as talin (69). Integrins are

heterodimeric proteins that contain non-covalently bound alpha and beta subunits; the combination of different alpha and beta subunits determines the ECM molecules that the integrin can bind to (70, 71). Integrins can exist in either an active-state, where they are unfolded and bound to ECM molecules, or in an inactive-state, where they are folded and not bound to ECM molecules; integrins can rapidly switch between these states to attach and detach from the ECM during processes such as cell migration (59, 72-74).

Talin acts as a bridge that links integrins to the actin cytoskeleton by either binding directly to the beta subunit of integrins and actin filaments or binding to these molecules indirectly via vinculin and α-actinin (75, 76). Together, the actomyosin network, talin and integrins work together to aid in cell migration. While there are several other molecules that mediate force transduction during cell migration, we will not discuss them here because they were not the focus of our studies.

Cell Migration Cycle:

The cell migration cycle begins when the cells sends out actin-rich cell membrane protrusions (58, 59, 61). Next, integrins in the protrusions are activated and the extracellular subunits bind to ECM while cytoplasmic tail binds to the actin cytoskeleton via adaptor proteins including Talin (76, 77). Contraction of the actomyosin network exerts force on the talin and integrin containing adhesions, which in turn exerts force on the ECM attached to the integrins. This force promotes the recruitment of additional integrins and signaling molecules to

the growing adhesion, promoting adhesion maturation (69). Finally, actomyosin contractility causes retraction of the cell rear and promotes focal adhesion disassembly in the back of the cell and protein recycling to the leading edge (78-81). When this process repeats in a polarized fashion, the cell is able to migrate in a specific direction.

The ability of a cell to polarize and migrate directionally is regulated by various signaling molecules, including the Rho family of GTPases (82). The Rho GTPases, RAC, RHOA and CDC42, are small G proteins that bind guanosine triphosphate (GTP) molecules. Guanine nucleotide exchange factors (GEFs) activate Rho GTPases by swapping GDP molecules that are bound by the GTPases with GTP molecules. GTPase activating proteins (GAPs) deactivate Rho GTPases, by promoting the hydrolysis of bound GTP to GDP(83, 84). Rho GTPases regulate many of the components of cell migration machinery and the spatial regulation of active Rho GTPases promote directional cell migration (85). For example, RAC and CDC42 stimulate Arp2/3, a protein complex that facilitates actin filament nucleation and branching, which produces lamellipodial protrusions (83, 86). RHOA induces actomyosin contractility, which is responsible for focal adhesion maturation and turnover in the cell rear. RHOA and RAC are mutually antagonistic (87). RAC is more active at the leading edge of a migrating cell due to the RAC GEFs that are activated by PI3 kinases at the leading edge, while RHOA is more active at the sides and rear(58). RHOA inhibits RAC at the sides and rear of the cell, preventing protrusions from occurring in locations other than the leading edge (88, 89). This spatial regulation restricting protrusions to

the front of the cell and retractions to the back of the cell promotes directional cell migration.

Force Transmission from the Cell to the Extracellular Matrix:

Not only do focal adhesions mediate the attachment of a cell to its extracellular environment to promote cell migration, they are also sites of force transmission where the contractile force produced by the actomyosin network is transmitted to the ECM via actin and talin (62). Cells are able to sense the stiffness of the ECM and remodel the cytoskeleton accordingly; less stiff substrates resist less tension and as a result the focal adhesions are unable to mature as they would on stiffer substrates (90, 91). Furthermore, as force is exerted on the ECM via focal adhesions, the ECM is remodeled. ECM remodeling has been shown to play a role in the collective migration of tumor cells. During collective migration of squamous cell carcinoma, fibroblasts migrate and remodel the ECM so that they align in the direction of the cell movement, and this remodeling is force dependent. The squamous cell carcinoma cells then follow the tracks of remodeled ECM to metastasize to new sites (92, 93). It is likely that, during mesothelial clearance by ovarian spheroids, the force exerted by the spreading ovarian cancer cells on the ECM surrounding the monolayer cells plays a role in regulating ovarian cancer spheroid invasion into the monolayer.

The Epithelial to Mesenchymal Transition and Cancer Metastasis:

The Epithelial to Mesenchymal Transition (EMT) is a transcriptional program that imparts increased migratory and invasive ability on cells. EMT is believed to occur during cancer progression, to convert immotile primary tumors cells to motile cells that can travel to secondary sites. Expression of EMT-inducing transcription factors SNAI1, ZEB1 and TWIST1 have been associated with tumor recurrence, metastasis and poor prognosis in many cancer, including breast, colon, squamous cell, colorectal, uterine, and prostate, and hepatocellular carcinomas (94-107). Furthermore, there is evidence linking transcription factors that regulate EMT with ovarian cancer invasion and progression. The expression of SNAIL, TWIST and ZEB1 is associated with metastasis and poor overall and progression-free survival in ovarian cancer (108-114). This raises the question of whether the EMT program may regulate mesothelial clearance during ovarian cancer metastasis.

What is EMT?

EMT is a process whereby apicobasal-polarized, immotile epithelial cells that are linked by cell-cell adhesions are converted to planar-polarized, migratory mesenchymal-like cells that display tractable cell-cell adhesions, increased invasiveness, resistance to apoptosis, and increased production of ECM components (115, 116). The epithelial and mesenchymal cell states can be thought of as two extremes on a continuum, as cells with varying degrees of

epithelial and mesenchymal characteristics have been observed. The reverse process, a Mesenchymal to Epithelial Transition (MET), can also occur (115, 117).

EMT occurs in several biological contexts: during embryo implantation, trophectoderm cells in the blastocyst undergo EMT to invade into the endometrium and anchor the placenta; during gastrulation, cells in a single germ layer migrate to produce three germ layers; during vertebrate nervous system development, epithelial cells located near the dorsal midline of the neural tube are converted to mesenchymal cells that migrate to distinct regions within the embryo (118-120); during wound healing, tissue regeneration and organ fibrosis, EMT converts epithelial cells to fibroblasts that reconstruct tissue after trauma or injury due to inflammation (121-123); and during neoplastic transformation, non-migratory epithelial carcinoma cells convert to migratory cells that physically detach from a primary tumor and metastasize to distant sites. Cells with the hallmarks of EMT transformation have been observed at the invasive front of primary tumors (124-127).

During development, EMT is induced by receptor tyrosine kinases that are activated by signaling molecules such as fibroblast growth factor (FGF), platelet derived growth factor (PDGF), epidermal growth factor (EGF), transforming growth factor-β (TGFβ), and vascular endothelial growth factor (VEGF) (125, 128, 129). These growth factors induce multiple transcription factors that have been shown to regulate programs associated with EMT, including SNAIL, SLUG, TWIST1, TWIST2, ZEB1, ZEB2, Goosecoid and FOXC2 (130). All of these

transcription factors regulate the expression of target genes that ultimately control the EMT phenotype (131).

SNAIL and SLUG, members of the snail family of transcription factors, are zinc finger transcriptional repressors (132). Each protein contains a highly conserved C-terminal region with four zinc fingers that act as sequence specific DNA binding domains that recognize consensus E2-box DNA binding elements. The N-terminal domain of the proteins contains a nuclear export sequence and a destruction box that regulate the proteins localization and function when subject to phosphorylation and other post-translational modifications (133-136).

TWIST1 and TWIST2 protein are class II bHLH proteins that each contain two parallel amphipatic α helices that are joined by a loop region. They bind to target DNA sequences as heterodimers with class I bHLH proteins. The proteins can act as transcriptional activators or repressors by recruiting molecules, such as histone acetyltransferases or deacetylases, that regulate transcription via post-translational DNA modifications (137, 138).

Members of the ZEB family (including ZEB1 and ZEB2) are E-box DNA binding proteins that contain two zinc finger clusters on either end of a homeodomain. The two zinc finger domains bind with high affinity to the E-box DNA sequences to induce or repress transcription (139-142).

In addition to transcription factors, microRNAs act downstream of growth factors to regulate EMT. miR10b, miR21, miR373 and miR520c positively regulate EMT, migration and invasion, while miR126, miR206, miR335 and miR200 suppress EMT (143, 144). For example, members of the miR200 family

of microRNAs can prevent EMT by blocking ZEB1 function (145).

During EMT, the transcription factors and microRNAs above repress the expression of epithelial genes, including E-cadherin, claudins, cytokeratins, mucins, plakophilin, occludin, syndecan, and ZO proteins, and enhance the expression of mesenchymal genes, including N-cadherin, vimentin, α-SMA, fibronectin and α5β1 integrin (115, 146). Transcriptional regulation of these genes can be direct or indirect (130, 131). Taube and coworkers identified a core signature of EMT gene that are consistently up-regulated or down-regulated in response to several conditions of EMT induction (146) -- Goosecoid, SNAIL or TWIST1 overexpression, TGFβ treatment, or E-cadherin knockdown -- in human mammary epithelial cells (HMEC). An overlapping set of 159 genes were down-regulated and 87 genes were up-regulated at least 2-fold as a result of each of those perturbations. Genes that were down-regulated included the epithelial genes E-cadherin, Keratin-18 and Rab25 while genes that were up-regulated included the mesenchymal genes N-cadherin, vimentin and ZEB1. This set of genes, therefore, represented a minimal set of genes that are associated with EMT in HMECs (146).

EMT in Cancer:

As stated previously, the expression of EMT-associated transcription factors is associated with ovarian cancer progression and metastasis (94-107). In addition, the expression of mesenchymal markers, including vimentin, α-SMA and laminin 5, or the repression of the epithelial marker E-cadherin, are

associated with invasiveness and metastasis in several types of cancer(127, 147-150). Furthermore, inducing EMT in cells promotes invasiveness. For example, over-expression of ZEB1 in epithelial cells results in a loss of E-cadherin expression and induction of invasion (149) and overexpression of FOXC2 or Goosecoid in weakly metastatic human carcinoma cells increases their ability to disseminate (151, 152). This suggests that EMT plays an important role in cancer progression, but how is EMT induced within the tumor microenvironment?

The induction of EMT has been studied extensively in breast cancer cells. Weinberg and colleagues have shown that components of the tumor stroma are able to induce EMT in epithelial carcinoma cells. They showed that breast cancer cells recruit mesenchymal stem cells to the breast-cancer associated stroma (153). IL-1 secreted by the breast cancer cells induces the mesenchymal stem cells to produce PGE2, IL-6, IL-8, and GRO-α. All of these cytokines secreted by the mesenchymal stem cells then induce EMT in the breast cancer cells(154).

Once outside of the EMT promoting microenvironment, cancer cells can maintain the mesenchymal-like state in a paracrine fashion if EMT inducing cytokines are in the new environment or in an autocrine fashion if the cancer cells produce their own cytokines. If these signaling loops are inhibited, the mesenchymal-like cancer cells convert back to an epithelial state (155).

The fact that mesenchymal-like cells lose their mesenchymal features and revert back to epithelial-like cells when they are removed from an environment with EMT-inducing cytokines suggests that carcinoma cells do not constitutively

express the properties that allow them to invade and metastasize, but rather only transiently become invasive in response to the microenvironment to which the cell is exposed (153). The reversion of mesenchymal-like carcinoma cells to an epithelial-like state may facilitate proliferate at the distant metastatic site (125, 156). This transient nature of EMT has made it difficult to observe EMT *in vivo,* which is why the existence of EMT during cancer metastasis is still under debate.

EMT in Ovarian Cancer:

The microenvironment and mode of metastasis of ovarian cancer is very different compared to that of breast cancer, however, so it is unclear if EMT plays a role in ovarian cancer metastasis, or how or when EMT would be induced in ovarian cancer cells. Several studies have attempted to address the role of EMT in ovarian cancer. Increased SNAI1 expression is associated with the degree of malignancy and overall survival in ovarian cancer. Specifically, increased SNAI1 expression in metastases is correlated with poor overall survival (108). Higher SNAI1 expression is observed in late stage ovarian cancer patients compared to early stage patients and SNAI1 protein expression is significantly lower in ovarian cancer effusions compared to primary and solid metastases (109, 110). TWIST1 is associated with shorter overall and progression free survival in ovarian cancer (108, 111, 112) and high levels of ZEB1 mRNA are observed in high-grade serous ovarian carcinomas (113). Furthermore, the expression levels of TWIST1, ZEB1 and vimentin are higher in metastases compared to primary tumors and effusions (114). The majority of studies on the role of E-cadherin in ovarian

cancer suggest a prognostic role in the disease. Loss of overall E-cadherin expression is associated with poor survival and low E-cadherin mRNA expression in carcinoma effusions is correlated with poor survival, as well (113). In high-grade serous ovarian carcinoma, high expression of E-cadherin and low expression of N- and P-cadherin are associated with better survival (157). These observations suggest that EMT plays a role in ovarian cancer progression.

Experimental data showed that EMT-inducing transcription factors could regulate the attachment of ovarian cancer cells to ECM and mesothelial monolayers and invasion through Matrigel. Down-regulation of SNAI1 or TWIST1 expression in ES2 or HEY ovarian cancer cells, respectively, suppressed invasion through Matrigel (114, 158). Furthermore, knockdown of PAK1, a known regulator of SNAI1, reduced ES2 cell attachment to ECM and mesothelial cell monolayers (114). TWIST1 overexpression in OVCA433 and OVCA432 ovarian cancer cells increased adhesion to ECM and mesothelial cell monolayers as well (112, 158). These studies did not, however, address the role of EMT-inducing transcription factors in mesothelial clearance by ovarian cancer cells.

Characterization of Mesothelial Clearance:

We first sought to describe the process of mesothelial clearance by ovarian cancer spheroids. Time-lapse, confocal microscopy revealed that ovarian cancer spheroids intercalate into mesothelial monolayers, protrude under the mesothelial cells, trigger mesothelial cell matrix adhesion disassembly, and ultimately, mesothelial cell migration away from the intercalating spheroid.

We showed that inhibiting α5β1 integrin, myosin II or Talin I function, in a clearance-competent cell line, inhibits mesothelial clearance. Furthermore, over-expression of α5 integrin in a clearance-incompetent cell line promotes mesothelial clearance. We show that α5β1 integrin reorganizes the fibronectin matrix surrounding the mesothelial cells and blocking α5β1 integrin function inhibits fibronectin remodeling. Furthermore, we show that over-expressing α5 integrin in ovarian cancer cells increases the amount of traction force exerted by the cell, while inhibiting myosin II or talin I function in the α5 integrin over-expressing cells blocks the increase in traction force cause by α5 integrin. Taken together, these experiments suggest that ovarian cancer spheroids use actomyosin generated traction force, via talin and α5β1 integrin, to drive mesothelial clearance (Chapter 3).

Transcriptional Regulation of Mesothelial Clearance:

To comprehensively and systematically investigate the mechanisms regulating mesothelial clearance, we measured clearance ability in large panels of both established ovarian cancer cell lines and primary ovarian cancer cells isolated from the ascites of ovarian cancer patients. Comparison of the clearance ability of 20 established ovarian cancer cell lines revealed that genes in an EMT core signature were enriched in clearance-competent compared to clearance-incompetent cell lines. Overexpression of EMT transcription factors in clearance-incompetent ovarian cancer spheroids promoted mesothelial clearance, while inhibition of EMT transcription factors in clearance-competent cell lines

attenuated mesothelial clearance. The correlation of EMT with mesothelial clearance was also found in a more clinically relevant large panel of primary ovarian tumor cell samples; clearance-competent primary cell spheroids were enriched for the mesenchymal marker, vimentin, while clearance-incompetent primary cell spheroids were enriched for the epithelial marker, E-cadherin. This heterogeneity was also observed in different subpopulations of tumor cells from the same primary patient sample. Taken together, these data suggest that a mesenchymal phenotype promotes mesothelial clearance ability by ovarian cancer spheroids (Chapter 4).

The findings in this dissertation provide important new insights into the mechanisms associated with metastatic progression of ovarian cancer and provide a framework for future studies on the mechanisms of clearance by ovarian cancer spheroids.

References:

1.Siegel R, Naishadham D, Jemal A. Cancer statistics, 2012. CA Cancer J Clin. 2012;62:10-29.

2.Integrated genomic analyses of ovarian carcinoma. Nature. 2011;474:609-15.

3.Lengyel E. Ovarian cancer development and metastasis. Am J Pathol. 2010;177:1053-64.

4.Kyriazi S, Kaye SB, deSouza NM. Imaging ovarian cancer and peritoneal metastases--current and emerging techniques. Nat Rev Clin Oncol. 2010;7:381-93.

5.Moyer VA. Screening for Ovarian Cancer: U.S. Preventive Services Task Force Reaffirmation Recommendation Statement. Ann Intern Med. 2012.

6.Vaughan S, Coward JI, Bast RC, Jr., Berchuck A, Berek JS, Brenton JD, et al. Rethinking ovarian cancer: recommendations for improving outcomes. Nat Rev Cancer. 2011;11:719-25.

7.Armstrong DK, Bundy B, Wenzel L, Huang HQ, Baergen R, Lele S, et al. Intraperitoneal cisplatin and paclitaxel in ovarian cancer. N Engl J Med. 2006;354:34-43.

8.Karst AM, Drapkin R. The new face of ovarian cancer modeling: better prospects for detection and treatment. F1000 Med Rep. 2011;3:22.

9.Schorge JO, McCann C, Del Carmen MG. Surgical debulking of ovarian cancer: what difference does it make? Rev Obstet Gynecol. 2010;3:111-7.

10.Bristow RE, Tomacruz RS, Armstrong DK, Trimble EL, Montz FJ. Survival effect of maximal cytoreductive surgery for advanced ovarian carcinoma during the platinum era: a meta-analysis. J Clin Oncol. 2002;20:1248-59.

11.Naora H. The heterogeneity of epithelial ovarian cancers: reconciling old and new paradigms. Expert Rev Mol Med. 2007;9:1-12.

12.Auersperg N, Wong AS, Choi KC, Kang SK, Leung PC. Ovarian surface epithelium: biology, endocrinology, and pathology. Endocr Rev. 2001;22:255-88.

13.Seidman JD, Horkayne-Szakaly I, Haiba M, Boice CR, Kurman RJ, Ronnett BM. The histologic type and stage distribution of ovarian carcinomas of surface epithelial origin. Int J Gynecol Pathol. 2004;23:41-4.

14.Kurman RJ, Shih Ie M. Molecular pathogenesis and extraovarian origin of epithelial ovarian cancer--shifting the paradigm. Hum Pathol. 2011;42:918-31.

15.Martin DC. Cancer and endometriosis: do we need to be concerned? Semin Reprod Endocrinol. 1997;15:319-24.

16.Rosenblatt KA, Thomas DB. Reduced risk of ovarian cancer in women with a tubal ligation or hysterectomy. The World Health Organization Collaborative Study of Neoplasia and Steroid Contraceptives. Cancer Epidemiol Biomarkers Prev. 1996;5:933-5.

17.Riopel MA, Ronnett BM, Kurman RJ. Evaluation of diagnostic criteria and behavior of ovarian intestinal-type mucinous tumors: atypical proliferative (borderline) tumors and intraepithelial, microinvasive, invasive, and metastatic carcinomas. Am J Surg Pathol. 1999;23:617-35.

18.Piek JM, van Diest PJ, Zweemer RP, Jansen JW, Poort-Keesom RJ, Menko FH, et al. Dysplastic changes in prophylactically removed Fallopian tubes of women predisposed to developing ovarian cancer. J Pathol. 2001;195:451-6.

19.Lee Y, Miron A, Drapkin R, Nucci MR, Medeiros F, Saleemuddin A, et al. A candidate precursor to serous carcinoma that originates in the distal fallopian tube. J Pathol. 2007;211:26-35.

20.Levanon K, Ng V, Piao HY, Zhang Y, Chang MC, Roh MH, et al. Primary ex vivo cultures of human fallopian tube epithelium as a model for serous ovarian carcinogenesis. Oncogene. 2010;29:1103-13.

21.Crum CP, Drapkin R, Miron A, Ince TA, Muto M, Kindelberger DW, et al. The distal fallopian tube: a new model for pelvic serous carcinogenesis. Curr Opin Obstet Gynecol. 2007;19:3-9.

22.Dubeau L. The cell of origin of ovarian epithelial tumors and the ovarian surface epithelium dogma: does the emperor have no clothes? Gynecol Oncol. 1999;72:437-42.

23.Marquez RT, Baggerly KA, Patterson AP, Liu J, Broaddus R, Frumovitz M, et al. Patterns of gene expression in different histotypes of epithelial ovarian cancer correlate with those in normal fallopian tube, endometrium, and colon. Clin Cancer Res. 2005;11:6116-26.

24.Kurman RJ, Shih Ie M. The origin and pathogenesis of epithelial ovarian cancer: a proposed unifying theory. Am J Surg Pathol. 2010;34:433-43.

25.Ahmed AA, Etemadmoghadam D, Temple J, Lynch AG, Riad M, Sharma R, et al. Driver mutations in TP53 are ubiquitous in high grade serous carcinoma of the ovary. J Pathol. 2010;221:49-56.

26.Kohler MF, Marks JR, Wiseman RW, Jacobs IJ, Davidoff AM, Clarke-Pearson DL, et al. Spectrum of mutation and frequency of allelic deletion of the p53 gene in ovarian cancer. J Natl Cancer Inst. 1993;85:1513-9.

27.Singer G, Stohr R, Cope L, Dehari R, Hartmann A, Cao DF, et al. Patterns of p53 mutations separate ovarian serous borderline tumors and low- and high-grade carcinomas and provide support for a new model of ovarian carcinogenesis: a mutational analysis with immunohistochemical correlation. Am J Surg Pathol. 2005;29:218-24.

28.Medeiros F, Muto MG, Lee Y, Elvin JA, Callahan MJ, Feltmate C, et al. The tubal fimbria is a preferred site for early adenocarcinoma in women with familial ovarian cancer syndrome. Am J Surg Pathol. 2006;30:230-6.

29.Kindelberger DW, Lee Y, Miron A, Hirsch MS, Feltmate C, Medeiros F, et al. Intraepithelial carcinoma of the fimbria and pelvic serous carcinoma: Evidence for a causal relationship. Am J Surg Pathol. 2007;31:161-9.

30.Gupta GP, Massague J. Cancer metastasis: building a framework. Cell. 2006;127:679-95.

31.Shield K, Ackland ML, Ahmed N, Rice GE. Multicellular spheroids in ovarian cancer metastases: Biology and pathology. Gynecol Oncol. 2009;113:143-8.

32.Naora H, Montell DJ. Ovarian cancer metastasis: integrating insights from disparate model organisms. Nat Rev Cancer. 2005;5:355-66.

33.Allen HJ, Porter C, Gamarra M, Piver MS, Johnson EA. Isolation and morphologic characterization of human ovarian carcinoma cell clusters present in effusions. Exp Cell Biol. 1987;55:194-208.

34.Burleson KM, Hansen LK, Skubitz AP. Ovarian carcinoma spheroids disaggregate on type I collagen and invade live human mesothelial cell monolayers. Clin Exp Metastasis. 2004;21:685-97.

35.Daya D, McCaughey WT. Pathology of the peritoneum: a review of selected topics. Semin Diagn Pathol. 1991;8:277-89.

36.Witz CA, Montoya-Rodriguez IA, Cho S, Centonze VE, Bonewald LF, Schenken RS. Composition of the extracellular matrix of the peritoneum. J Soc Gynecol Investig. 2001;8:299-304.

37.Kenny HA, Nieman KM, Mitra AK, Lengyel E. The First Line of Intra-abdominal Metastatic Attack: Breaching the Mesothelial Cell Layer. Cancer Discovery. 2011;1:100-2.

38.Bristow RE, del Carmen MG, Kaufman HS, Montz FJ. Radical oophorectomy with primary stapled colorectal anastomosis for resection of locally advanced epithelial ovarian cancer. J Am Coll Surg. 2003;197:565-74.

39.Niedbala MJ, Crickard K, Bernacki RJ. Interactions of human ovarian tumor cells with human mesothelial cells grown on extracellular matrix. An in vitro model system for studying tumor cell adhesion and invasion. Exp Cell Res. 1985;160:499-513.

40.Burleson KM, Casey RC, Skubitz KM, Pambuccian SE, Oegema TR, Jr., Skubitz AP. Ovarian carcinoma ascites spheroids adhere to extracellular matrix components and mesothelial cell monolayers. Gynecol Oncol. 2004;93:170-81.

41.Shield K, Riley C, Quinn MA, Rice GE, Ackland ML, Ahmed N. Alpha2beta1 integrin affects metastatic potential of ovarian carcinoma spheroids by supporting disaggregation and proteolysis. J Carcinog. 2007;6:11.

42.Burleson KM, Boente MP, Pambuccian SE, Skubitz AP. Disaggregation and invasion of ovarian carcinoma ascites spheroids. J Transl Med. 2006;4:6.

43Ahmed N, Riley C, Rice G, Quinn M. Role of integrin receptors for fibronectin, collagen and laminin in the regulation of ovarian carcinoma functions in response to a matrix microenvironment. Clin Exp Metastasis. 2005;22:391-402.

44.Strobel T, Cannistra SA. Beta1-integrins partly mediate binding of ovarian cancer cells to peritoneal mesothelium in vitro. Gynecol Oncol. 1999;73:362-7.

45.Lessan K, Aguiar DJ, Oegema T, Siebenson L, Skubitz AP. CD44 and beta1 integrin mediate ovarian carcinoma cell adhesion to peritoneal mesothelial cells. Am J Pathol. 1999;154:1525-37.

46.Slack-Davis JK, Atkins KA, Harrer C, Hershey ED, Conaway M. Vascular cell adhesion molecule-1 is a regulator of ovarian cancer peritoneal metastasis. Cancer Res. 2009;69:1469-76.

47.Cannistra SA, Ottensmeier C, Niloff J, Orta B, DiCarlo J. Expression and function of beta 1 and alpha v beta 3 integrins in ovarian cancer. Gynecol Oncol. 1995;58:216-25.

48.Kaur S, Kenny HA, Jagadeeswaran S, Zillhardt MR, Montag AG, Kistner E, et al. {beta}3-integrin expression on tumor cells inhibits tumor progression,

reduces metastasis, and is associated with a favorable prognosis in patients with ovarian cancer. Am J Pathol. 2009;175:2184-96.

49.Heyman L, Kellouche S, Fernandes J, Dutoit S, Poulain L, Carreiras F. Vitronectin and its receptors partly mediate adhesion of ovarian cancer cells to peritoneal mesothelium in vitro. Tumour Biol. 2008;29:231-44.

50.Cannistra SA, Kansas GS, Niloff J, DeFranzo B, Kim Y, Ottensmeier C. Binding of ovarian cancer cells to peritoneal mesothelium in vitro is partly mediated by CD44H. Cancer Res. 1993;53:3830-8.

51.Strobel T, Swanson L, Cannistra SA. In vivo inhibition of CD44 limits intra-abdominal spread of a human ovarian cancer xenograft in nude mice: a novel role for CD44 in the process of peritoneal implantation. Cancer Res. 1997;57:1228-32.

52.Kenny HA, Krausz T, Yamada SD, Lengyel E. Use of a novel 3D culture model to elucidate the role of mesothelial cells, fibroblasts and extra-cellular matrices on adhesion and invasion of ovarian cancer cells to the omentum. Int J Cancer. 2007;121:1463-72.

53.Casey RC, Koch KA, Oegema TR, Jr., Skubitz KM, Pambuccian SE, Grindle SM, et al. Establishment of an in vitro assay to measure the invasion of ovarian carcinoma cells through mesothelial cell monolayers. Clin Exp Metastasis. 2003;20:343-56.

54.Acloque H, Adams MS, Fishwick K, Bronner-Fraser M, Nieto MA. Epithelial-mesenchymal transitions: the importance of changing cell state in development and disease. J Clin Invest. 2009;119:1438-49.

55.Swann JB, Smyth MJ. Immune surveillance of tumors. J Clin Invest. 2007;117:1137-46.

56.Lamprecht SA, Lipkin M. Migrating colonic crypt epithelial cells: primary targets for transformation. Carcinogenesis. 2002;23:1777-80.

57.Mierke CT, Frey B, Fellner M, Herrmann M, Fabry B. Integrin alpha5beta1 facilitates cancer cell invasion through enhanced contractile forces. J Cell Sci. 2011;124:369-83.

58.Ridley AJ, Schwartz MA, Burridge K, Firtel RA, Ginsberg MH, Borisy G, et al. Cell migration: integrating signals from front to back. Science. 2003;302:1704-9.

59.Lauffenburger DA, Horwitz AF. Cell migration: a physically integrated molecular process. Cell. 1996;84:359-69.

60.Mouneimne G, Hansen SD, Selfors LM, Petrak L, Hickey MM, Gallegos LL, et al. Differential remodeling of actin cytoskeleton architecture by profilin isoforms leads to distinct effects on cell migration and invasion. Cancer Cell. 2012;22:615-30.

61.Pollard TD, Borisy GG. Cellular motility driven by assembly and disassembly of actin filaments. Cell. 2003;112:453-65.

62.Ingber DE. Cellular mechanotransduction: putting all the pieces together again. FASEB J. 2006;20:811-27.

63.Schwartz IM, Ehrenberg M, Bindschadler M, McGrath JL. The role of substrate curvature in actin-based pushing forces. Curr Biol. 2004;14:1094-8.

64.Wolenski JS. Regulation of calmodulin-binding myosins. Trends Cell Biol. 1995;5:310-6.

65.Hynes RO. The emergence of integrins: a personal and historical perspective. Matrix Biol. 2004;23:333-40.

66.Tamkun JW, DeSimone DW, Fonda D, Patel RS, Buck C, Horwitz AF, et al. Structure of integrin, a glycoprotein involved in the transmembrane linkage between fibronectin and actin. Cell. 1986;46:271-82.

67.Plow EF, Haas TA, Zhang L, Loftus J, Smith JW. Ligand binding to integrins. J Biol Chem. 2000;275:21785-8.

68.van der Flier A, Sonnenberg A. Function and interactions of integrins. Cell Tissue Res. 2001;305:285-98.

69.Petit V, Thiery JP. Focal adhesions: structure and dynamics. Biol Cell. 2000;92:477-94.

70.Lin EC, Ratnikov BI, Tsai PM, Carron CP, Myers DM, Barbas CF, 3rd, et al. Identification of a region in the integrin beta3 subunit that confers ligand binding specificity. J Biol Chem. 1997;272:23912-20.

71.Mould AP, Askari JA, Humphries MJ. Molecular basis of ligand recognition by integrin alpha 5beta 1. I. Specificity of ligand binding is determined by amino acid sequences in the second and third NH2-terminal repeats of the alpha subunit. J Biol Chem. 2000;275:20324-36.

72.Lock JG, Wehrle-Haller B, Stromblad S. Cell-matrix adhesion complexes: master control machinery of cell migration. Semin Cancer Biol. 2008;18:65-76.

73.Puklin-Faucher E, Sheetz MP. The mechanical integrin cycle. J Cell Sci. 2009;122:179-86.

74.Hynes RO. Integrins: bidirectional, allosteric signaling machines. Cell. 2002;110:673-87.

75.Zhang X, Jiang G, Cai Y, Monkley SJ, Critchley DR, Sheetz MP. Talin depletion reveals independence of initial cell spreading from integrin activation and traction. Nat Cell Biol. 2008.

76.del Rio A, Perez-Jimenez R, Liu R, Roca-Cusachs P, Fernandez JM, Sheetz MP. Stretching single talin rod molecules activates vinculin binding. Science. 2009;323:638-41.

77.Wegener KL, Partridge AW, Han J, Pickford AR, Liddington RC, Ginsberg MH, et al. Structural basis of integrin activation by talin. Cell. 2007;128:171-82.

78.Jay PY, Pham PA, Wong SA, Elson EL. A mechanical function of myosin II in cell motility. J Cell Sci. 1995;108 (Pt 1):387-93.

79.Rubino S, Fighetti M, Unger E, Cappuccinelli P. Location of actin, myosin, and microtubular structures during directed locomotion of Dictyostelium amebae. J Cell Biol. 1984;98:382-90.

80.Palecek SP, Schmidt CE, Lauffenburger DA, Horwitz AF. Integrin dynamics on the tail region of migrating fibroblasts. J Cell Sci. 1996;109 (Pt 5):941-52.

81.Regen CM, Horwitz AF. Dynamics of beta 1 integrin-mediated adhesive contacts in motile fibroblasts. J Cell Biol. 1992;119:1347-59.

82.Nobes CD, Hall A. Rho GTPases control polarity, protrusion, and adhesion during cell movement. J Cell Biol. 1999;144:1235-44.

83.Schwartz M. Rho signalling at a glance. J Cell Sci. 2004;117:5457-8.

84.Bishop AL, Hall A. Rho GTPases and their effector proteins. Biochem J. 2000;348 Pt 2:241-55.

85.Etienne-Manneville S, Hall A. Rho GTPases in cell biology. Nature. 2002;420:629-35.

86.Mullins RD, Pollard TD. Rho-family GTPases require the Arp2/3 complex to stimulate actin polymerization in Acanthamoeba extracts. Curr Biol. 1999;9:405-15.

87.Evers EE, Zondag GC, Malliri A, Price LS, ten Klooster JP, van der Kammen RA, et al. Rho family proteins in cell adhesion and cell migration. Eur J Cancer. 2000;36:1269-74.

88.Worthylake RA, Burridge K. RhoA and ROCK promote migration by limiting membrane protrusions. J Biol Chem. 2003;278:13578-84.

89.Xu J, Wang F, Van Keymeulen A, Herzmark P, Straight A, Kelly K, et al. Divergent signals and cytoskeletal assemblies regulate self-organizing polarity in neutrophils. Cell. 2003;114:201-14.

90.Maniotis AJ, Chen CS, Ingber DE. Demonstration of mechanical connections between integrins, cytoskeletal filaments, and nucleoplasm that stabilize nuclear structure. Proc Natl Acad Sci U S A. 1997;94:849-54.

91.Wang N, Butler JP, Ingber DE. Mechanotransduction across the cell surface and through the cytoskeleton. Science. 1993;260:1124-7.

92.Gaggioli C, Hooper S, Hidalgo-Carcedo C, Grosse R, Marshall JF, Harrington K, et al. Fibroblast-led collective invasion of carcinoma cells with differing roles for RhoGTPases in leading and following cells. Nat Cell Biol. 2007;9:1392-400.

93.Gaggioli C. Collective invasion of carcinoma cells: when the fibroblasts take the lead. Cell Adh Migr. 2008;2:45-7.

94.Blanco MJ, Moreno-Bueno G, Sarrio D, Locascio A, Cano A, Palacios J, et al. Correlation of Snail expression with histological grade and lymph node status in breast carcinomas. Oncogene. 2002;21:3241-6.

95.Cheng CW, Wu PE, Yu JC, Huang CS, Yue CT, Wu CW, et al. Mechanisms of inactivation of E-cadherin in breast carcinoma: modification of the two-hit hypothesis of tumor suppressor gene. Oncogene. 2001;20:3814-23.

96.Come C, Magnino F, Bibeau F, De Santa Barbara P, Becker KF, Theillet C, et al. Snail and slug play distinct roles during breast carcinoma progression. Clin Cancer Res. 2006;12:5395-402.

97.Moody SE, Perez D, Pan TC, Sarkisian CJ, Portocarrero CP, Sterner CJ, et al. The transcriptional repressor Snail promotes mammary tumor recurrence. Cancer Cell. 2005;8:197-209.

98.Roy HK, Smyrk TC, Koetsier J, Victor TA, Wali RK. The transcriptional repressor SNAIL is overexpressed in human colon cancer. Dig Dis Sci. 2005;50:42-6.

99.Takeno S, Noguchi T, Fumoto S, Kimura Y, Shibata T, Kawahara K. E-cadherin expression in patients with esophageal squamous cell

carcinoma: promoter hypermethylation, Snail overexpression, and clinicopathologic implications. Am J Clin Pathol. 2004;122:78-84.

100.Pena C, Garcia JM, Silva J, Garcia V, Rodriguez R, Alonso I, et al. E-cadherin and vitamin D receptor regulation by SNAIL and ZEB1 in colon cancer: clinicopathological correlations. Hum Mol Genet. 2005;14:3361-70.

101.Spoelstra NS, Manning NG, Higashi Y, Darling D, Singh M, Shroyer KR, et al. The transcription factor ZEB1 is aberrantly expressed in aggressive uterine cancers. Cancer Res. 2006;66:3893-902.

102.Hoek K, Rimm DL, Williams KR, Zhao H, Ariyan S, Lin A, et al. Expression profiling reveals novel pathways in the transformation of melanocytes to melanomas. Cancer Res. 2004;64:5270-82.

103.Yuen HF, Chan YP, Wong ML, Kwok WK, Chan KK, Lee PY, et al. Upregulation of Twist in oesophageal squamous cell carcinoma is associated with neoplastic transformation and distant metastasis. J Clin Pathol. 2007;60:510-4.

104.Martin TA, Goyal A, Watkins G, Jiang WG. Expression of the transcription factors snail, slug, and twist and their clinical significance in human breast cancer. Ann Surg Oncol. 2005;12:488-96.

105.Kyo S, Sakaguchi J, Ohno S, Mizumoto Y, Maida Y, Hashimoto M, et al. High Twist expression is involved in infiltrative endometrial cancer and affects patient survival. Hum Pathol. 2006;37:431-8.

106.Kwok WK, Ling MT, Lee TW, Lau TC, Zhou C, Zhang X, et al. Up-regulation of TWIST in prostate cancer and its implication as a therapeutic target. Cancer Res. 2005;65:5153-62.

107.Lee TK, Poon RT, Yuen AP, Ling MT, Kwok WK, Wang XH, et al. Twist overexpression correlates with hepatocellular carcinoma metastasis through induction of epithelial-mesenchymal transition. Clin Cancer Res. 2006;12:5369-76.

108.Yoshida J, Horiuchi A, Kikuchi N, Hayashi A, Osada R, Ohira S, et al. Changes in the expression of E-cadherin repressors, Snail, Slug, SIP1, and Twist, in the development and progression of ovarian carcinoma: the important role of Snail in ovarian tumorigenesis and progression. Med Mol Morphol. 2009;42:82-91.

109.Jin H, Yu Y, Zhang T, Zhou X, Zhou J, Jia L, et al. Snail is critical for tumor growth and metastasis of ovarian carcinoma. Int J Cancer. 2010;126:2102-11.

110.Sivertsen S, Hadar R, Elloul S, Vintman L, Bedrossian C, Reich R, et al. Expression of Snail, Slug and Sip1 in malignant mesothelioma effusions is associated with matrix metalloproteinase, but not with cadherin expression. Lung Cancer. 2006;54:309-17.

111.Hosono S, Kajiyama H, Terauchi M, Shibata K, Ino K, Nawa A, et al. Expression of Twist increases the risk for recurrence and for poor survival in epithelial ovarian carcinoma patients. Br J Cancer. 2007;96:314-20.

112.Kajiyama H, Hosono S, Terauchi M, Shibata K, Ino K, Yamamoto E, et al. Twist expression predicts poor clinical outcome of patients with clear cell carcinoma of the ovary. Oncology. 2006;71:394-401.

113.Davidson B, Trope CG, Reich R. Epithelial-mesenchymal transition in ovarian carcinoma. Front Oncol. 2012;2:33.

114.Elloul S, Vaksman O, Stavnes HT, Trope CG, Davidson B, Reich R. Mesenchymal-to-epithelial transition determinants as characteristics of ovarian carcinoma effusions. Clin Exp Metastasis. 2010;27:161-72.

115.Kalluri R, Weinberg RA. The basics of epithelial-mesenchymal transition. J Clin Invest. 2009;119:1420-8.

116.Hay ED. An overview of epithelio-mesenchymal transformation. Acta Anat (Basel). 1995;154:8-20.

117.Rothenpieler UW, Dressler GR. Pax-2 is required for mesenchyme-to-epithelium conversion during kidney development. Development. 1993;119:711-20.

118.Vicovac L, Aplin JD. Epithelial-mesenchymal transition during trophoblast differentiation. Acta Anat (Basel). 1996;156:202-16.

119.Bischof P, Aplin JD, Bentin-Ley U, Brannstrom M, Casslen B, Castrillo JL, et al. Implantation of the human embryo: research lines and models. From the implantation research network 'Fruitful'. Gynecol Obstet Invest. 2006;62:206-16.

120.Hay ED. The mesenchymal cell, its role in the embryo, and the remarkable signaling mechanisms that create it. Dev Dyn. 2005;233:706-20.

121.Zeisberg EM, Tarnavski O, Zeisberg M, Dorfman AL, McMullen JR, Gustafsson E, et al. Endothelial-to-mesenchymal transition contributes to cardiac fibrosis. Nat Med. 2007;13:952-61.

122.Zeisberg M, Yang C, Martino M, Duncan MB, Rieder F, Tanjore H, et al. Fibroblasts derive from hepatocytes in liver fibrosis via epithelial to mesenchymal transition. J Biol Chem. 2007;282:23337-47.

123.Okada H, Danoff TM, Kalluri R, Neilson EG. Early role of Fsp1 in epithelial-mesenchymal transformation. Am J Physiol. 1997;273:F563-74.

124.Hanahan D, Weinberg RA. The hallmarks of cancer. Cell. 2000;100:57-70.

125.Thiery JP. Epithelial-mesenchymal transitions in tumour progression. Nat Rev Cancer. 2002;2:442-54.

126.Yang J, Weinberg RA. Epithelial-mesenchymal transition: at the crossroads of development and tumor metastasis. Dev Cell. 2008;14:818-29.

127.Sarrio D, Rodriguez-Pinilla SM, Hardisson D, Cano A, Moreno-Bueno G, Palacios J. Epithelial-mesenchymal transition in breast cancer relates to the basal-like phenotype. Cancer Res. 2008;68:989-97.

128.Thiery JP, Sleeman JP. Complex networks orchestrate epithelial-mesenchymal transitions. Nat Rev Mol Cell Biol. 2006;7:131-42.

129.Huber MA, Kraut N, Beug H. Molecular requirements for epithelial-mesenchymal transition during tumor progression. Curr Opin Cell Biol. 2005;17:548-58.

130.Nieto MA. The ins and outs of the epithelial to mesenchymal transition in health and disease. Annu Rev Cell Dev Biol. 2011;27:347-76.

131.Peinado H, Olmeda D, Cano A. Snail, Zeb and bHLH factors in tumour progression: an alliance against the epithelial phenotype? Nat Rev Cancer. 2007;7:415-28.

132.Barrallo-Gimeno A, Nieto MA. The Snail genes as inducers of cell movement and survival: implications in development and cancer. Development. 2005;132:3151-61.

133.Nieto MA. The snail superfamily of zinc-finger transcription factors. Nat Rev Mol Cell Biol. 2002;3:155-66.

134.Hemavathy K, Ashraf SI, Ip YT. Snail/slug family of repressors: slowly going into the fast lane of development and cancer. Gene. 2000;257:1-12.

135.Dominguez D, Montserrat-Sentis B, Virgos-Soler A, Guaita S, Grueso J, Porta M, et al. Phosphorylation regulates the subcellular location and activity of the snail transcriptional repressor. Mol Cell Biol. 2003;23:5078-89.

136.Zhou BP, Deng J, Xia W, Xu J, Li YM, Gunduz M, et al. Dual regulation of Snail by GSK-3beta-mediated phosphorylation in control of epithelial-mesenchymal transition. Nat Cell Biol. 2004;6:931-40.

137.Massari ME, Murre C. Helix-loop-helix proteins: regulators of transcription in eucaryotic organisms. Mol Cell Biol. 2000;20:429-40.

138.Ellenberger T, Fass D, Arnaud M, Harrison SC. Crystal structure of transcription factor E47: E-box recognition by a basic region helix-loop-helix dimer. Genes Dev. 1994;8:970-80.

139.Eger A, Aigner K, Sonderegger S, Dampier B, Oehler S, Schreiber M, et al. DeltaEF1 is a transcriptional repressor of E-cadherin and regulates epithelial plasticity in breast cancer cells. Oncogene. 2005;24:2375-85.

140.Comijn J, Berx G, Vermassen P, Verschueren K, van Grunsven L, Bruyneel E, et al. The two-handed E box binding zinc finger protein SIP1 downregulates E-cadherin and induces invasion. Mol Cell. 2001;7:1267-78.

141.Postigo AA, Depp JL, Taylor JJ, Kroll KL. Regulation of Smad signaling through a differential recruitment of coactivators and corepressors by ZEB proteins. EMBO J. 2003;22:2453-62.

142.Remacle JE, Kraft H, Lerchner W, Wuytens G, Collart C, Verschueren K, et al. New mode of DNA binding of multi-zinc finger transcription factors: deltaEF1 family members bind with two hands to two target sites. EMBO J. 1999;18:5073-84.

143.Ocana OH, Nieto MA. A new regulatory loop in cancer-cell invasion. EMBO Rep. 2008;9:521-2.

144.Castilla MA, Moreno-Bueno G, Romero-Perez L, Van De Vijver K, Biscuola M, Lopez-Garcia MA, et al. Micro-RNA signature of the epithelial-mesenchymal transition in endometrial carcinosarcoma. J Pathol. 2011;223:72-80.

145.Brabletz S, Brabletz T. The ZEB/miR-200 feedback loop--a motor of cellular plasticity in development and cancer? EMBO Rep. 2010;11:670-7.

146.Taube JH, Herschkowitz JI, Komurov K, Zhou AY, Gupta S, Yang J, et al. Core epithelial-to-mesenchymal transition interactome gene-expression signature is associated with claudin-low and metaplastic breast cancer subtypes. Proc Natl Acad Sci U S A. 2010;107:15449-54.

147.Raymond WA, Leong AS. Vimentin--a new prognostic parameter in breast carcinoma? J Pathol. 1989;158:107-14.

148.Carpenter PM, Wang-Rodriguez J, Chan OT, Wilczynski SP. Laminin 5 expression in metaplastic breast carcinomas. Am J Surg Pathol. 2008;32:345-53.

149.Vandewalle C, Van Roy F, Berx G. The role of the ZEB family of transcription factors in development and disease. Cell Mol Life Sci. 2009;66:773-87.

150.Frixen UH, Behrens J, Sachs M, Eberle G, Voss B, Warda A, et al. E-cadherin-mediated cell-cell adhesion prevents invasiveness of human carcinoma cells. J Cell Biol. 1991;113:173-85.

151.Hartwell KA, Muir B, Reinhardt F, Carpenter AE, Sgroi DC, Weinberg RA. The Spemann organizer gene, Goosecoid, promotes tumor metastasis. Proc Natl Acad Sci U S A. 2006;103:18969-74.

152.Mani SA, Yang J, Brooks M, Schwaninger G, Zhou A, Miura N, et al. Mesenchyme Forkhead 1 (FOXC2) plays a key role in metastasis and is associated with aggressive basal-like breast cancers. Proc Natl Acad Sci U S A. 2007;104:10069-74.

153.Karnoub AE, Dash AB, Vo AP, Sullivan A, Brooks MW, Bell GW, et al. Mesenchymal stem cells within tumour stroma promote breast cancer metastasis. Nature. 2007;449:557-63.

154.Li HJ, Reinhardt F, Herschman HR, Weinberg RA. Cancer-stimulated mesenchymal stem cells create a carcinoma stem cell niche via prostaglandin E2 signaling. Cancer Discov. 2012;2:840-55.

155.Scheel C, Eaton EN, Li SH, Chaffer CL, Reinhardt F, Kah KJ, et al. Paracrine and autocrine signals induce and maintain mesenchymal and stem cell states in the breast. Cell. 2011;145:926-40.

156.Tsai JH, Donaher JL, Murphy DA, Chau S, Yang J. Spatiotemporal Regulation of Epithelial-Mesenchymal Transition Is Essential for Squamous Cell Carcinoma Metastasis. Cancer Cell. 2012.

157.Quattrocchi L, Green AR, Martin S, Durrant L, Deen S. The cadherin switch in ovarian high-grade serous carcinoma is associated with disease progression. Virchows Arch. 2011;459:21-9.

158.Terauchi M, Kajiyama H, Yamashita M, Kato M, Tsukamoto H, Umezu T, et al. Possible involvement of TWIST in enhanced peritoneal metastasis of epithelial ovarian carcinoma. Clin Exp Metastasis. 2007;24:329-39.

Chapter 2

In vitro Mesothelial Clearance Assay that Models the Early Steps of Ovarian Cancer Metastasis

Statement of Contribution:

This chapter embodies a manuscript published in the *Journal of Visualized Experiments* by R.A. Davidowitz, M.P. Iwanicki and J.S. Brugge*. I wrote the manuscript and performed the mesothelial clearance assay in the video. MPI developed the assay. MPI and JSB participated in the writing of the manuscript.

*Corresponding authors

Journal of Visualized Experiments Video:

See Supplementary Movie 2.1 or

www.jove.com/video/3888/in-vitro-mesothelial-clearance-assay-that-models-early-steps-ovarian

Short Abstract:

The mesothelial clearance assay described here takes advantage of fluorescently labeled cells and time-lapse video microscopy to visualize and quantitatively measure the interactions of ovarian cancer multicellular spheroids and mesothelial cell monolayers. This assay models the early steps of ovarian cancer metastasis.

Long Abstract:

Ovarian cancer is the fifth leading cause of cancer related deaths in the United States(1). Despite a positive initial response to therapies, 70 to 90 percent of women with ovarian cancer develop new metastases, and the recurrence is often fatal(2). It is, therefore, necessary to understand how secondary metastases arise in order to develop better treatments for intermediate and late stage ovarian cancer. Ovarian cancer metastasis occurs when malignant cells detach from the primary tumor site and disseminate throughout the peritoneal cavity. The disseminated cells can form multicellular clusters, or spheroids, that will either remain unattached, or implant onto organs within the peritoneal cavity(3) (Figure 2.1).

All of the organs within the peritoneal cavity are lined with a single, continuous, layer of mesothelial cells(4-6) (Figure 2.2). However, mesothelial cells are absent from underneath peritoneal tumor masses, as revealed by electron micrograph studies of excised human tumor tissue sections(3, 5-7) (Figure 2.2). This suggests that mesothelial cells are excluded from underneath the tumor mass by an unknown process.

Previous *in vitro* experiments demonstrated that primary ovarian cancer cells attach more efficiently to extracellular matrix than to mesothelial cells(8), and more recent studies showed that primary peritoneal mesothelial cells actually provide a barrier to ovarian cancer cell adhesion and invasion (as compared to adhesion and invasion on substrates that were not covered with mesothelial cells)(9, 10). This would suggest that mesothelial cells act as a barrier against ovarian cancer metastasis. The

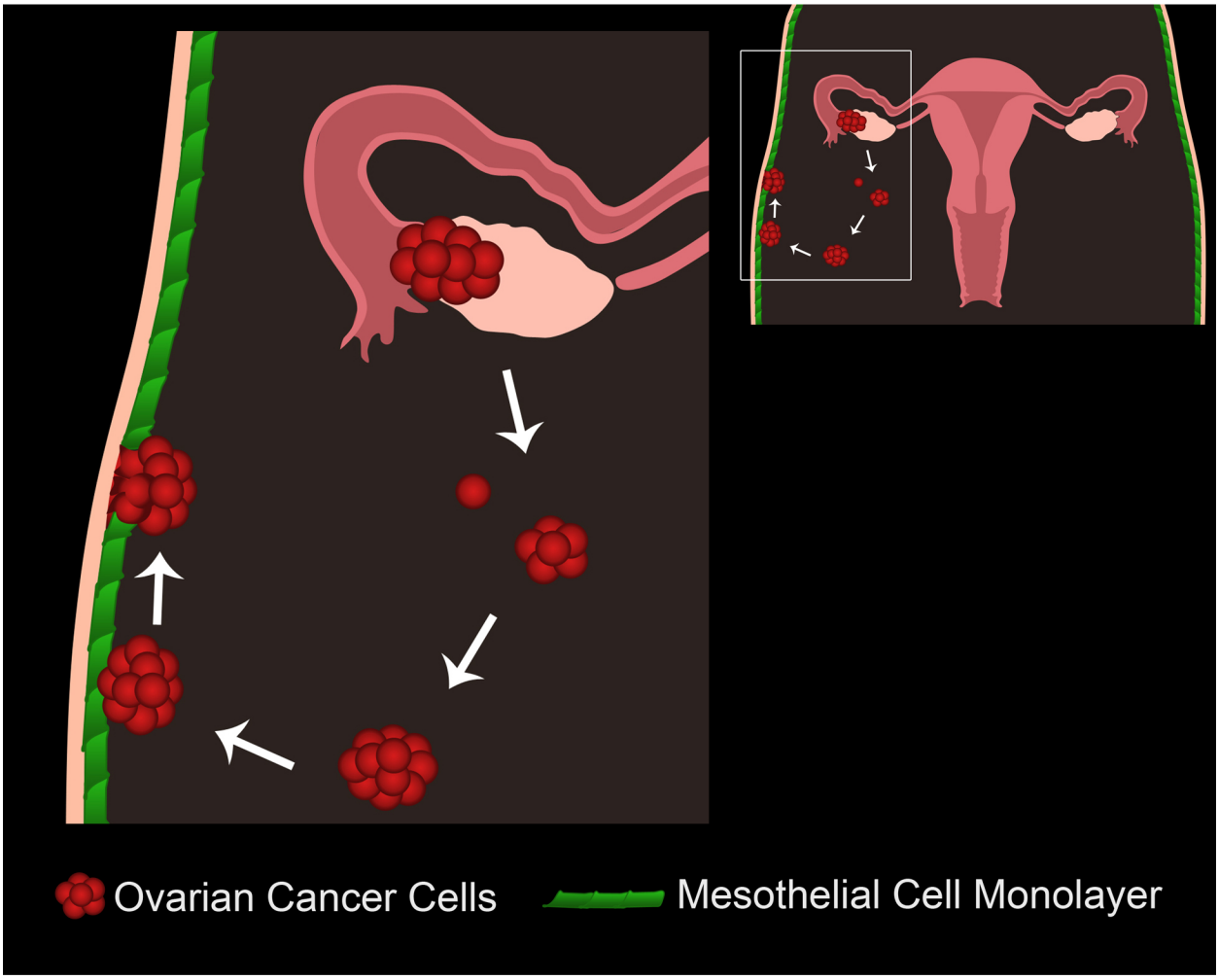

FIGURE 2.1: Ovarian Cancer Metastasis. Primary ovarian tumors develop either from the ovarian surface epithelium or fallopian tubes. Tumor cells/ clusters break off from the primary tumor and collect in the peritoneal cavity. Tumor cells can then aggregate to form multicellular spheroids. Spheroids then attach to the mesothelial cell monolayers lining the peritoneal cavity. The mesothelial cells are excluded from underneath the attached ovarian cancer spheroid, allowing the spheroids to gain access to the underlying basement membrane.

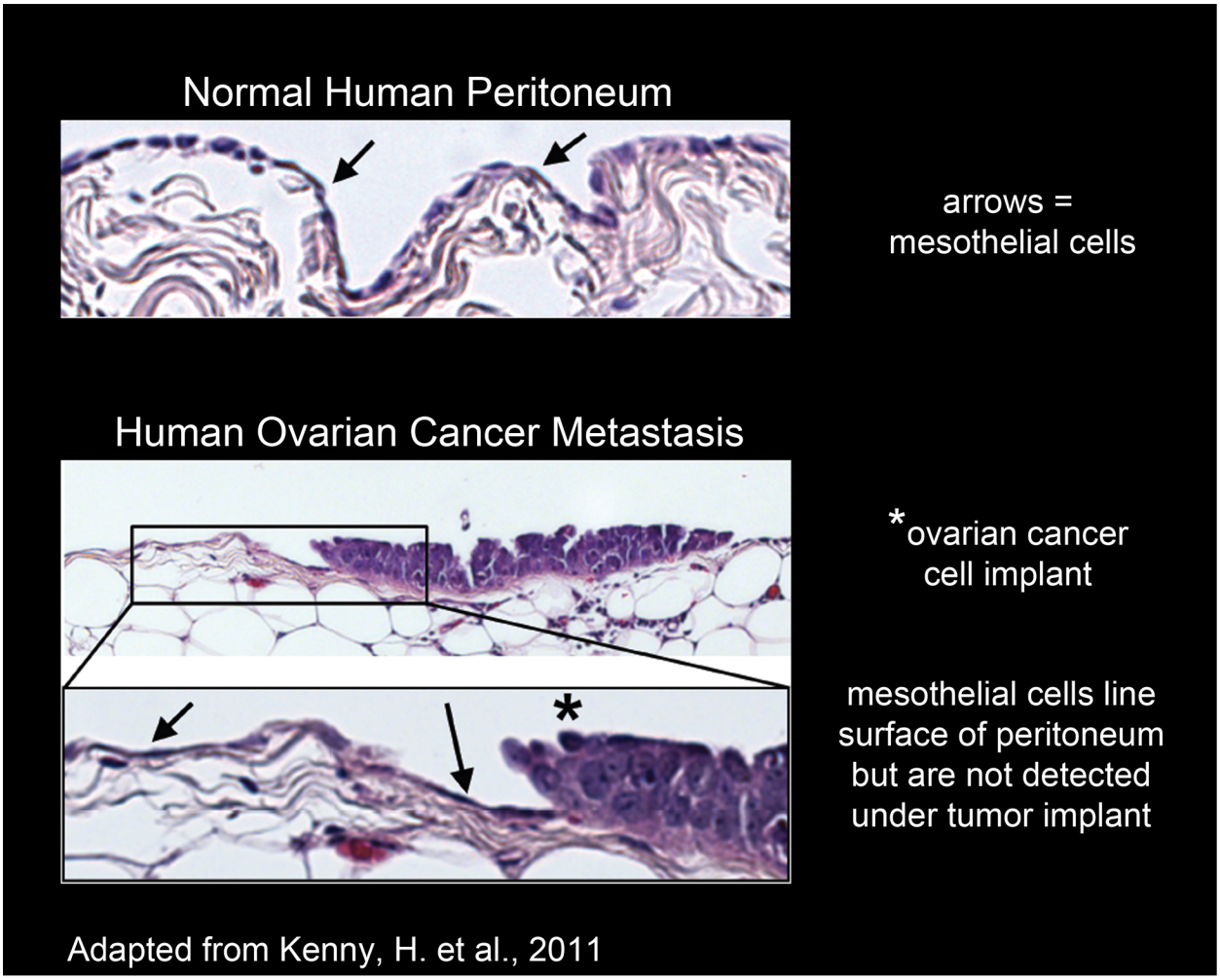

FIGURE 2.2: Mesothelial cells line the surface of human peritoneal tissue and are excluded from underneath ovarian cancer cell implants.

cellular and molecular mechanisms by which ovarian cancer cells breach this barrier, and exclude the mesothelium have, until recently, remained unknown.

Here we describe the methodology for an *in vitro* assay that models the interaction between ovarian cancer cell spheroids and mesothelial cells *in vivo* (Figure 2.3). Our protocol was adapted from previously described methods for analyzing ovarian tumor cell interactions with mesothelial monolayers(8-16), and was first described in a report showing that ovarian tumor cells utilize an integrin –dependent activation of myosin and traction force to promote the exclusion of the mesothelial cells from under a tumor spheroid(17). This model takes advantage of time-lapse fluorescence microscopy to monitor the two cell populations in real time, providing spatial and temporal information on the interaction. The ovarian cancer cells express red fluorescent protein (RFP) while the mesothelial cells express green fluorescent protein (GFP). RFP-expressing ovarian cancer cell spheroids attach to the GFP-expressing mesothelial monolayer. The spheroids spread, invade, and force the mesothelial cells aside creating a hole in the monolayer. This hole is visualized as the negative space (black) in the GFP image. The area of the hole can then be measured to quantitatively analyze differences in clearance activity between control and experimental populations of ovarian cancer and/ or mesothelial cells. This assay requires only a small number of ovarian cancer cells (100 cells per spheroid X 20-30 spheroids per condition), so it is feasible to perform this assay using precious primary tumor cell samples. Furthermore, this assay can be easily adapted for high throughput screening.

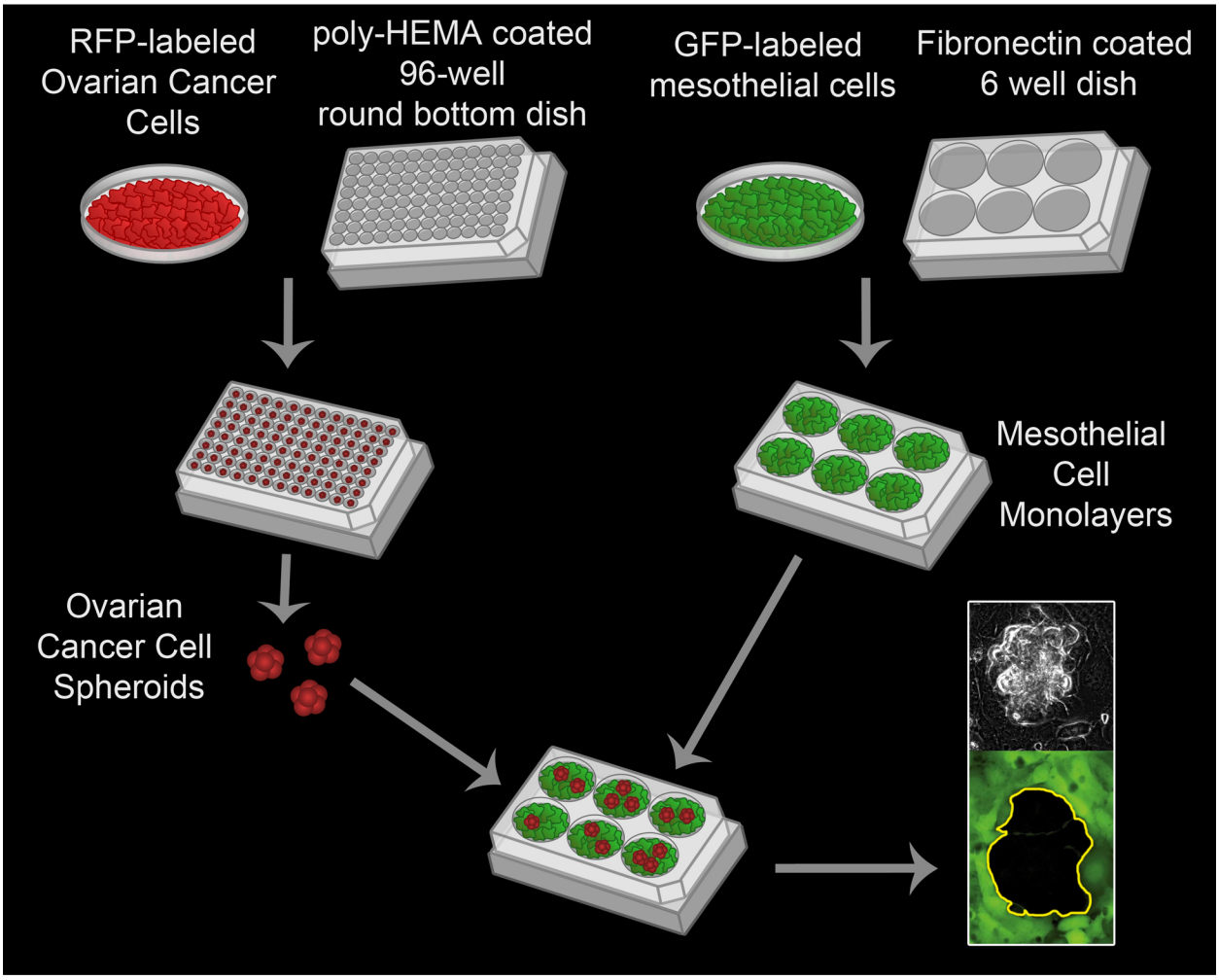

FIGURE 2.3: Mesothelial Clearance Assay. Ovarian cancer spheroids are formed by incubating 100 RFP-expressing ovarian cancer cells per well in a poly-HEMA coated 96 well round bottom culture dish at 37°C for 16 hours. Poly-HEMA prevents the cells from attaching to the culture dish, allowing the cells to remain in suspension and adhere to one another to form a single cluster per well. Mesothelial cell monolayers are prepared by plating 3x105 mesothelial cells per well in a fibronectin coated 6 well MatTek dish and incubating the plate at 37°C for 16 hours. The spheroids are then transferred to the MatTek dish with the mesothelial monolayer and the two cell populations are imaged every 10 minutes for 8 hours using a Nikon Ti-E Inverted Motorized Widefield Fluorescence time-lapse microscope and Elements software.

Protocol Text:

1. Ovarian Cancer Cell Spheroid Formation

1.1 RFP-expressing ovarian cancer cells are cultured in 10% Base Medium (a custom cell culture medium containing a 50:50 mixture of 199 and MCDB105, 10% inactivated fetal bovine serum and 1% pen-strep). To express RFP in unlabeled ovarian cancer cells, transfect the cells with a plasmid containing RFP and select for cells expressing RFP. Alternatively, viral vectors can be used to transiently express fluorescent proteins, or cells can be pre-incubate with a red fluorescent cell tracker dye (Invitrogen).

1.2 Prior to forming of ovarian cancer spheroids, it is necessary to prepare low-adhesion 96 well round bottom culture dishes. To produce the low-adhesion culture plates, 30ul poly-HEMA (6mg polyhydroxyethylmethacrylate in 95% EtOH) solution is added to each well of a 96 well Corning cell culture dish. The 96 well plates are incubated in a 37°C non-humidified incubator to evaporate the ethanol, leaving a film of poly-HEMA on each well. This poly-HEMA film prevents cells from attaching to the bottom of the well, forcing the cells to grow in suspension(18). [Alternatively, Ultra-Low Attachment culture plates (Corning) can be used instead of poly-HEMA coated dishes.]

1.3 After the low-adhesion culture plates are prepared, trypsinize a plate of ovarian cancer cells, pellet the cells in a tabletop centrifuge (Heraeus) at 900 RCF for 3 minutes, aspirate the supernatant and re-suspend in 10% Base Medium.

1.4 Count the cells using a hemocytometer.

1.5 Adjust the concentration of cells such that there are 100 cells per 50ul of 10% Base Medium.

1.6 Add 50ul of the uniformly suspended diluted cell suspension to each well of the 96 well poly-HEMA coated culture dish.

1.7 Incubate the 96 well plate in a 37°C cell culture incubator for 16 hours (this amount of time should be increased or decreased depending on the amount of time it takes for a particular cell line to form multicellular spheroids or desired experimental conditions) to allow the ovarian cancer cells to cluster together, forming a single multicellular spheroid in each well. Some tumor cells can undergo apoptosis during this period, so it is important to choose a time prior to induction of apoptosis.

2. Mesothelial Cell Monolayer Formation

2.1 In a cell culture hood, pre-coat the wells of a 6 well glass-bottom MatTek dish with fibronectin by adding 2mL of a 5ug fibronectin/ mL PBS solution to each well of the dish and incubating at room temperature for 30 minutes. The optical quality of the glass-bottoms in MatTek dishes allow for high-resolution microscopic imaging.

2.2 GFP-expressing mesothelial cells are cultured in 10% Base Medium. Trypsinize a plate of mesothelial cells, spin down in a tabletop centrifuge (Heraeus) at 900RPM for 3 minutes, aspirate the supernatant, and re-suspend in 10% Base Medium. The mesothelial cells used here were already expressing GFP when they were obtained, but unlabeled mesothelial cells can be produced by transfecting with a plasmid containing GFP cDNA, or preincubating the cells in a green fluorescent cell tracker dye (Invitrogen).

2.3 After the 30-minute fibronectin incubation (in step 2.1), wash the wells of the MatTek dish with 2mL PBS.

2.4 Aspirate the PBS and plate $3x10^5$ mesothelial cell per well in each well of the 6 well MatTek dish. Incubate the MatTek dish in a 37°C cell culture incubator overnight to allow the mesothelial cells to attach to the dish and form a monolayer.

3. Mesothelial Cell Clearance Assay

3.1 Use a pipet to collect the ovarian cancer spheroids from the 96 well poly-HEMA coated plate.

3.2 Aspirate the medium from one well of the 6 well MatTek dish containing a mesothelial cell monolayer. Wash once with 2mL PBS. Add all of the spheroids from the 96 well plate to one well of the MatTek dish (~3x the number of spheroids that are going to be imaged to account for spheroids landing on the part of the dish that cannot be imaged).

3.3 Place the MatTek dish on the stage of an inverted widefield fluorescence microscope capable of performing time-lapse imaging for the duration of at least 8 hours. Use a motorized stage to image multiple positions in the dish, with multiple spheroid intercalation events, in a single experiment. We use a Nikon Ti-E Inverted Motorized Widefield Fluorescence time-lapse microscope with integrated Perfect Focus System and low [20×-0.75 numerical aperture (NA)] magnification/NA differential interference contrast (DIC) optics, a Nikon halogen transilluminator with 0.52 NA long working distance (LWD) condenser, Nikon fast (<100-millisecond switching time) excitation and emission filters (GFP Ex 480/40, Em 525/50, RFP-mCherry Ex 575/50

Em 640/50), Sutter fast transmitted and epifluorescence light path Smart Shutters, a Nikon linear-encoded motorized stage, a Hamamatsu ORCA-AG cooled charge-coupled device (CCD) camera, a custom-built microscope incubation chamber with temperature and CO_2 control, Nikon NIS-Elements AR software version 3, and a TMC vibration isolation table.

3.4 The ovarian cancer cell spheroids will settle to the bottom of dish and attach to the mesothelial cell monolayer. Collect GFP, RFP and phase images of 20+ spheroid/monolayer interactions, every 10 minutes, for 8 hours.

3.5 The RFP-expressing ovarian cancer cell spheroids will invade into the GFP-expressing mesothelial cell monolayer creating a hole in the monolayer. After 8 hours, measure the sizes of the holes by tracing the black holes in the GFP images using Elements software (or another suitable software such as image J) . Normalize the hole size to the initial spheroid size by dividing the hole size at 8 hours by the size of the spheroid in the corresponding RFP image at time zero. In this example, the hole size was only measured once, but it can be measured multiple times throughout the eight hour experiment to better understand the dynamics of intercalation.

Representative Results:

In this example, we compared the mesothelial clearance ability of OVCA433 ovarian cancer cell spheroids that have attenuated expression of talin-1 and -2 to control OVCA433 spheroids. OVCA433 spheroids from each group were added to a MatTek dish containing ZT mesothelial cell monolayers. Six spheroids from each group were imaged every 10 minutes for eight hours (Figure 2.4). The holes produced in the monolayer by the spreading spheroids were measured and six positions from each group were averaged. Figure 2.4 shows that the average clearance area created by talin 1 and 2 knockdown spheroids was significantly smaller than the average area created by control spheroids, suggesting that talin is required for mesothelial clearance by OVCA433 ovarian cancer spheroids.

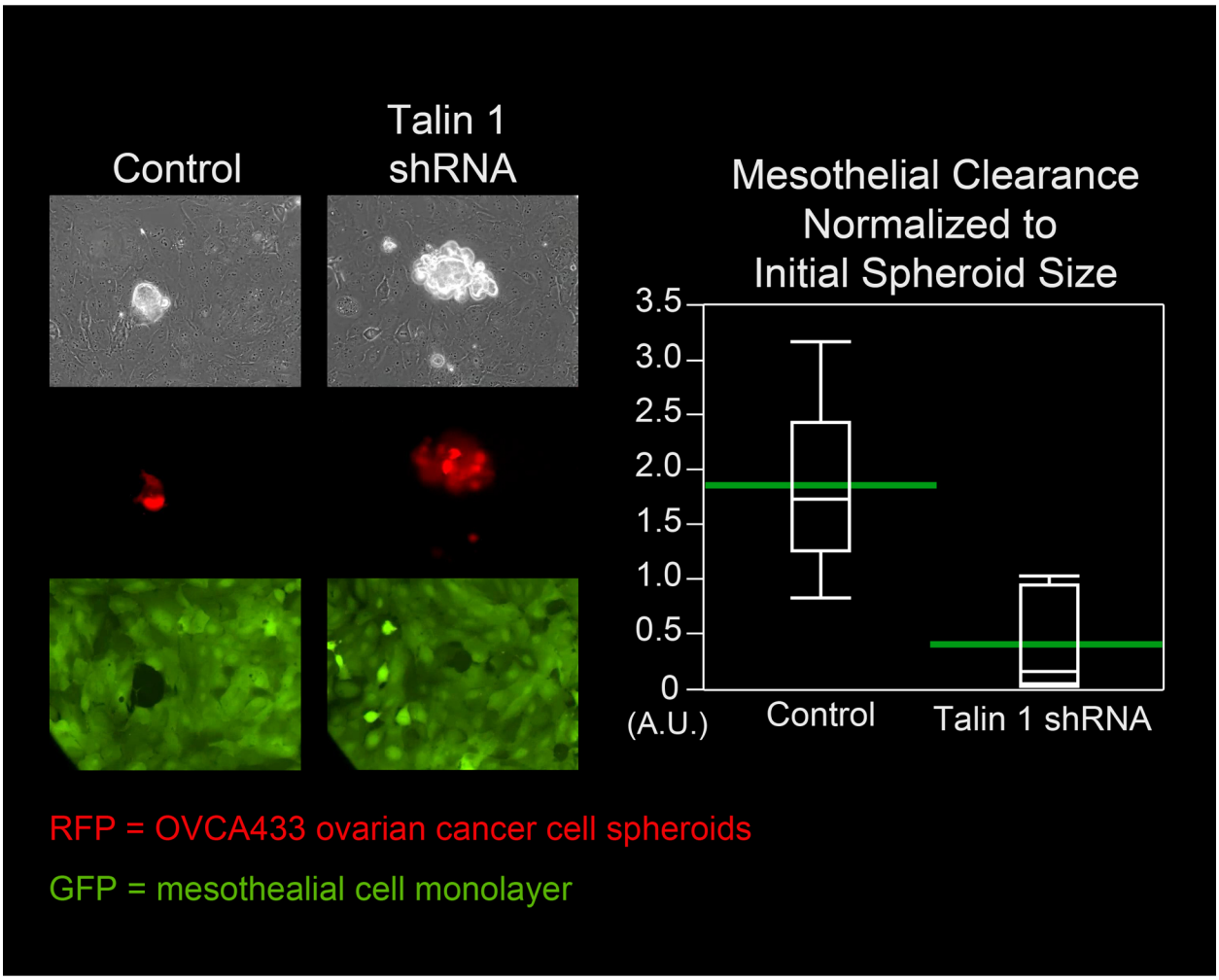

FIGURE 2.4: Attenuation of talin 1/2 expression in OVCA433 spheroids decreases mesothelial clearance ability. OVCA433 spheroids (red) with and without attenuated expression of talin 1 and 2 were allowed to attach to and invade into a ZT mesothelial monolayer (green). The two cell populations were imaged every 10 minutes for 8 hours using a Nikon Ti-E Inverted Motorized Widefield Fluorescence time-lapse microscope and elements software. The graph shows that talin 1 and 2 attenuation significantly decreases mesothelial cell clearance. (Quantile plot with green bars at the means)

Discussion:

The “Mesothelial Clearance Assay” presented here uses time-lapse microscopy to monitor the interactions of ovarian cancer multicellular spheroids and mesothelial cell monolayers, in great spatial and temporal detail. Previously, several groups(8-14) had used endpoint assays to show that ovarian cancer cells attach to and invade into mesothelial cell monolayers. This assay is unique in that it uses fluorescently labeled cells to distinguish tumor cells from mesothelial cells, so that the dynamics of these two cell populations can be monitored throughout the assay. The process of intercalation can be visualized in real time and the rate of mesothelial clearance can be quantitatively measured over time. The use of timelapse microscopy allows one to closely monitor the dynamics of the interaction between the two cell populations under different experimental conditions. Additionally, a small percentage of either the mesothelial cells or the ovarian cancer cells can be labeled with a third fluorescent marker to monitor the dynamics of individual cells within the population. By tracking individual cells over time, the directionality and rate of migration can be calculated. To perform higher resolution analyses of mesothelial clearance, total internal reflection fluorescence (TIRF) microscopy can be used. If focal adhesions are labeled in the mesothelial cells, the dissociation of mesothelial adhesions by protrusive extensions of the tumor cells can be monitored, as described in our previous publication(17).

This assay can be used to compare the invasion ability of ovarian cancer cell spheroids that have been genetically or pharmacologically modified to elucidate the molecular mechanisms by which ovarian cancer cell spheroids clear the mesothelial monolayer or to identify small molecule inhibitors of the process. Furthermore, the

assay requires a very small number of ovarian cancer cells, so primary tumor cells from fluid exudates can be used (see limitations below) if labeled by preincubating the cells with cytotracker dyes (Invitrogen). The assay is also amenable to high throughput analysis. To perform high throughput genetic or pharmacological studies, the ovarian cancer cells can be transfected with different siRNA vectors or treated with different pharmacological inhibitors in each well of the 96-well plate. Mesothelial cell monolayers can be plated in 96 well glass-bottom culture dishes, and the spheroids can be transferred 1:1 from the poly-HEMA coated plates to the monolayer-containing plates. All of these steps can be optimized for use with screening robots so that hundreds of siRNAs or inhibitors can screened at one time.

One of the strengths of this assay is to be able to model the force-dependent intercalation of ovarian cancer cells into the mesothelial monolayer. Our lab used traction force microscopy (TFM) to determine whether mechanical force regulates mesothelial clearance(17). We found that overexpression of α5 integrin increased the contractility of cells plated on a fibronectin-coated substrate, while RNAi-mediated knockdown of talin, or myosin II decreased cell contractility(17). Since downregulation of α5 integrin, talin, or myosin II in the ovarian cancer cell spheroids also decreased mesothelial clearance, our TFM measurements support the idea that mesothelial clearance in an event dependent on cellular contractile forces, in which cells with higher contractile forces caused greater mesothelial clearance. Therefore, the mesothelial clearance assay can be used to further understand intercalation events, associated with ovarian spheroid metastasis, that are dependent on mechanical forces.

This assay has a few limitations to consider. First, in order to form the multicellular spheroids, the cells must be cultured in suspension for at least 6 hours. If the cells are unable to survive without matrix contact their clearance ability will be compromised. Second, it is advantageous to use ovarian cancer cells that form uniform, compact multicellular spheroids. If the ovarian cancer cells only form loose clusters, they may break apart in the transfer from the polyHEMA-coated plate to the dish containing the mesothelial monolayer, creating spheroids of different shapes and sizes that will add variability to the data. Third, if the cells used are heterogeneous, this will add additional variability to the sizes of holes created in the monolayer. It is important to use multiple replicate wells (10-20/sample) due to the variability in extent of intercalation after eight hours. In the assays described here, well-established ovarian cancer (OVCA433) and mesothelial (ZT) cell lines were used. To make this assay more clinically relevant, primary ovarian cancer cells, from the ascites fluid of patients, can be used. It would be interesting to determine if *in vitro* mesothelial cell clearance ability correlates with clinical outcome. The limitations above are particularly important to consider when using primary samples, as the number of primary cells available is a limiting factor. Additionally, it is important to check the integrity of the mesothelial monolayer before performing this assay. The mesothelial monolayer can be fixed and stained for cell-cell junction proteins to ensure that mesothelial cell junctions are intact.

Finally, the mesothelial clearance assay can be easily modified to answer specific experimental questions. Here, we used fibronectin as the ECM component that allows the ovarian and mesothelial cells to adhere to the glass-bottom culture dishes, however, other ECM components can be used including collagen and laminin.

Furthermore, other cell types that are found under the basement membrane, including fibroblasts, can be added to this experimental system, to assess the role of these cell types in mesothelial clearance(9, 19, 20). Lastly, interactions of other types of tumor cells (e.g. pancreatic, breast, etc) with mesothelial cells can also be modeled using this assay. And it is feasible to study interactions between cancer cells and an endothelial monolayer, using this assay, to mimic intravasation or extravasation (Similar assays have been described in: (15, 16, 21-27))

Acknowledgements:

We would like to thank the Nikon Imaging Center at Harvard Medical School, specifically Jennifer Waters, Lara Petrak and Wendy Salmon, for training and the use of their timelapse microscopes. We would also like to thank Rosa Ng and Achim Besser for valuable discussions. This work was supported by NIH Grant 5695837 (to M. Iwanicki) and GM064346 to JSB; by a grant from Dr. Miriam and Sheldon G. Adelson Medical Research Foundation (to JSB).

Table 2.1: Specific Reagents and Equipment

Reagent	Company	Catalog Number	Comments
OVCA433 Ovarian Cancer Cells			Gift from Dr. Dennis Slamon
ZT Mesothelial Cells			Gift from Dr. Tan Ince
Medium 199	Gibco	19950	
MCDB105	Cell Applications Inc.	117-500	
FBS-heat inactivated	Gibco	10082	
Pen-Strep	Gibco	15070	
96 well plates	Corning Costar	3799	
Polyhydroxyethylmethacrylate (poly-HEMA)	Sigma Aldrich	192066-25G	For poly-HEMA solution dissolve 6mg poly-HEMA powder in 1ml of 95% EtOH
EtOH	Pharmco-aaper	111ACS200	Dilute to 95% in dH20
Cell culture hood	Nuaire	NU-425-300	
Tissue culture incubator	Thermo Scientific	3110	
incubator for poly-HEMA plates	Labline Instruments	Imperial III 305	
Tabletop centrifuge	Heraeus	75003429/01	
6 well glass-bottom dish	MatTek corp.	P06G-1.5-20-F	
Fibronectin	Sigma	F1141-1MG	
PBS	Cellgro	21-040-CV	

Table 2.1, cont'd.

Timelapse Microscope:			
Microscope	Nikon		Ti-E Inverted Motorized Fluorescence time-lapse microscope with integrated Perfect Focus System
Lens	Nikon		20X-0.75 numerical apeture
Halogen transilluminator	Nikon		0.52 NA long working distance condenser
Excitation and emission filters	Chroma single pass filters in Nikon housing		GFP Ex 480/40, Em 525/50 RFP-mCherry Ex 575/50 Em 640/50
Transmitted and Epifluoresce light path	Sutter		Smart Shutters
Linear-encoded motorized stage	Nikon		
Cooled charged-coupled device camera	Hamamatsu	ORCA-AG	
Microscope incubation chamber with temperature and CO2 control	custom-built		
Vibration isolation table	TMC		
NIS-Elements software	Nikon		Version 3

References:

1.Jemal A, Siegel R, Ward E, Hao Y, Xu J, Thun MJ. Cancer statistics, 2009. CA Cancer J Clin. 2009;59:225-49.

2.Ries LG MD, Krapcho M, Stinchcomb DG, Howlader N, Horner MJ, Mariotto A, Miller BA, Feuer EJ, Altekruse SF, Lewis DR, Clegg L, Eisner MP, Reichman M, Edwards BK. SEER Cancer Statistics Review. http://seercancergov/csr/1975_2005: National Cancer Institute. Bethesda, MD; 2007.

3.Burleson KM, Casey RC, Skubitz KM, Pambuccian SE, Oegema TR, Jr., Skubitz AP. Ovarian carcinoma ascites spheroids adhere to extracellular matrix components and mesothelial cell monolayers. Gynecol Oncol. 2004;93:170-81.

4.Birbeck MS, Wheatley DN. An Electron Microscopic Study of the Invasion of Ascites Tumor Cells into the Abdominal Wall. Cancer Res. 1965;25:490-7.

5.Witz CA, Monotoya-Rodriguez IA, Schenken RS. Whole explants of peritoneum and endometrium: a novel model of the early endometriosis lesion. Fertil Steril. 1999;71:56-60.

6.Zhang XY, Pettengell R, Nasiri N, Kalia V, Dalgleish AG, Barton DP. Characteristics and growth patterns of human peritoneal mesothelial cells: comparison between advanced epithelial ovarian cancer and non-ovarian cancer sources. J Soc Gynecol Investig. 1999;6:333-40.

7.Kenny HA, Nieman KM, Mitra AK, Lengyel E. The First Line of Intra-abdominal Metastatic Attack: Breaching the Mesothelial Cell Layer. Cancer Discovery. 2011;1:100-2.

8.Niedbala MJ, Crickard K, Bernacki RJ. Interactions of human ovarian tumor cells with human mesothelial cells grown on extracellular matrix. An in vitro model system for studying tumor cell adhesion and invasion. Exp Cell Res. 1985;160:499-513.

9.Kenny HA, Krausz T, Yamada SD, Lengyel E. Use of a novel 3D culture model to elucidate the role of mesothelial cells, fibroblasts and extra-cellular matrices on adhesion and invasion of ovarian cancer cells to the omentum. Int J Cancer. 2007;121:1463-72.

10.Ksiazek K, Mikula-Pietrasik J, Korybalska K, Dworacki G, Jorres A, Witowski J. Senescent peritoneal mesothelial cells promote ovarian cancer cell adhesion: the role of oxidative stress-induced fibronectin. Am J Pathol. 2009;174:1230-40.

11.Burleson KM, Boente MP, Pambuccian SE, Skubitz AP. Disaggregation and invasion of ovarian carcinoma ascites spheroids. J Transl Med. 2006;4:6.

12.Heyman L, Kellouche S, Fernandes J, Dutoit S, Poulain L, Carreiras F. Vitronectin and its receptors partly mediate adhesion of ovarian cancer cells to peritoneal mesothelium in vitro. Tumour Biol. 2008;29:231-44.

13.Heyman L, Leroy-Dudal J, Fernandes J, Seyer D, Dutoit S, Carreiras F. Mesothelial vitronectin stimulates migration of ovarian cancer cells. Cell Biol Int. 2010;34:493-502.

14.Lessan K, Aguiar DJ, Oegema T, Siebenson L, Skubitz AP. CD44 and beta1 integrin mediate ovarian carcinoma cell adhesion to peritoneal mesothelial cells. Am J Pathol. 1999;154:1525-37.

15.Leroy-Dudal J, Heyman L, Gauduchon P, Carreiras F. Adhesion of human ovarian adenocarcinoma IGROV1 cells to endothelial cells is partly mediated by the alphav integrins-vitronectin adhesive system and induces an alteration of endothelial integrity. Cell Biol Int. 2005;29:482-8.

16.Leroy-Dudal J, Demeilliers C, Gallet O, Pauthe E, Dutoit S, Agniel R, et al. Transmigration of human ovarian adenocarcinoma cells through endothelial extracellular matrix involves alphav integrins and the participation of MMP2. Int J Cancer. 2005;114:531-43.

17.Iwanicki M, Davidowitz RA, Ng MR, Besser A, Muranen T, Merritt M, et al. Ovarian cancer spheroids use myosin-generated force to clear the mesothelium. Cancer Discovery. 2011;1:144-57.

18.Folkman J, Moscona A. Role of cell shape in growth control. Nature. 1978;273:345-9.

19.Gregoire L, Munkarah A, Rabah R, Morris RT, Lancaster WD. Organotypic culture of human ovarian surface epithelial cells: a potential model for ovarian carcinogenesis. In Vitro Cell Dev Biol Anim. 1998;34:636-9.

20.Roberts PC, Mottillo EP, Baxa AC, Heng HH, Doyon-Reale N, Gregoire L, et al. Sequential molecular and cellular events during neoplastic progression: a mouse syngeneic ovarian cancer model. Neoplasia. 2005;7:944-56.

21.Okada T, Okuno H, Mitsui Y. A novel in vitro assay system for transendothelial tumor cell invasion: significance of E-selectin and alpha 3 integrin in the transendothelial invasion by HT1080 fibrosarcoma cells. Clin Exp Metastasis. 1994;12:305-14.

22.Zervantonakis IK, Kothapalli CR, Chung S, Sudo R, Kamm RD. Microfluidic devices for studying heterotypic cell-cell interactions and tissue specimen cultures under controlled microenvironments. Biomicrofluidics. 2011;5:13406.

23.Brandt B, Heyder C, Gloria-Maercker E, Hatzmann W, Rotger A, Kemming D, et al. 3D-extravasation model -- selection of highly motile and metastatic cancer cells. Semin Cancer Biol. 2005;15:387-95.

24.Condeelis J, Segall JE. Intravital imaging of cell movement in tumours. Nat Rev Cancer. 2003;3:921-30.

25.Dai J, Ting-Beall HP, Hochmuth RM, Sheetz MP, Titus MA. Myosin I contributes to the generation of resting cortical tension. Biophys J. 1999;77:1168-76.

26.Laferriere J, Houle F, Taher MM, Valerie K, Huot J. Transendothelial migration of colon carcinoma cells requires expression of E-selectin by endothelial cells and activation of stress-activated protein kinase-2 (SAPK2/p38) in the tumor cells. J Biol Chem. 2001;276:33762-72.

27.Dong C, Slattery MJ, Rank BM, You J. In vitro characterization and micromechanics of tumor cell chemotactic protrusion, locomotion, and extravasation. Ann Biomed Eng. 2002;30:344-55.

Chapter 3

Ovarian Cancer Spheroids Use Myosin-generated Force to Clear the Mesothelium

Statement of Contribution:

This chapter embodies a manuscript published in *Cancer Discovery* by M.P. Iwanicki, R.A. Davidowitz, M.R. Ng, A. Besser, T. Muranen, M. Merritt, G. Danuser, T. Ince, and J.S. Brugge*. I designed, performed and analyzed the experiments examining the role of integrins in mesothelial clearance as well as the experiments examining the behavior of individual mesothelial cells within a mesothelial monolayer during invasion by ovarian cancer spheroids. I also contributed to the writing of the manuscript. MPI designed, performed and analyzed the other experiments and wrote the manuscript. MRN, AB and GD assisted with the traction force microscopy and analysis. TM isolated the primary cells and MM and TI prepared immortalized GFP-expressing mesothelial cells. JSB provided guidance and participated in the writing of the manuscript.

*Corresponding authors

Abstract:

Dissemination of ovarian tumors involves the implantation of cancer spheroids into the mesothelial monolayer on the walls of peritoneal and pleural cavity organs. Biopsies of tumors attached to peritoneal organs show that mesothelial cells are not present under tumor masses. We have developed a live, image-based *in vitro* model in which interactions between tumor spheroids and mesothelial cells can be monitored in real time to provide spatial and temporal understanding of mesothelial clearance. Here we provide evidence that ovarian cancer spheroids utilize integrin – and talin - dependent activation of myosin and traction force to promote mesothelial cells displacement from underneath a tumor cell spheroid. These results suggest that ovarian tumor cell clusters gain access to the sub-mesothelial environment by exerting force on the mesothelial cells lining target organs, driving migration and clearance of the mesothelial cells.

Significance:

This study employs state of the art microscopy to reveal that ovarian cancer cell clusters physically displace mesothelial cells and gain access to the sub-mesothelial environment. Blockade of force- conducting molecules including α5 integrin, talin I and non-muscle myosin II in cancer cells abrogated mesothelial displacement from underneath attached cancer spheroids.

Introduction:

During the progression of ovarian cancer, tumor cells detach from the primary tumor site and form cell clusters, or spheroids, that can either remain unattached in the peritoneal cavity or implant onto peritoneal organs (1). Formation of implants depends on the ability of tumor cells to invade into the mesothelial layer that covers peritoneal and pleural organs (2). Electron micrographs of mesothelial tissue sections with and without peritoneal metastases (3, 4) revealed that normal peritoneal mesothelial cells are flat and cover the entire surface of the peritoneum, such that cell-cell boundaries are difficult to discern, whereas, the mesothelial cells with peritoneal metastases are more rounded and separated from each other, revealing the sub-mesothelial surface. These studies suggested that mesothelial cells retracted in the presence of the tumor. Furthermore, the cancer cells did not adhere to the mesothelial cells, but rather to connective tissue under the mesothelial cells. In addition, electron micrographs of excised human peritoneum-associated tumors revealed that mesothelial cells are not present directly under the tumor mass, suggesting mesothelial clearance from the area beneath the tumor mass (4). Early, in vitro, experiments also provided evidence that mesothelial cells retract after coming in contact with tumor cells (5, 6). In these studies ovarian cancer cell clusters disrupted mesothelial cell-cell junctions and penetrated matrix under mesothelial cells, suggesting that the integrity of the mesothelial cell monolayer is altered by the attached tumor cells that bind with high affinity to sub-mesothelial matrix (6, 7). The cellular and molecular mechanisms of mesothelial clearance, however, are unknown.

We have used a live, image-based *in vitro* model in which interactions between tumor spheroids and mesothelial cells can be monitored in real time to provide spatial and temporal understanding of the process of mesothelial clearance. Using this model, we demonstrate that tumor spheroid attachment and spreading on a mesothelial monolayer promotes clearance of the mesothelial cells from the area underneath the spheroid. We provide evidence that force generation on the mesothelial cell-associated extra-cellular matrix provokes mesothelial cells to migrate and clear from underneath the tumor spheroid. This mechanism might be relevant to processes involved in implantation of ovarian tumor aggregates into the sub-mesothelial environment of the organs of the peritoneal and pleural cavities.

Results:

Interaction of ovarian cancer spheroids with mesothelial monolayers promotes mesothelial cell clearance.

To investigate the interaction between ovarian cancer spheroids (OVCA433 ovarian cancer cell line) and GFP-expressing mesothelial cells (normal immortalized lung mesothelium), we used time-lapse microscopy to follow the dynamics of a mesothelial monolayer after cancer spheroid attachment, in real time. As the spheroid spread on the mesothelial monolayer, mesothelial cells were displaced from the area directly underneath the spreading spheroid. This phenomenon will be referred to as mesothelial clearance. (Figure 3.1A and Supplementary Movie 3.1). The clearance area increased with time as the spheroid became more incorporated into the mesothelial monolayer (Figure 3.1B). We also observed that primary tumor clusters isolated from the peritoneal fluid of ovarian cancer patients are able to attach to and clear the mesothelium (Figure 3.1C and Supplementary Movie 3.2). Overall, these data indicate that, following attachment to a mesothelial monolayer, clusters of ovarian cancer cells are able to induce clearance of the mesothelial cells directly underneath the tumor spheroid.

In vivo, mesothelial cells are separated from the underlying soft connective tissue by a layer of matrix (8). To examine whether mesothelial clearance can occur on more physiologically relevant substrates (of similar stiffness to connective tissue), mesothelial monolayers were plated on fibronectin-coated polyacrylamide gels with elastic moduli of 0.3 kPa or 10kPa. OVCA433 tumor spheroids were able to induce mesothelial clearance on both substrates (Supplementary Figure 3.1A), indicating that mesothelial

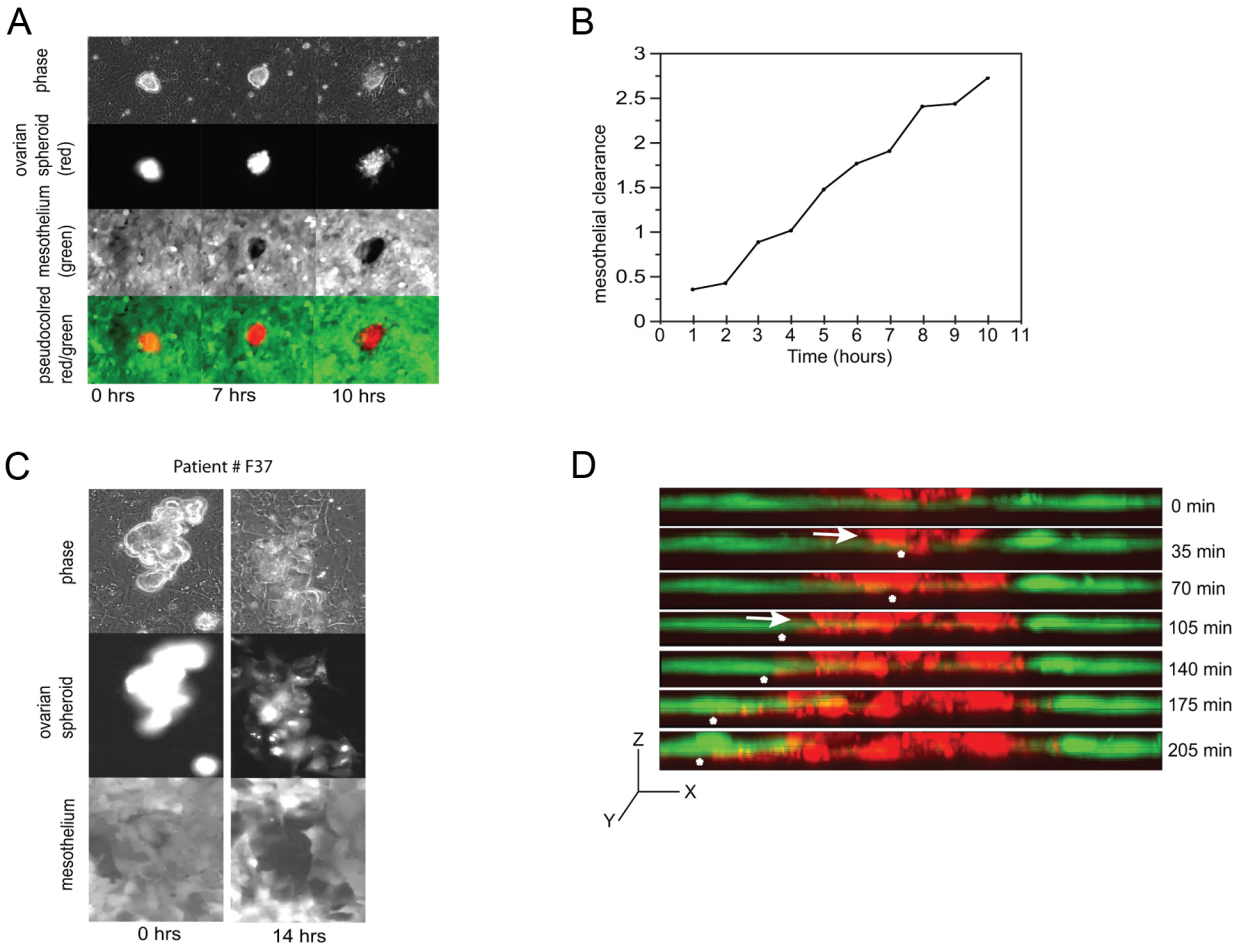

FIGURE 3.1: Interaction of cancer spheroids with mesothelium prompts mesothelial cell clearance. A. Ovarian cancer spheroids (OVCA433) labeled with CMTCX cell tracker dye (red) were pipetted on top of a confluent monolayer of GFP-labeled primary TERT immortalized human lung mesothelial cells (green) and incubated for 60 min. The dynamics of these two cell populations were followed in parallel for 10 hours. Images show a time course of mesothelial clearance at 0, 7 and 10 hours. Scale bar = 100μm **B.** Quantification of mesothelial clearance from experiment shown in (A). **C.** Representative images from a mesothelial clearance assay utilizing a primary tumor cluster isolated from the ascites fluid of an ovarian cancer patient. The sample was labeled and assayed as in (A) Scale bar = 50μm. **D.** Time lapse images of multiple Z sections (side view) of OVCA433 CMTCX-labeled spheroids inducing clearance of GFP- labeled lung mesothelial cells.

clearance can indeed occur on softer, more physiologically relevant substrates, and that the mesothelial clearance observed is not an artifact of cells grown on stiff glass surfaces.

To study the spheroid-mesothelial interaction more closely, we imaged a spheroid during the process of intercalation into a mesothelial monolayer in multiple focal planes and reconstructed the x-z planes to observe ovarian-mesothelial cell interactions at the ventral and dorsal cell surfaces. In the early stages of clearance (as shown in Figure 3.1D and Supplementary Movie 3.3), cancer cells spread on top of the monolayer (as indicated by the arrows) and then penetrated under the mesothelium (as indicated by *). From these observations, we hypothesized that cancer spheroids adhere to the mesothelial monolayer and induce localized de-adhesion of the mesothelial cells to ultimately prompt movement of the mesothelial cells away from the spheroid.

To examine whether localized de-adhesion of mesothelial cell matrix adhesions indeed occurs upon contact with a tumor spheroid, we used Total Internal Reflection Fluorescent Microscopy (TIRFM) to monitor mesothelial cell adhesions labeled with paxillin-GFP (this protein localizes to integrin-matrix engagement sites in multiple cell types). TIRFM allows for the visualization of florescent molecules present within 100nm above the surface of the cover slip, thereby minimizing background intensity from cytoplasm. We observed that cancer spheroids (labeled with RFP-actin) approached the mesothelial cell's adhesions (GFP) and promoted matrix adhesion disassembly (Figure 3.2A and Supplementary Movie 3.4). Furthermore, there was little adhesion assembly within the area of contact. In contrast, mesothelial cell matrix adhesions that were not in

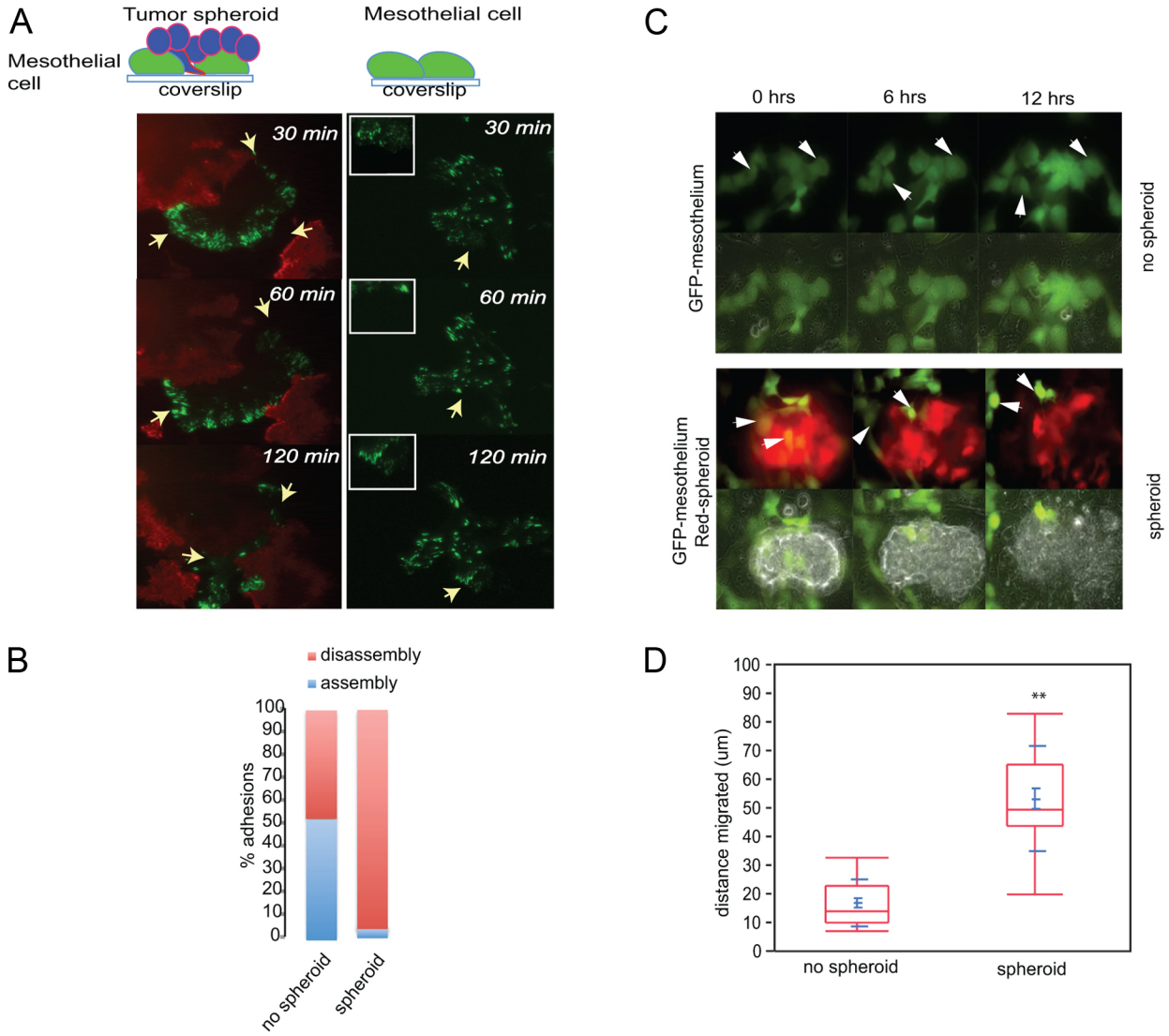

FIGURE 3.2: Tumor spheroid induces mesothelial cell migration. A. Temporal analysis of adhesion dynamics of Paxillin-GFP labeled LP9 human peritoneal mesothelial cells incubated with or without RFP-actin expressing OVCA433 cancer spheroids. Events of adhesion asembly and disassembly were scored. Scale bar = 5μm **B.** The bar graph shows the ratio of adhesion assembly and disassembly events within the same area. A total of 150 assembly and disassembly events were analyzed per condition. **C.** GFP-labeled lung mesothelial cells were mixed at 1:500 ratio with non -labeled lung mesothelial cells. Images show temporal behavior of single mesothelial cells in the prescence or absence of cancer spheroids. Scale bar =100μm **D.** The migration distance of single mesothelial cells was measured in the presence and absence of OVCA433 cancer spheroids. 50 GFP-labeled mesothelial cells were analyzed per condition.

contact with a tumor spheroid displayed spontaneous adhesion assembly and disassembly events (Figure 3.2B and Supplementary Movie 3.5). In a separate experiment, we labeled approximately one in 500 mesothelial cells with GFP to track the movement of individual mesothelial cells and observed that mesothelial cells that contacted a cancer spheroid migrated significantly longer distances than the mesothelial cells that did not contact a cancer spheroid (Figure 3.2C,D and Supplementary Movie 3.6). Overall, our results are consistent with the hypothesis that ovarian cancer spheroids can attach to a mesothelial monolayer, intercalate into the monolayer, and trigger mesothelial cell matrix adhesion disassembly and migration, ultimately leading to mesothelial clearance.

Coupling of myosin contractility to integrins in cancer spheroids is required for mesothelial clearance.

Ovarian cancer cell adhesion to a mesothelial monolayer has been shown to involve integrins (9). Cells exert force on the extracellular matrix by coupling myosin contractility to integrins (10) (11). Therefore, we examined whether tumor spheroid expression of myosin II is required to promote mesothelial clearance. OVCA433 cancer spheroids express non-muscle myosin isoforms IIA and IIB (Figure 3.3A). Both myosin II isoforms were downregulated in OVCA433 cells using small hairpin RNA (shRNA) and small interfering RNA (siRNA) targeting myosin IIA and II B heavy chain respectively (Figure 3.3A). Myosin heavy chain IIA and IIB attenuation did not prevent the ovarian cancer cells from spreading on surfaces coated with fibronectin and collagen I, indicating that myosin IIA and IIB are not required for spheroid attachment

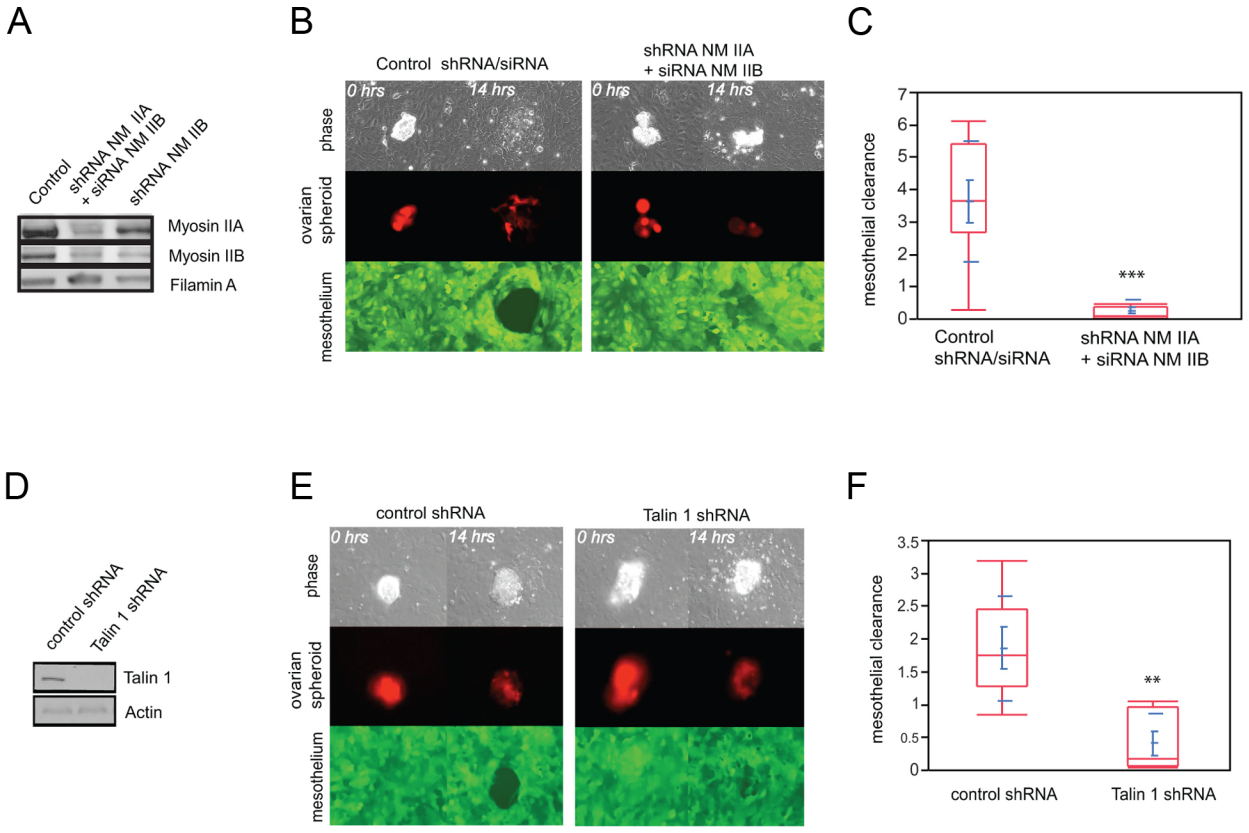

FIGURE 3.3: Coupling of myosin to integrins in cancer spheroids is required for mesothelial clearance. A. Western blot of non-muscle myosin heavy chain A and B (NM IIA or NM IIB) expression levels in control or NM IIA/NM IIB shRNA treated OVCA433 cells. **B.** Images show the temporal behavior of mesothelial cells contacting control or myosin shRNA expressing OVCA433 ovarian cancer cells. Scale bar = 50μm **C.** Quantification of mesothelial clearance from (B). 20 spheroid attachment sites were analyzed per condition. **D.** Western blot of talin I expression levels in control or talin 1 shRNA expressing OVCA433 cells. **E.** Images show temporal behavior of mesothelial cells contacting control or talin 1 shRNA expressing OVCA433 ovarian cancer cells. Scale bar = 50μm **F.** Quantification of mesothelial clearance from (E). 15 randomly chosen regions were analyzed per condition.

and spreading on fibronectin and collagen coated glass surfaces (Supplementary Figure 3.1B). However, OVCA433 spheroids with reduced levels of myosin IIA/IIB initiated but were unable to sustain mesothelial clearance (Figure 3.3B,C and Supplementary Movie 3.7). Attenuation of myosin II in OVCA433 cells by shRNA/siRNA did not prevent adhesion of spheroids to the mesothelial monolayer (Supplementary Figure 3.1C left panel) or induce apoptosis (Supplementary Figure 3.1C right panel), suggesting that myosin II expression in these cells is dispensable for spheroid attachment. We validated these results with two additional independent shRNA sequences targeting myosin IIA combined with the same siRNA pool for myosin IIB molecules (Supplementary Figure 3.1D). Taken together, these results suggest that OVCA433 cancer spheroids require myosin to induce mesothelial clearance.

The ability of cells to exert force on the outside environment depends on linkage of the actin and myosin network to integrins through recruitment of talin I to adhesion sites (10). We used small hairpin RNA (shRNA) to attenuate the expression of talin I in the spheroids (Figure 3.3D). Attenuation of talin I expression in OVCA433 spheroids did not induce apoptosis (Supplementary Figure 3.1C right panel) and had no effect on spreading on glass surfaces coated with fibronectin and collagen I (Supplementary Figure 3.2A). However, decreased expression of talin I but not talin II significantly reduced mesothelial clearance, even though spheroid adherence to the monolayer was unaffected (Figure 3.3C,Supplementary Movie 3.8 and Supplementary Figure 3.2B,C). We validated these results with two additional independent shRNA sequences targeting talin I molecule in OVCA433, DOV13 and SKOV3 ovarian cancer cell lines (Supplementary Figure 3.2D). These data indicate that talin I is required for tumor cell

interaction and suggest that the linkage of integrins to the actomyosin network in ovarian spheroids contributes to mesothelial clearance.

α5β1 integrin is required for spheroid – induced mesothelial clearance and contributes to the activation of myosin in cancer cells

Because expression of the α5 integrin fibronectin receptor has been shown to correlate with the development of myosin-driven contractility(12) and increased invasion of ovarian cancer cells (13, 14), we addressed whether α5β1 integrin-mediated activation of contractility contributes to ovarian spheroid–induced mesothelial clearance. First, we blocked the function of α5 integrin in cells that express high levels of α5 integrin (OVCA433 ovarian cancer cells) (Figure 3.4 A). Treatment of OVCA433 cell spheroids, which express high levels of α5 integrin, with α5 integrin blocking antibody significantly decreased spheroid-induced mesothelial clearance (Figure 3.4B, 3.4C, Supplementary Movie 3.9). Blocking α5 integrin on DOV13 and SKOV3 spheroids also significantly decreased mesothelial clearance (Supplementary Figure 3.3A). α5 blocking antibodies did not, however, prevent the OVCA433 spheroids from adhering to the mesothelial monolayer (Supplementary Movie 3.8, and Supplementary Figure 3.3B). Blocking other adhesion receptors expressed by OVCA433 spheroid (data not shown), including CD44 and integrins α_2 and α_v, did not have any significant effect on spheroid-induced mesothelial clearance (Supplementary Figure 3.3C).

In parallel experiments, we over-expressed α5 integrin in ovarian cancer cells that have a low level of α5 integrin expression (OVCAR5) and are unable to clear a mesothelial monolayer (Supplementary Figure 3.3D). Ectopic expression of α5 integrin

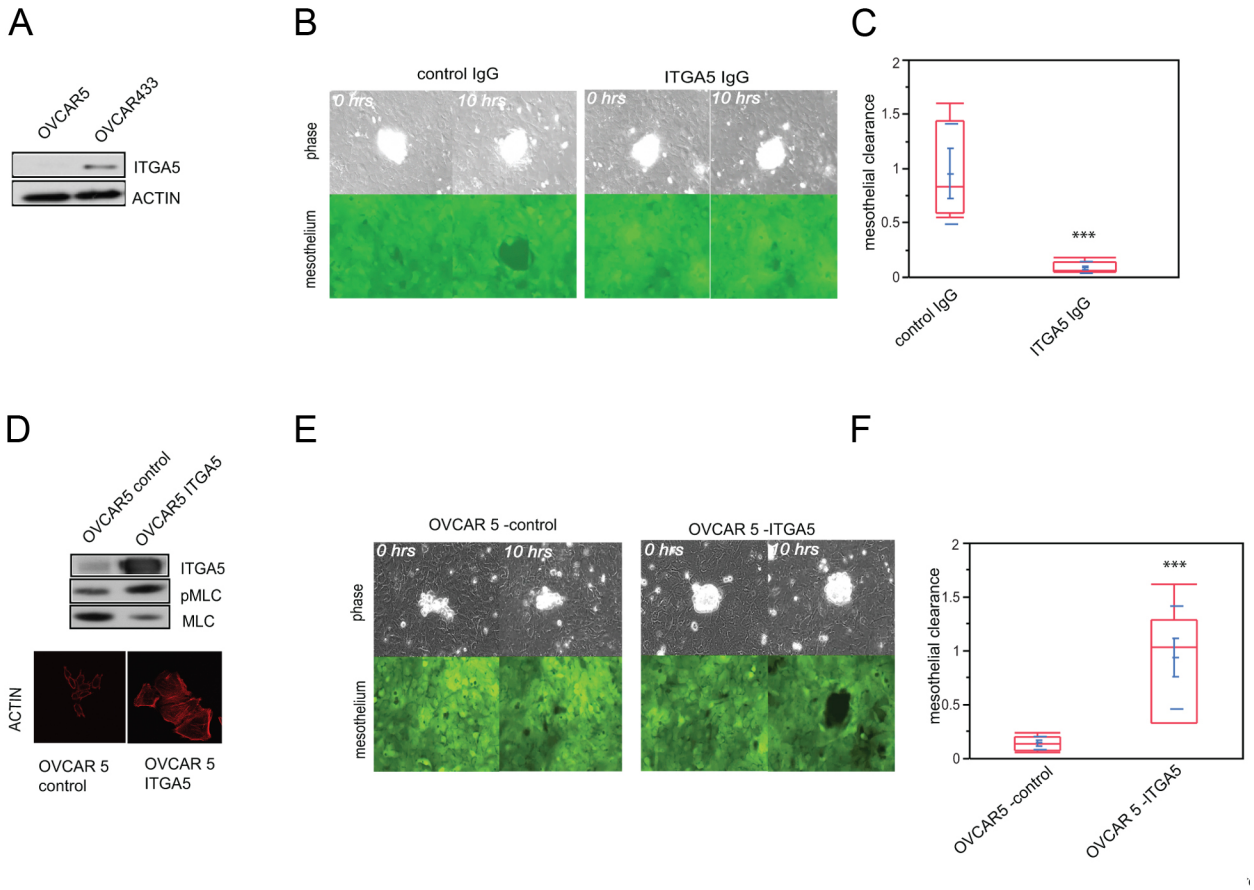

FIGURE 3.4: α5β1 integrin contributes to the activation of myosin in OVAR5 ovarian cancer cells and is required for OVCAR5 spheroid-induced mesothelial clearance. A. Western blot analysis of α5 integrin expression levels in OVCAR5 and OVCA433 ovarian cancer cells. Scale Bar = 10μm **B.** Images depict mesothelial clearance induced by OVCA433 cancer spheroids in the presence of control or α5β1 integrin blocking antibody at 0 and 10 hour time points. Scale bar = 50μm **C.** Quantification of mesothelial clearance from E. 12 independent regions were analyzed per condition. **D.** Western blot analysis of α5 integrin, phospho-MLC and MLC expression levels in control or α5 overexpressing OVCAR5 ovarian cancer cells plated on fibronectin-coated glass. Images show organization of the actin cytoskeleton in control and α5 integrin overexpressing OVCAR5 ovarian cancer cells plated on fibronectin-coated glass. **E.** Images represent mesothelial clearance induced by control or α5 integrin overexpressing OVCAR5 cells at 0 and 10 hour time points. Scale bar = 50μm **F.** Quantification of mesothelial clearance from B. 20 randomly chosen regions were analyzed per condition.

in OVCAR5 cells increased activation of myosin, promoted cell spreading and an increase in stress fibers and other cortical actin contractile structures and increased mesothelial clearance (Figure 3.4D,E,F and Supplementary Movie 3.10). These results support the hypothesis that $\alpha5\beta1$–dependent activation of myosin in ovarian cancer spheroids is required for spheroid-mediated mesothelial clearance.

Cancer spheroids expressing functional $\alpha5\beta1$ integrin detach fibronectin fibrils from the surface of the mesothelium.

Our data suggests that engagement of the fibronectin receptor $\alpha5\beta1$ integrin is an important step in spheroid-induced mesothelial clearance. Fibronectin has been found to be present on the surface of murine mesothelial cells (15). Thus, we addressed whether ovarian cancer spheroids re-organize the fibronectin matrix presented on dorsal surface of the mesothelial monolayer. To determine if fibronectin is organized on the dorsal surface of the mesothelial monolayer, the monolayer was immunostained with an antibody that recognized human fibronectin. We observed that fibronectin fibrils were present on top of the mesothelial monolayer (Figure 3.5A and Supplementary Movie 3.11). We also detected organized collagen fibers on top of the mesothelium (data not shown); however, blocking the $\alpha_2\beta_1$ integrin collagen receptor did not affect mesothelial clearance (Supplementary Figure 3.3C). Because fibronectin fibrils contacting the periphery of an intercalated spheroid appeared to be preferentially associated with the spheroid, but not the mesothelial cells (Supplementary Movie 3.11), we investigated whether cancer spheroids detach fibronectin from the mesothelial monolayer. We followed the dynamics of rhodamine-labeled fibronectin organized on

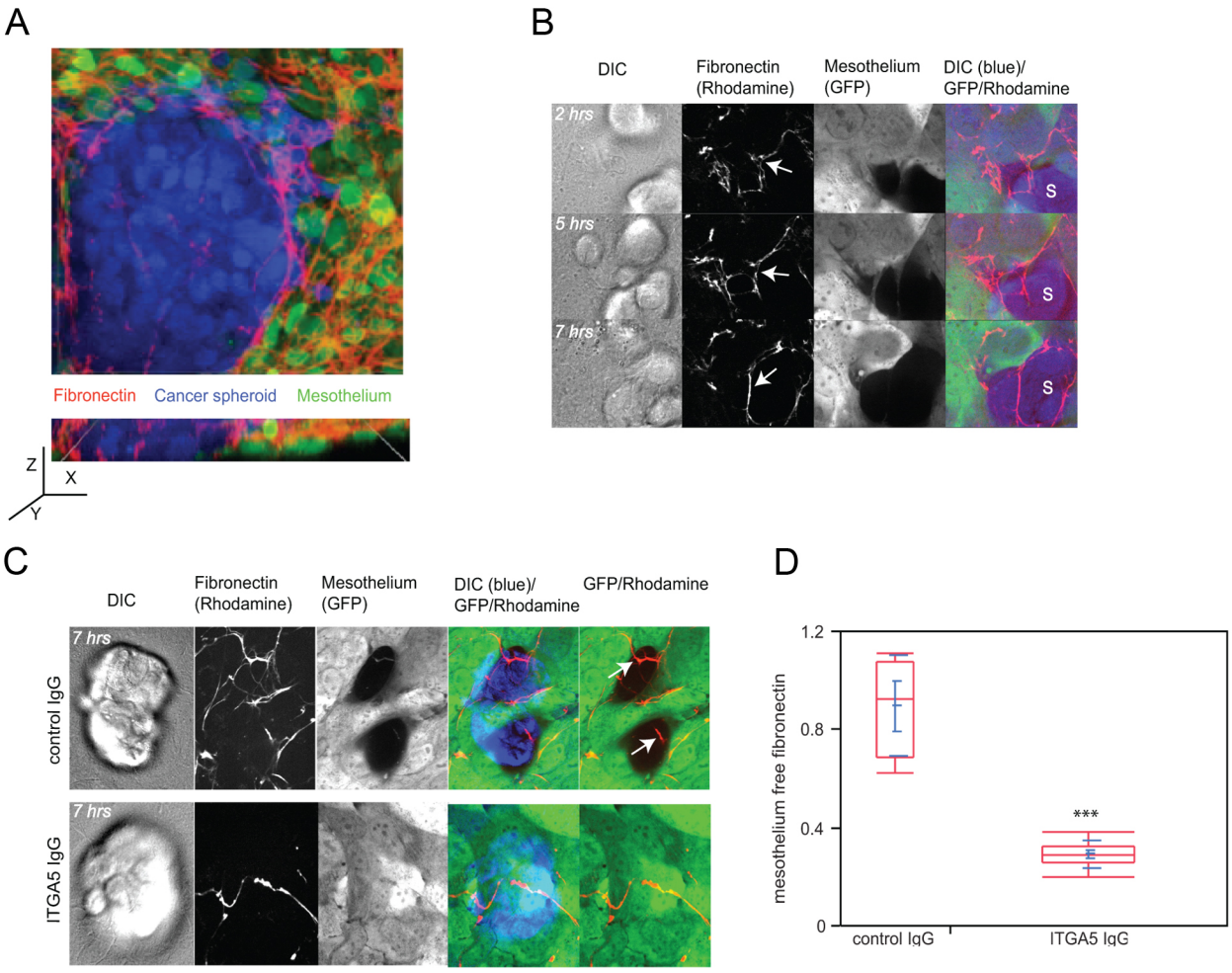

FIGURE 3.5: Cancer spheroids expressing functional α5β1 integrin dissociate fibronectin fibrils from the surface of the mesothelium. A. The upper image shows a laser scanning confocal image shows the top view of an OVCA433 cancer spheroid (blue) inserted into a mesothelial monolayer (green) stained with an antibody directed against human fibronectin (red). Scale bar = 10μm. The lower image shows a side view reconstruction of multiple Z planes of the same image. **B.** Images show temporal acquisition of mesothelium (green) associated fibronectin (red) by OVCA433 cancer spheroids (blue). Scale bar = 10μm **C.** Dissociation of fibronectin (red) from mesothelial monolayer (green) after 7 hours in response to spheroids (blue) pretreated with either control or α5β1 blocking antibody. Scale bar = 10μm. **D.** Quantification of fibronectin dissociation from a mesothelial monolayer in response to an attached cancer spheroid pretreated with either control or α5β1 antibody. 8 randomly chosen regions were analyzed in the control group and 20 randomly chosen regions were analyzed in the ITGA5 group.

top of the mesothelial monolayer in the presence of OVCA433 cancer spheroids. As shown in Figure 3.5B and Supplementary Movie 3.12, cancer spheroids induced detachment of fibronectin fibrils from the mesothelial cells. As time progressed, some of the fibronectin fibrils organized around the spheroid. In addition, when $\alpha5\beta1$ integrin was inhibited by an $\alpha5$ function blocking antibody, fibronectin did not dissociate from the mesothelial cells, suggesting that dissociation of fibronectin from the top of the mesothelial monolayer was dependent on functional $\alpha5\beta1$ integrin expressed by the cancer spheroids (Figure 3.5C,D). These data suggest that ovarian cancer spheroids utilize $\alpha5\beta1$ integrin to dissociate fibronectin from the mesothelial monolayer during clearance.

Cancer cells exert force on a fibronectin-coated substrate in an $\alpha5\beta1$ integrin-, talin 1- and myosin-dependent manner.

The data presented above show that $\alpha5\beta1$ integrin, myosin, and talin are all required in ovarian cancer cells for mesothelial clearance and that $\alpha5\beta1$ integrin-dependent binding of the ovarian cancer spheroids to fibronectin organized by the mesothelium is important for the clearance processes. This would suggest that the traction force exerted on the substratum by the spreading spheroids contributes to mesothelial clearance. To determine if modulation of $\alpha5$, talin I, or myosin affects force generation in the ovarian cancer cells, we used traction force microcopy (16, 17). This microscopy technique involves tracking fluorescent beads embedded in the substrate on which cell spread / migrate. Displacement of these beads is used to measure traction force exerted by cells on substrate during spreading/migration. Control OVCAR5 cells,

OVCAR5 cells over-expressing α5 integrin, and α5 over-expressing cells treated with either talin I siRNA or blebbistatin were allowed to spread on fibronectin–coated polyacrylamide substrates embedded with fluorescently labeled beads. Spreading caused deformation of the substrate, as indicated by the movement of the embedded beads. Tracking the bead displacement and reconstructing the cellular traction stresses allowed us to measure the strain energy invested by the cells to deform the elastic substrate (16). The strain energy can be used as a measure for the contractile strength of cells. As shown in Figure 3.6A, increased expression of α5 integrin in cancer cells correlated with an increase in cellular contractility, as measured by strain energy exerted by the cells. α5 integrin-induced force generation was dependent on myosin activation because treatment of OVCAR5 cells overexpressing α5 integrin with blebbistatin significantly decreased elastic energy exerted on the matrix (Figure 3.5A). We also observed that downregulation of talin I, but not talin II, in OVCAR5 cells overexpressing α5 integrin decreased force generation on fibronectin substrates (Figure 3.6B). These results are consistent with a model in which talin I and myosin act downstream of α5 integrin to generate force as ovarian cancer cells interact with fibronectin matrix.

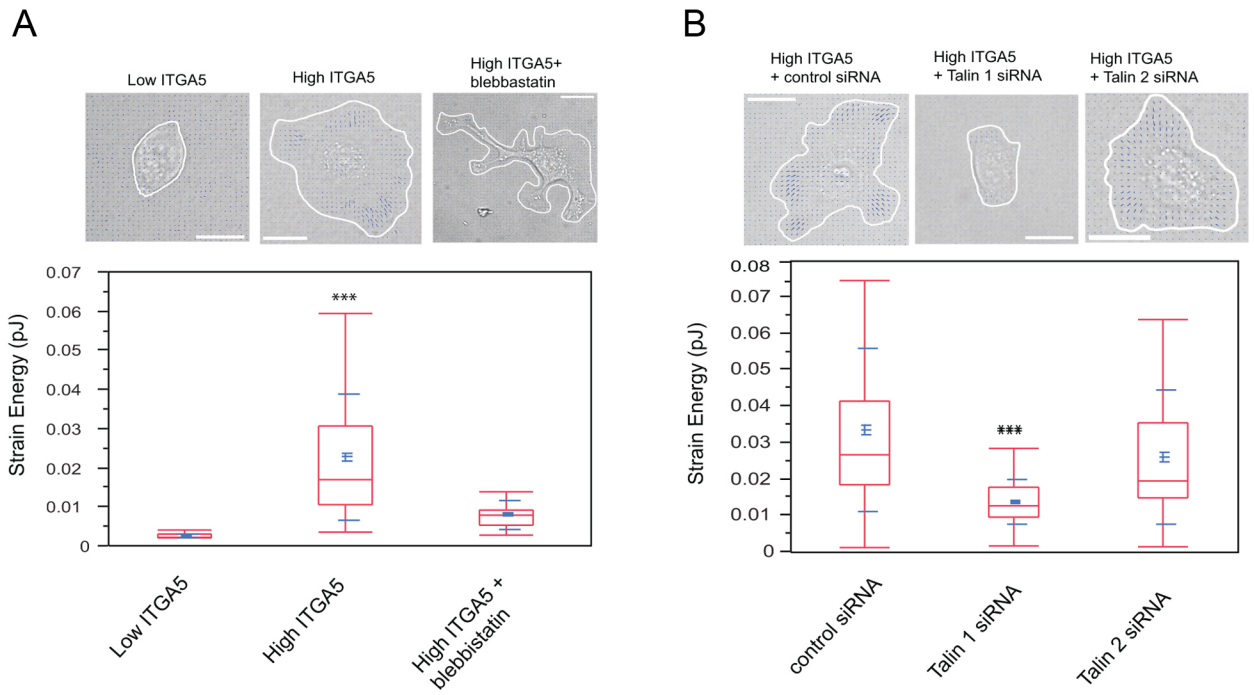

FIGURE 3.6: Cancer cells exert forces on a fibronectin-coated polyacrylamide gel in an α5β1 integrin, talin 1 and myosin-dependent manner. OVCAR5 ovarian cancer cells were plated on a polyacrylamide (PAA) gel substrate coated with fibronectin (10ug/ml). Cells were allowed to adhere to and spread on the PAA substrate and the displacement of fluorescently labeled beads embedded in the substrate was monitored. The strain energy was calculated from measured bead displacement data and used to reconstruct traction stresses. The strain energy is the energy invested by the cells to deform the substrate and a measure for the overall contractility of a cell (37). **A.** OVCAR5 cells have low endogenous α5-integrin (ITGA5) expression levels, and are significantly less contractile than OVCAR5 cells overexpressing ITGA5 ($p<0.001$). The high contractility of ITGA5-overexpressing OVCAR5 cells is attenuated by treatment with 1uM blebbistatin ($p<0.001$). **B.** The contractility of ITGA5-overexpressing OVCAR5 cells can also be significantly attenuated by siRNA-mediated knockdown of Talin 1, but only slightly attenuated by knockdown of Talin II. Bar = 20μm.

Discussion:

In summary, these studies provide new insights into the mechanism whereby ovarian tumor spheroids induce mesothelial cell clearance. Clearance-competent tumor spheroids were found to adhere to the dorsal surface of the mesothelial cells and initiate spreading. Protrusions from the spreading cells penetrated underneath the mesothelial cells causing localized breakdown of the mesothelial cell matrix adhesions, and provoked migration of the mesothelial cells. In tumor spheroids, $\alpha 5\beta 1$ integrin, talin I and myosin II were found to be required for spheroid –induced mesothelial clearance. These experiments suggest that ovarian cancer spheroids use actomyosin contractility to exert force via matrix adhesion to the fibronectin organized on the mesothelial monolayer, ultimately leading to mesothelial clearance (see model**,** Figure 3.7). The mesothelial clearance we observe in vitro may be relevant in human tumors since it has been shown that mesothelial cells are not present under ovarian tumor masses found attached to the peritoneal tissues.

In contrast to other epithelial tumors that employ hematogenous or lymphatogenous routes to metastasize, ovarian cancer cells predominantly move within the ascites fluid to metastasize to new sites within the peritoneal cavity(8). The mesothelial monolayer surface provides a variety of ligands to support the attachment of ovarian cancer cells (1). These ligands include hyaluronic acid, mesothelin and extracellular matrix molecules that are able to engage integrins (18-20). Both CD44 and $\beta 1$-containing integrin dimers have been implicated as receptors that can mediate ovarian cancer cells adherence to the mesothelium. However, function-blocking antibodies directed against $\beta 1$ integrin or CD44 only partially block ovarian cancer cells

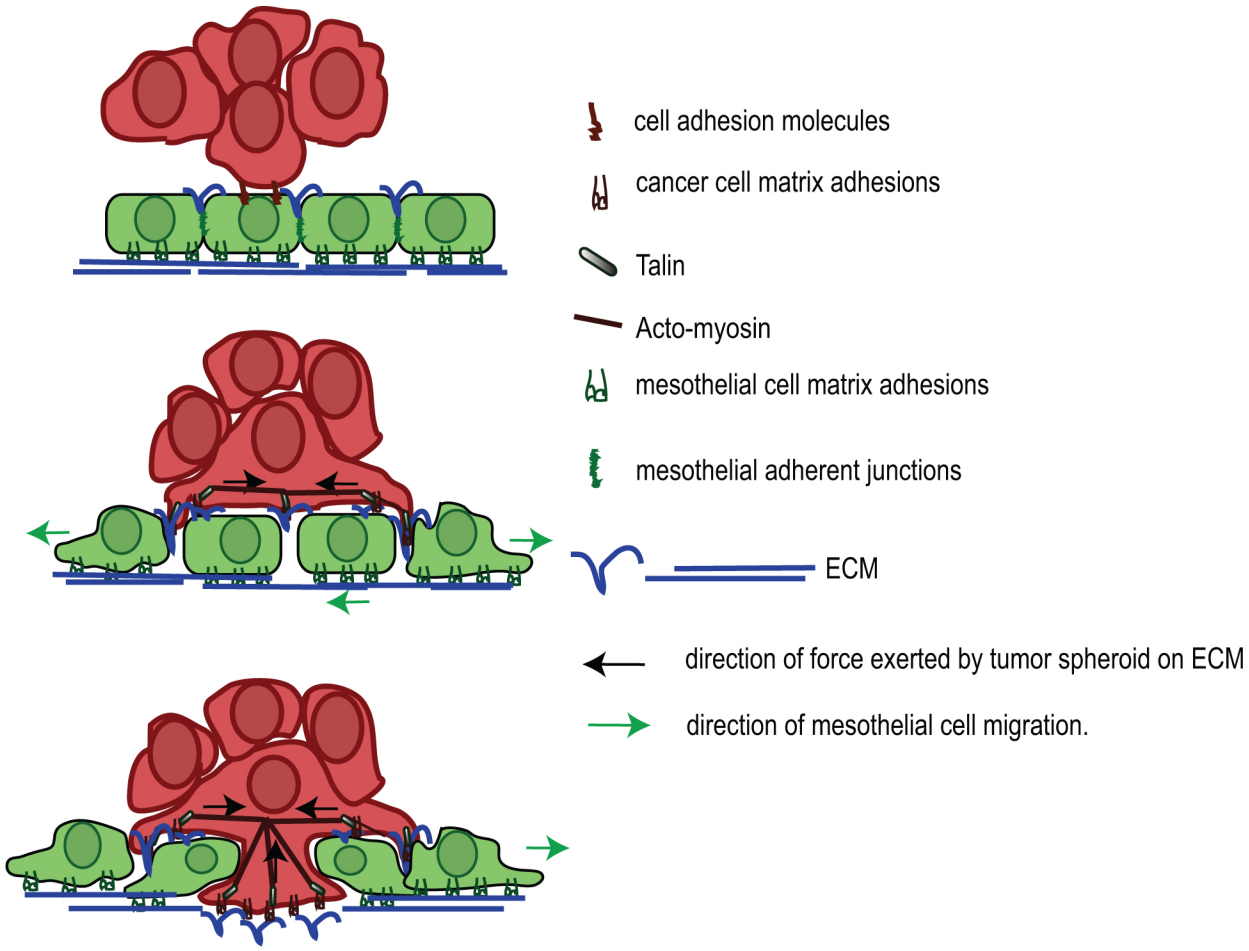

FIGURE 3.7: Model depicting the events associated with ovarian tumor cell intercalation into a mesothelial monolayer. Cancer spheroids attach to the mesothelial monolayer using various cell adhesion molecules including CD44,α5β1, αvβ1 and α2β1 integrins. Interaction of α5β1 integrin, expressed on cancer spheroids with fibronectin presented on the mesothelium promotes activation of myosin in the tumor spheroids and transmission of the force from the spheroid to the fibronectin on the monolayer. This promotes dissociation of mesothelial cells adhesions and their migration away form intruding tumor cells, leading to mesothelial cells exclusion from the base of cancer spheroid.

adherence to the mesothelial monolayer in short term, in vitro adhesion assays(9)'(18, 21) . This suggests that multiple ligands and receptors can support ovarian tumor cell adhesion to the mesothelial monolayer and targeting a single molecule will not abrogate cancer cell interaction with mesothelial cells. Consistent with this, we found that blocking CD44 or selected β1 integrin containing integrin heterodimers expressed by OVCA433 spheroids ($\alpha_2\beta_1$, $\alpha_v\beta_3$, $\alpha_5\beta_1$) did not significantly block OVCA433 spheroid attachment to the mesothelium after 10 hours of co-culture. Interestingly, however, our data indicated that interfering with the function of α5β1 integrin alone can significantly decrease OVCA433, DOV13 and SKOV3 spheroid-induced mesothelial clearance over a period of 10 hours (Supplementary Figure 3.3A,C). As α5β1 integrin is a fibronectin receptor, these results suggest that cancer spheroids can utilize α5β1 to bind to the fibronectin surrounding the mesothelial cells to mediate mesothelial clearance. Supporting this, we found that as a spheroid clears a space in a mesothelial monolayer, the fibronectin fibrils organized on the top of the mesothelial cells are redistributed away from the mesothelial cells and under the spheroid. This process was dependent on functional α5β1 integrin expressed by the cancer spheroids. In addition, we also observed that the expression level of α5β1 integrin in various ovarian cancer cell lines correlated with the ability of these cells to clear the mesothelium (data not shown). However, it is likely that other, $\alpha_5\beta_1$ integrin-independent mechanisms can mediate clearance as well.

Integrins are the major molecules that can transmit traction forces to the outside environment (22). While α_2 integrin binding to collagen I can induce fibril reorganization and transmit traction forces to the ECM in certain contexts (23), OVCAR5 ovarian tumor

spheroids that express high levels of α_2, but not α_5 integrin, were unable to clear the mesothelium in our experiments (Supplementary Figure 3.3C). In addition, blocking α_2 integrin in OVCA433 cells that express both α_2 and α_5 integrin did not prevent mesothelial clearance (Supplementary Figure 3.3C). It is possible that α2 integrin does not transmit sufficient traction force under conditions of adherence to mesothelial cells to induce clearance of the mesothelial cells. The generation of traction force on fibronectin has been shown to involve two steps: First, clustering of $\alpha_5\beta_1$ integrins promotes strong adhesiveness to matrix and second, recruitment of talin I stabilizes and reinforces formed $\alpha_5\beta_1$ adhesions (24) promoting the exertion of traction force on the matrix force. Our study indicated that the interaction between fibronectin receptor $\alpha_5\beta_1$ integrin expressed by tumor cells and mesothelial-associated fibronectin is a molecular event that contributes to the clearance process. In addition, we show that expression of talin I by tumor spheroids is required for $\alpha_5\beta_1$ -mediated formation of traction force and mesothelial clearance. We found that interfering with the function of another fibronectin receptor, $\alpha_v\beta_3$ integrin, did not affect spheroid–induced mesothelial clearance (Supplementary Figure 3.3C), suggesting that these receptors do not contribute to development of myosin contractility by OVCA433 spheroids that adhered to the mesothelial monolayer. This is consistent with previous experiments implicating $\alpha_5\beta_1$ but not $\alpha_v\beta_3$ integrins, in the development of contractility (25-27). Our data as well as earlier findings(3) show that the mesothelial cells retract in response to cancer cluster attachment. This raises an interesting question: how does the tumor induce retraction in the mesothelial cells? One possibility is that retraction is induced by the physical force of the spreading tumor cells pulling on the mesothelial cell's associated ECM and

provoking mesothelial cells migration away from the spheroid. Alternatively, the retraction of mesothelial cells could be provoked by a repulsive ligand presented on the tumor cells. In this study, we have shown that force produced by a spreading ovarian cancer cell cluster, via $\alpha_5\beta_1$ integrin, myosin II and talin I, is important for mesothelial clearance. The evidence that ovarian cancer spheroids deficient in non-muscle myosin II were unable to sustain mesothelial clearance suggests that mere contact between tumor cells and mesothelial cells is not sufficient to induce retraction and migration of mesothelial cells and that a repulsive ligand presented by spheroid does not trigger retraction of the mesothelial cells. However, it is possible that interfering with myosin function also perturbs expression or activity of repulsive ligands present on tumor cell plasma membrane. Spheroid-induced mesothelial clearance was accompanied by disassembly of mesothelial cell matrix adhesion sites, indicating that force induced on the mesothelium by cancer spheroids initiates migratory response in individual mesothelial cells. In spheroid-induced matrix adhesion turnover experiments mesothelial cells that originated from peritoneal wall (LP9) exhibited much more dynamic integrin adhesion when compared to mesothelium isolated from lungs (MET5A) (compare movies 3.4A and 3.4B). This suggests that mesothelial cells covering different organs might elicit distinct migratory responses when contacting tumor spheroids.

Earlier studies implicated mesothelial apoptosis as a mechanism of clearance as result of tumor cluster attachment (28). In our assays clearance of the mesothelium started about 30 minutes after spheroid attachment and was accompanied by migration of individual mesothelial cells from underneath of tumor spheroid. This observation

argues that in our assay mesothelial cells respond to contacting tumor cells by activating migratory, but not apoptotic pathways. However it is possible that mesothelial cells that are “stuck” underneath the spheroid and cannot escape, undergo apoptosis. In patients with advanced disease ovarian tumor clusters predominantly implant into mesothelial lining of peritoneal cavity-associated organs. Invasive tumor implants are able to cross mesothelial layer and gain access to stroma beneath mesothelium (29). These observations suggest that the mesothelium presents a functional barrier to the spread and progression of ovarian tumors. Hence, one would expect that progression toward invasive disease would be associated with alterations that enable the tumor cells to adhere to the mesothelium and brake mesothelial barrier by provoking mesothelial clearance. Our studies suggest that integrin-dependent activation of myosin contractility in tumor cells is required to perturb the mesothelial barrier. Therefore, our results suggest that acquisition of contractile phenotypes in ovarian tumor cells represents a step towards malignant progression.

Materials and Methods:

Cell Culture. All cells used in this study were cultured in a 1:1 ratio of Medium 199 (GIBCO) and MCDB 105 (Cell Applications, INC) supplemented with 10% fetal bovine serum (GIBCO). Normal lung mesothelial cells were obtained from a benign pleural effusion from a patient with pneumothorax. These cells were immortalized by simultaneous inactivation of p53 and Rb through ectopic expression of SV40 T antigen and overexpression of human telomerase (fused to GFP) as described previously (30, 31). In experiments involving a mixture of labeled and unlabeled mesothelial cells MET5A (human mesothelioma cells -ATTC) were used as a source of unlabeled cells. In focal adhesion tracking experiments, LP9s, a peritoneum-derived mesothelial cell line (Coriell Cell Repositories) was used. Primary lung mesothelial cells were under passage 20. LP9 cells were used as passage under 10. MET5A mesothelial cells were used under passage 10 and these cells morphologically resembled primary lung mesothelilal cells that we used during the course of this experiment. OVCA433 and OVCAR5 ovarian cancer cell lines were a generous gift from Dr. Dennis Slamon (University of California, Los Angeles).

Spheroid-induced mesothelial clearance assay: The mesothelial cells were plated on glass-bottom dishes (Mat-TEK Corporation) coated with 5ug/ml of fibronectin (Sigma, USA) and/or collagen I (Sigma, USA). Cells were maintained in culture until confluent (48 hrs after plating). To generate spheroids, cells were dissociated by trypsinization, labeled with CMTX-red membrane dye (Molecular Probes), washed 2x with PBS, re-suspended in culture medium and plated on Poly-Hema-coated culture

dishes (32). Spheroids were collected for experiments 36-48hrs later. The cell number varied from 100 to 500 cells per spheroid. OVCAR5 spheroids were generated in the presence of 10ug/ml of soluble bovine fibronectin to increase spheroid cohesion (33, 34). In co-culture experiments, spheroids were added to a confluent mesothelial monolayer, allowed to attach for 60 minutes, and imaged for the indicated time. Only spheroids that remained attached during the experiment were used for quantification.

Fibronectin labeling of mesothelial cells and quantification of fibronectin dissociation – 20 ug of rhodamine conjugated fibronectin (Cytoskeleton, USA) was added for a period of 24 hrs to a confluent monolayer of human lung mesothelial cells expressing GFP. To quantify fibronectin dissociation from the top of the mesothelial monolayer in the presence of cancer spheroids, we divided total fluorescent intensity of the fibronectin present beneath the cancer spheroid by the total intensity of GFP labeled mesothelial cells.

Western blots and antibodies. Cells were lysed in 100 µl of RIPA buffer (50 mM HEPES pH 7.4, 1% Triton X-100, 1% sodium deoxycholate, 0.1% SDS, 0.1 M NaCl, 1 mM sodium orthovanadate, 0.1 M sodium pyrophosphate, 100 mM NaF and 1 mM PMSF). Lysates were clarified by centrifugation at 13,000 ***g*** for 10 minutes. Clarified lysates were boiled in 1x sample buffer (0.04 M Tris-HCl pH 6.8, 1% SDS, 1% β-mercaptoethanol and 10% glycerol) for 10 minutes and resolved by SDS-PAGE. Proteins were transferred to Immobilon membranes (Whatman) and blocked with 5% BSA in PBS (140 mM NaCl, 0.27 mM KCl, 0.43 mM $Na_2HPO_4 \cdot 7H_2O$, 0.14 mM KH_2PO_4

pH 7.3), 0.1% Tween 20, pH 7.2 for 1 hour at room temperature. Membranes were incubated overnight at 4°C with one of the following antibodies: anti-talin I polyclonal antibody (Cell Signalling, 1:1000), anti-actin monoclonal antibody (Sigma, 1:1000), anti-myosin heavy chain IIA polyclonal antibody (Covance, 1:1000), anti-myosin heavy chain IIB polyclonal antibody (1:1000, Covance), anti-filamin A polyclonal antibody (1:1000, Cell Signaling), anti –cleaved caspase -3 polyclonal antibody (1:1000 , Cell Signaling) anti-α5 integrin polyclonal antibody (1:1000, Cell Signaling), anti-phosphorylated myosin light chain serine 18 polyclonal antibody (1:1000, Cell Signaling), or anti-myosin light chain polyclonal antibody (1:1000, Cell Signaling). Membranes were subsequently probed with secondary antibodies linked to horserasish peroxidase (HRP; Santa Cruz). Western blot membranes were developed using enhanced chemiluminescent substrate for detection of HRP (VWR). Western blot results were visualized using kodak film developer and an Epson 3000 scanner. OVCA433 spheroids were treated for 45 min in the presence of low serum medium (OPTIMEM) with the following cell adhesion blocking antibodies: anti-α5β1 (5ug/ml, BD Biosciences), anti-α2β1 (5ug/ml, BD Biosciences) integrins, anti-CD44 (5ug/ml, Sigma). We used non specific serum IgG (10ug/ml, Sigma) in function blocking experiments. Treated spheroids were washed twice with PBS (CellGrow), re-suspended in culture medium and added to the mesothelial monolayer.

shRNAs, siRNAs, cDNA plasmids and reagents. To attenuate the expression level of talin 1 and non-muscle myosin heavy chain IIA, OVCA433 cells were infected with

lentiviruses lacking an shRNA sequence (pLKO) as a control, or plasmid containing talin 1 (OpenBiosystems)
(seq#1:CCGGGCAGTGAAAGATGTAGCCAAACTCGAGTTTGGCTACATCTTTCACTG
CTTTTTG
seq#2:CCGGGCCTCAGATAATCTGGTGAAACTCGAGTTTCACCAGATTATCTGAGG
CTTTTTG
seq#3:CCGGCGCATTGGCATCACCAATCATCTCGAGATGATTGGTGATGCCAATGC
GTTTTTG) or non-muscle myosin IIA shRNA sequences (OpenBiosystems)
seq#1:CCGGCGCATCAACTTTGATGTCAATCTCGAGATTGACATCAAAGTTGATGCG
TTTTTG
seq#2:CCGGCGCATCAACTTTGATGTCAATCTCGAGATTGACATCAAAGTTGATGCG
TTTTT
seq#3:CCGGGACAGCAATCTGTACCGCATTCTCGAGAATGCGGTACAGATTGCTGT
CTTTTT). Lentivirus-infected cells were selected for 72 hours in medium containing 1ug/ml of puromycin (Dulbecco). To attenuate the expression level of non-muscle myosin IIB in OVCAR433 cells or talin 1 in OVCAR5 cells, we also used a pool of siRNA oligonucleotides against NMIIB or talin 1 respectively (Dharmacon). To ectopically express α5 integrin in OVCAR5 cells, we used a retroviral vector (pLZRS) encoding the human α5 integrin gene (generous gift from Dr.Erik Danen, The Netherlands Cancer Institute). Infected cells were selected in growth medium containing 600ug/ml G418 (Dulbecco). Staurosporin was purchased from CalBiochem (USA).

Live cell imaging.

Spheroid-induced mesothelial clearance assay: Imaging was performed using a Nikon Ti-E Inverted Motorized Widefield Fluorescence Microscope with integrated Perfect Focus System and low (20x-0.75 NA) magnification/NA DIC optics, Nikon halogen trans illuminator with 0.52 NA LWD condenser, Nikon fast (<100ms switching time) excitation and emission filter wheels, Sutter fast transmitted and epi-fluorescence light path Smart shutters, Nikon linear-encoded motorized stage, Hamamatsu ORCA-AG cooled CCD camera, custom-built microscope incubation chamber with temperature and CO_2 control, Nikon NIS-Elements AR software v3 and TMC vibration-isolation table

Total Internal Reflection Fluorescence (TIRF) analysis: Mesothelial cell adhesion dynamics were visualized using Nikon Ti-E inverted microscope with integrated Perfect Focus System, Nikon 1.49 NA TIRF DIC optics (60x), Nikon halogen trans illuminator with 0.52 NA LWD and 0.85 NA Dry condenser, Nikon dual-port TIRF/Epi illuminator with motorized laser incident angle adjustment and motorized switching between TIRF and epi-illumination, Solamere laser launch with 100mW 491nm, 75mW 561nm and 30mW 640nm solid state lasers with fiber-optic delivery system and 4-channel AOTF, Prior controller, Prior fast excitation and emission filter wheels, Prior fast transmitted and epi-fluorescence light path shutters, Prior linear-encoded motorized stage, Hamamatsu ImagEM 512x512 back-thinned electron multiplying cooled CCD camera, 20/20 Technologies Bionomic Controller/ Stage heater insert, Molecular Devices MetaMorph v7.7 and TMC vibration-isolation table

Analysis of the dynamics of rhodamine-labeled fibronectin: Imaging was performed using a Spinning Disk Confocal Microscope: Nikon Ti-E inverted motorized microscope equipped with integrated Perfect Focus System, Nikon Plan Apo 1.4 NA DIC optics (60x), Nikon halogen trans illuminator with 0.52 NA LWD and 0.85 NA Dry condenser, Yokogawa CSU-X1 spinning disk confocal head with internal motorized high speed emission filter wheel and Spectral Applied Research Borealis modification for increased light throughput and illumination homogeneity, Spectral Applied Research custom laser merge module (LMM-7) with AOTF and 100-200mW solid state 442nm, 491nm, 515nm, 561nm, and 642 nm lasers, Semrock 405/488/561/647 and 442/514/647 dichroic mirrors, Prior ProScan II controller, Prior NanoScan piezo Z stage insert for high speed z-series, Prior fast transmitted and epi-fluorescence light path shutters, Hamamatsu ORCA-AG cooled CCD camera, custom built 37°C microscope incubator enclosure with 5% CO_2 delivery, Molecular Devices MetaMorph v7.7 and TMC vibration-isolation table.

Quantification of mesothelial clearance and dissociation of fibronectin. To quantify mesothelial clearance, the non-fluorescent area in the GFP mesothelial monolayer was measured over time and divided by the initial area of the cancer spheroid. To quantify the dissociation of fibronectin from the mesothelial cells, the total fluorescence intensity of rhodamine-labeled fibronectin (enclosed within the area of the spheroid) was divided by the total fluorescent intensity of GFP-labeled mesothelial cells beneath the spheroid. Data was plotted as a point distribution using JMP8 statistical software. We used the non-parametric Mann-Whitney t-test to calculate statistical significance.* denotes p=0.05, ** denotes p =0.01, *** denotes p=0.001.

Cancer spheroid adhesion assay. OVCA433 spheroids were co-cultured with mesothelial monolayers for five hours. Spheroids that did not adhere to the monolayer within this time were removed and re-plated on fibronectin and collagen I coated glass bottom dish for 60 minutes, the spheroids were counted. All spheroids that adhered to the mesothelial monolayer were counted. The number of spheroids adhered to the mesothelial monolayer plus the number of spheroids adhered to the matrix-coated dish represented the total number of spheroids. The percentage of spheroids adhered to the mesothelium was calculated by dividing the amount of spheroids attached to the mesothelium by the total number of spheroids (mesothelium + culture dish).

Preparation of Polyacrylamide (PAA) Gel Substrates for Traction Force Microscopy (TFM). Fibronectin-coated PAA gels containing 0.2um fluorescent microspheres (Invitrogen) were prepared on glass-bottomed dishes as described previously (Wang and Pelham, 1998). In brief, the glass surfaces were incubated with 0.1N NaOH and air dried. The surfaces were then subsequently incubated with 3-aminopropyltrimethoxysilane (Sigma) and 0.5% glutaraldehyde (Sigma), and washed in distilled H_2O between incubations. After drying, a drop of acrylamide/bis-acrylamide solution containing ammonium persulfate (BioRad), tetramethylethylenediamine (TEMED; Sigma) and 0.2um fluorescent microspheres was pipetted onto the modified glass surface. A coverslip was then placed over the droplets to ensure a flat gel surface after polymerization. Fibronectin was coupled to the PAA substrates via the bi-functional crosslinker sulfosuccinimidyl hexanoate (sulfo-SANPAH; Pierce). For traction force

measurements of OvCar5 and OvCar5 cells overexpressing α5 integrin, gels with elastic moduli of approximately 10-20kPa were used.

Traction Force Microscopy and Calculations of Traction Forces.

Cells on PAA substrates were imaged with a multispectral multimode spinning disk confocal microscope consisting of a Nikon Ti-E inverted motorized microscope equipped with a custom built 37°C microscope incubator enclosure with 5% CO_2 delivery, an integrated Perfect Focus System, a 40x 0.95NA Plan Apo objective, a Yokogawa CSU-X1 spinning disk confocal head with internal motorized high speed emission filter wheel and Spectral Applied Research Borealis modification for increased light throughput and illumination homogeneity, and a Hamamatsu ORCA-AG cooled CCD camera. Images were acquired with MetaMorph software (MDS Analytical Technologies). Cells were trypsinized with 0.25% trypsin after imaging to obtain an image of unstrained bead positions as reference frames for analyses. Positions of fluorescent beads were extracted from image series and tracked using time-integrated cross-correlation tracking as described previously. Traction forces generated by the cells were determined using custom MatLab programs following the boundary element and Fourier transform traction cytometry methods described by Sabass et al (16). Square image blocks with a template size of 25pixels (= 4.1um) were centered on each reference bead position, identified as intensity maxima in the reference frame. Bead displacements were defined as the x-y-shift that maximizes the cross-correlation score of these image blocks in a corresponding region of the deformed bead image. To minimize false positive template matching, bead displacements with an insignificant

maxima in the cross-correlation score function are rejected (35).Traction forces were reconstructed from the measured bead displacements using an implementation of the regularized Fast Fourier Traction Cytometry (FTTC) method (36) provided by (16). For this study we regarded the PAA substrate as isotropic, linear elastic, infinite half-space, and thus applied the Boussinesq Green function. In order to solve the ill-posed inversion problem, we applied zero-order Tikhonov regularization (37). The regularization parameter λ has been determined using the L-curve method and we used the strain energy U, invested by the cell to deform the substrate, as a measure for cellular contractility (36) $U = \frac{1}{2}\int_{\Omega} \vec{T}(\vec{r}) \cdot \vec{u}(\vec{r}) d\vec{r}$

Here, $\vec{T}$ and $\vec{u}$ denote the measured displacement and reconstructed traction stress, respectively. To avoid possible boundary artifacts introduced by the FTTC algorithm (36) integration was performed over a hand drawn elliptical domain Ω that just covered the whole footprint of the cell. Data was plotted as a point distribution using JMP8 statistical software. We used the non-parametric Mann-Whitney t-test to calculate statistical significance.* -denotes p=0.05 ** - denotes p =0.01 *** - denotes p=0.001.

Acknowledgements:

We thank Ghassan Mouneimne and Cheuk Leung for lab meeting discussions and valued input into the direction of this project. We thank Benedikt Sabass and Ulrich Schwarz for providing the regularized FTTC algorithm. We also thank the Nikon Imaging Center at Harvard Medical School for help with light microscopy especially: Jennifer Waters, Wendy Salmon, Lara Petrak and Cassandra Rogers. This study was funded by NIH Grant 5695837 (to M.I) and by Miriam and Sheldon Adelson Research Foundation grant to J.B.

A.B. and G.D were funded by the NIH Grant R01 GM071868 and the Deutsche Forschungsgemeinschaft through fellowship BE4547/1-1.

References:

1.Burleson KM, Casey RC, Skubitz KM, Pambuccian SE, Oegema TR, Jr., Skubitz AP. Ovarian carcinoma ascites spheroids adhere to extracellular matrix components and mesothelial cell monolayers. Gynecol Oncol. 2004;93:170-81.

2.Burleson KM, Boente MP, Pambuccian SE, Skubitz AP. Disaggregation and invasion of ovarian carcinoma ascites spheroids. J Transl Med. 2006;4:6.

3.Birbeck MS, Wheatley DN. An Electron Microscopic Study of the Invasion of Ascites Tumor Cells into the Abdominal Wall. Cancer Res. 1965;25:490-7.

4.Witz CA, Monotoya-Rodriguez IA, Schenken RS. Whole explants of peritoneum and endometrium: a novel model of the early endometriosis lesion. Fertil Steril. 1999;71:56-60.

5.Niedbala MJ, Crickard K, Bernacki RJ. Interactions of human ovarian tumor cells with human mesothelial cells grown on extracellular matrix. An in vitro model system for studying tumor cell adhesion and invasion. Exp Cell Res. 1985;160:499-513.

6.Kiyasu Y, Kaneshima S, Koga S. Morphogenesis of peritoneal metastasis in human gastric cancer. Cancer Res. 1981;41:1236-9.

7.Koga S, Kudo H, Kiyasu Y, Kaneshima S, Iitsuka Y, Takeuchi T, et al. A scanning electron microscopic study on the peritoneal implantation of ascites hepatoma AH100B cells in rats. Gann. 1980;71:8-13.

8.Lengyel E. Ovarian Cancer Development and Metastasis. Am J Pathol.

9.Strobel T, Cannistra SA. Beta1-integrins partly mediate binding of ovarian cancer cells to peritoneal mesothelium in vitro. Gynecol Oncol. 1999;73:362-7.

10.Bershadsky AD, Balaban NQ, Geiger B. Adhesion-dependent cell mechanosensitivity. Annu Rev Cell Dev Biol. 2003;19:677-95.

11.Zhang X, Jiang G, Cai Y, Monkley SJ, Critchley DR, Sheetz MP. Talin depletion reveals independence of initial cell spreading from integrin activation and traction. Nat Cell Biol. 2008;10:1062-8.

12.Huveneers S, Truong H, Fassler R, Sonnenberg A, Danen EH. Binding of soluble fibronectin to integrin alpha5 beta1 - link to focal adhesion redistribution and contractile shape. J Cell Sci. 2008;121:2452-62.

13.Sawada K, Mitra AK, Radjabi AR, Bhaskar V, Kistner EO, Tretiakova M, et al. Loss of E-cadherin promotes ovarian cancer metastasis via alpha 5-integrin, which is a therapeutic target. Cancer Res. 2008;68:2329-39.

14.Mitra AK, Sawada K, Tiwari P, Mui K, Gwin K, Lengyel E. Ligand-independent activation of c-Met by fibronectin and alpha(5)beta(1)-integrin regulates ovarian cancer invasion and metastasis. Oncogene.

15.Kenny HA, Kaur S, Coussens LM, Lengyel E. The initial steps of ovarian cancer cell metastasis are mediated by MMP-2 cleavage of vitronectin and fibronectin. J Clin Invest. 2008;118:1367-79.

16.Sabass B, Gardel ML, Waterman CM, Schwarz US. High resolution traction force microscopy based on experimental and computational advances. Biophys J. 2008;94:207-20.

17.Wang N, Tolic-Norrelykke IM, Chen J, Mijailovich SM, Butler JP, Fredberg JJ, et al. Cell prestress. I. Stiffness and prestress are closely associated in adherent contractile cells. Am J Physiol Cell Physiol. 2002;282:C606-16.

18.Cannistra SA, Kansas GS, Niloff J, DeFranzo B, Kim Y, Ottensmeier C. Binding of ovarian cancer cells to peritoneal mesothelium in vitro is partly mediated by CD44H. Cancer Res. 1993;53:3830-8.

19.Kaneko O, Gong L, Zhang J, Hansen JK, Hassan R, Lee B, et al. A binding domain on mesothelin for CA125/MUC16. J Biol Chem. 2009;284:3739-49.

20.Casey RC, Burleson KM, Skubitz KM, Pambuccian SE, Oegema TR, Jr., Ruff LE, et al. Beta 1-integrins regulate the formation and adhesion of ovarian carcinoma multicellular spheroids. Am J Pathol. 2001;159:2071-80.

21.Strobel T, Swanson L, Cannistra SA. In vivo inhibition of CD44 limits intra-abdominal spread of a human ovarian cancer xenograft in nude mice: a novel role for CD44 in the process of peritoneal implantation. Cancer Res. 1997;57:1228-32.

22.Baker EL, Zaman MH. The biomechanical integrin. J Biomech.43:38-44.

23.Friedrichs J, Taubenberger A, Franz CM, Muller DJ. Cellular remodelling of individual collagen fibrils visualized by time-lapse AFM. J Mol Biol. 2007;372:594-607.

24.Roca-Cusachs P, Gauthier NC, Del Rio A, Sheetz MP. Clustering of alpha(5)beta(1) integrins determines adhesion strength whereas alpha(v)beta(3) and talin enable mechanotransduction. Proc Natl Acad Sci U S A. 2009;106:16245-50.

25.Moyano JV, Maqueda A, Casanova B, Garcia-Pardo A. Alpha4beta1 integrin/ligand interaction inhibits alpha5beta1-induced stress fibers and focal adhesions via down-regulation of RhoA and induces melanoma cell migration. Mol Biol Cell. 2003;14:3699-715.

26.Danen EH, Sonneveld P, Brakebusch C, Fassler R, Sonnenberg A. The fibronectin-binding integrins alpha5beta1 and alphavbeta3 differentially modulate RhoA-GTP

loading, organization of cell matrix adhesions, and fibronectin fibrillogenesis. J Cell Biol. 2002;159:1071-86.

27.Mierke CT, Frey B, Fellner M, Herrmann M, Fabry B. Integrin {alpha}5{beta}1 facilitates cancer cell invasion through enhanced contractile forces. J Cell Sci.124:369-83.

28.Heath RM, Jayne DG, O'Leary R, Morrison EE, Guillou PJ. Tumour-induced apoptosis in human mesothelial cells: a mechanism of peritoneal invasion by Fas Ligand/Fas interaction. Br J Cancer. 2004;90:1437-42.

29.Seidman JD, Kurman RJ. Ovarian serous borderline tumors: a critical review of the literature with emphasis on prognostic indicators. Hum Pathol. 2000;31:539-57.

30.Hahn WC, Counter CM, Lundberg AS, Beijersbergen RL, Brooks MW, Weinberg RA. Creation of human tumour cells with defined genetic elements. Nature. 1999;400:464-8.

31.Ince TA, Richardson AL, Bell GW, Saitoh M, Godar S, Karnoub AE, et al. Transformation of different human breast epithelial cell types leads to distinct tumor phenotypes. Cancer Cell. 2007;12:160-70.

32.Schafer ZT, Grassian AR, Song L, Jiang Z, Gerhart-Hines Z, Irie HY, et al. Antioxidant and oncogene rescue of metabolic defects caused by loss of matrix attachment. Nature. 2009;461:109-13.

33.Robinson EE, Foty RA, Corbett SA. Fibronectin matrix assembly regulates alpha5beta1-mediated cell cohesion. Mol Biol Cell. 2004;15:973-81.

34.Robinson EE, Zazzali KM, Corbett SA, Foty RA. Alpha5beta1 integrin mediates strong tissue cohesion. J Cell Sci. 2003;116:377-86.

35.Ji L, Danuser G. Tracking quasi-stationary flow of weak fluorescent signals by adaptive multi-frame correlation. J Microsc. 2005;220:150-67.

36.Butler JP, Tolic-Norrelykke IM, Fabry B, Fredberg JJ. Traction fields, moments, and strain energy that cells exert on their surroundings. Am J Physiol Cell Physiol. 2002;282:C595-605.

37.Schwarz US, Balaban NQ, Riveline D, Bershadsky A, Geiger B, Safran SA. Calculation of forces at focal adhesions from elastic substrate data: the effect of localized force and the need for regularization. Biophys J. 2002;83:1380-94.

Chapter 4

Mesothelial Clearance Ability of Ovarian Cancer Spheroids is Associated with a Mesenchymal Gene Expression Program

Statement of contribution:

This chapter embodies a manuscript submitted to *Cancer Discovery* by R.A. Davidowitz, L.M. Selfours, M.P. Iwanicki, A. Karst, H. Piao, T.A. Ince, M.G. Drage, J. Dering, G.E. Koneckny, U. Matulonis, G.B. Mills, D.J. Slamon, R. Drapkin*, and J.S. Brugge*. I designed and performed all experiments in this chapter, analyzed the data and wrote the manuscript. LMS performed the bioinformatics analyses. MGD prepared cell blocks. AK and HP performed the IHC. TAI provided the primary cell media. JD, GEK, and DJS performed the cell line microarrays. UM provided the primary cell samples. GBM provided the RPPA data. MPI, RD and JSB provided guidance throughout the project and participated in the writing of the manuscript.

*Co-corresponding authors

KEYWORDS: ovarian cancer, mesothelium, EMT, mesenchymal

Abstract:

Metastatic dissemination of ovarian tumors involves the invasion of tumor cell clusters into the mesothelial cell lining of peritoneal cavity organs. We used an *in vitro* mesothelial clearance assay that models this initial step of ovarian cancer metastasis to determine the clearance ability of a large panel of both established and primary ovarian cancer cell lines. Comparison of the gene and protein expression profiles of clearance-competent and clearance-incompetent cell lines revealed that mesenchymal genes are enriched in cell lines that showed strong clearance activity, while epithelial genes are enriched in cell lines with weak or undetectable activity. Over-expression of the EMT-regulatory transcription factors SNAI1, TWIST1 and ZEB1 promoted mesothelial clearance in cell lines with weak activity, while knockdown of the EMT-regulatory transcription factors TWIST1 and ZEB1 attenuated mesothelial clearance in lines with strong activity. These findings provide important new insights into the mechanisms associated with metastatic progression of ovarian cancer.

Significance:

The current treatment course for ovarian cancer involves cytoreductive surgery followed by platinum-taxane based chemotherapy. These treatments are insufficient because chemoresistant disease often recurs and advanced disease is often complicated by bowel obstruction. Our data suggest that inhibiting pathways that drive mesenchymal programs may suppress tumor cell invasion of peritoneal tissues and may be a useful treatment option in addition to existing therapies to prevent or partially thwart the development of late stage disease complications.

Introduction:

Ovarian cancer has the highest mortality rate of all gynecological cancers and the fifth highest mortality rate of all cancers in the United States(1, 2). Because early disease is asymptomatic, ovarian cancer is rarely diagnosed until late stages, when the cancer has spread beyond the primary tumor site(3). Ovarian cancer metastasis involves detachment of tumor cells from the primary tumor site and attachment on the surface of other organs within the peritoneal cavity(4, 5), including the omentum, peritoneum, diaphragm, and small bowel mesentery(6). Generally, tumor nodules develop on the surface of the peritoneal organs and subsequently intercalate through the mesothelial lining into the underlying tissues. This can often lead to significant clinical complications, including bowel obstructions.

All of the organs within the peritoneal cavity are lined with a continuous monolayer of mesothelial cells(7-9). Electron micrograph studies of ovarian cancer nodules attached to peritoneal cavity organs revealed that mesothelial cells are absent from underneath the attached tumor mass(8-11). Interestingly, *in vitro* studies have shown that ovarian cancer cells are able to attach more firmly to extracellular matrix (ECM) components compared to either plastic culture dishes or mesothelial cell monolayers(12). Furthermore, attachment and invasion of ovarian cancer cells into a 3D collagen gel is delayed when the gel is covered with a mesothelial monolayer(13). These observations suggest that mesothelial cells can act as a protective barrier against ovarian cancer metastasis, and that mesothelial cells are excluded during processes leading to successful tumor cell

implantation on peritoneal tissue.

Ovarian cancer cells can attach and spread on multiple ECM proteins, including collagen I, collagen IV, laminin, vitronectin and fibronectin; α and β integrins, as well as CD44, have been shown to serve as tumor cell receptors for these ligands(10, 12, 14-22). While ovarian cancer cell adhesion and spreading on mesothelial monolayers has been well characterized, there has been much less focus on understanding the mechanisms associated with ovarian cancer cell invasion into and displacement of cells in the mesothelial monolayer. Several groups have examined the ability of single ovarian cancer cells to transverse through a mesothelial monolayer and found that inhibiting VCAM, a4-integrin, β1-integrin, MMP-2, or MMP-9 could decrease the extent of invasion(22-24). Previously, we have shown that ovarian cancer multicellular spheroids are able to attach to and clear a hole in a mesothelial cell monolayer through an integrin- and force-dependent process involving α5 integrin, talin I and myosin II; inhibiting any of those molecules significantly decreases mesothelial clearance ability(25).

In this paper, we sought to better understand the mechanisms by which ovarian cancer multicellular spheroids clear the mesothelial monolayer by characterizing the clearance abilities of a panel of 20 established ovarian cancer cell lines and 21 primary ovarian cancer cell samples. Comparison of the gene and protein expression profiles of ovarian cancer spheroids that are competent or incompetent to clear mesothelial monolayers revealed distinct differences in the expression of mesenchymal and epithelial cell markers that correlated with clearance competency. Modulation of mesenchymal transcription factors to

promote or inhibit mesenchymal gene expression altered the clearance ability of the tumor cell lines. These studies provide important new insights into the mechanisms involved in mesothelial cell invasion.

Results:

Differential Ability of Ovarian Cancer Spheroids to Clear a Mesothelial Monolayer:

We have previously shown that OVCA433 ovarian cancer multicellular spheroids are able to attach to, intercalate into, and form a hole in a ZT mesothelial cell monolayer, while OVCAR5 ovarian cancer multicellular spheroids are unable to clear the monolayer(25). To explore the differences in gene and protein expression that distinguish clearance-competent ovarian cancer multicellular spheroids from clearance-incompetent spheroids, we first analyzed the ability of preformed multicellular spheroids from 20 different ovarian cancer cell lines to form a hole in GFP-expressing ZT mesothelial monolayers using time lapse video microscopy (Figure 4.1A).

After 8 hours of co-culture, clearance ability was scored. 11 ovarian cancer cell lines (ES2, CP70, OVCAR3, OVCA433, OV207, A2780, TOV112D, DOV13, OVCA432, HEYC2, OV2008) were able to clear the mesothelial monolayer, three (OVSAHO, C13, OAW28) cleared weakly, and six (PE06, CAOV3, OVCA429, EFO21, MCAS, RMG1) did not clear (FIGURE 4.1B, Supplementary Figure 4.1, Supplementary Movie 4.). These results indicate that there is a continuum of clearance abilities among ovarian cancer spheroids. The cell lines with a normalized clearance area greater than one will be referred to as clearance-competent, while the cell lines with a normalized clearance area less than one will be considered clearance-incompetent.

FIGURE 4.1: Spheroids from ovarian cancer cell lines display differential clearance ability that correlates with epithelial and mesenchymal marker expression. A. Representative images from mesothelial clearance assays of two ovarian cancer cell lines that display strong or weak clearance activity. The extent of clearance of a ZT mesothelial monolayer (green) by OVCA433 (top) or CAOV3 (bottom) ovarian cancer spheroids (red) was imaged at 0, 4 and 8 hours after co-incubation. **B.** Quantification of clearance by ovarian tumor cell lines. Clearance area was measured in 20 established ovarian cancer cell lines by co-culturing pre-formed multicellular spheroids with ZT mesothelial cell monolayers. After 8 hours of co-incubation, the negative space created in the mesothelial monolayer by the ovarian cancer spheroid was measured and divided by the initial size of the ovarian cancer spheroid at time zero to determine the normalized clearance area. Cell lines with a normalized clearance area >1 were classified as strong/clearance-competent. Cell lines with a normalized clearance area <1 were classified as weak/clearance-incompetent. >10 spheroids scored over two replicates. **C.** Analysis of the enrichment of mRNAs associated with EMT. Heat map showing mRNA expression of genes associated with the Taube EMT core signature and three additional transcription factors that are significantly differentially expressed in the strong and weak ovarian tumor cell lines. Ovarian cancer cell line data in the left columns and manipulations to HMLE cells from Taube et al.(1) in the right columns. Both data sets were log2 transformed for visualization. ***D.*** Western Blot analysis of E-cadherin and vimentin expression in the 20 established ovarian cancer cell lines. **E, F.** Average E-cadherin (E) or vimentin (F) protein expression levels in Clearance-competent and Clearance-incompetent cell lines measured by densiometry. Error bars denote SEM. *, $p<0.05$ using Student's t-test.

Figure 4.1, cont'd.

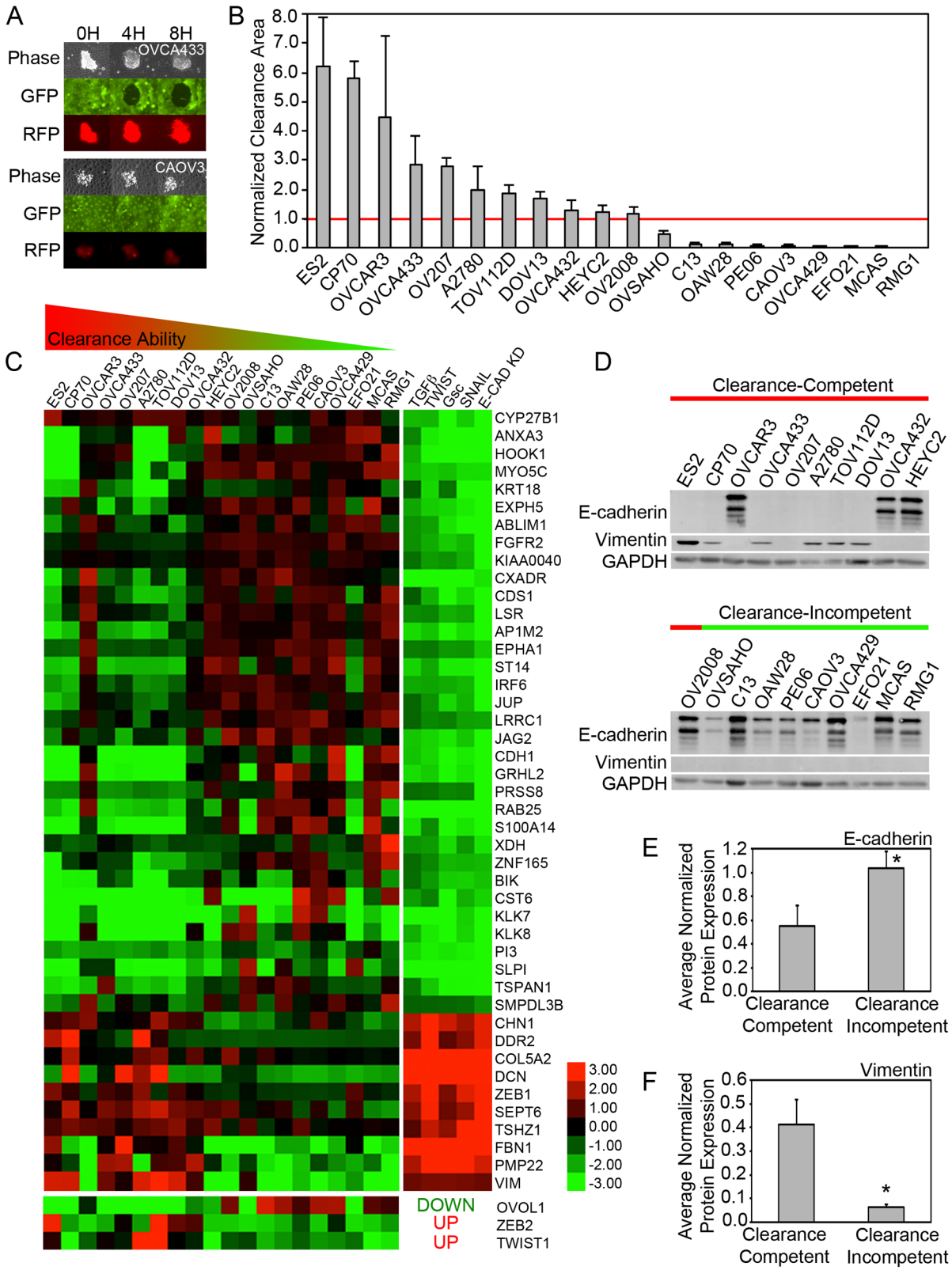

Ovarian Cancer Spheroid Clearance Ability Correlates with the Expression of Mesenchymal and Epithelial Markers:

To explore differences between cell lines with distinct clearance competencies, relative gene expression was measured in the 2O ovarian cancer cell lines using an Agilent Human 44K expression microarray. 1426 unique genes were identified that distinguished the clearance-competent cell lines from the clearance-incompetent cell lines ($p<0.05$, Supplementary Table 4.1). Enrichment analysis demonstrated that this set was enriched for genes in the GeneGo Pathway Maps: "TGFβ dependent induction of Epithelial-to-Mesenchymal Transition (EMT) via SMADs" and "regulation of epithelial-to-mesenchymal transition" ($p<7.37X10^{-5}$ and $p<5.69x10^{-4}$ respectively, GeneGo). To further validate this pathway enrichment, we analyzed the overlap between our set of differentially expressed genes and an EMT signature consisting of a 159 gene- EMT core signature (26) and 6 established EMT transcriptional regulators (TWIST1, TWIST2, ZEB2, SNAI1, SLUG, OVOL1)(27). The genes differentially regulated in clearance competent cell lines were 2.4-fold enriched for genes in the core EMT signature ($p=1.94X10^{-8}$, Figure 4.1C, fold enrichment is defined as the observed frequency divided by the expected frequency). Figure 4.1C shows that genes characteristic of a mesenchymal phenotype are enriched in the clearance-competent ovarian cancer cell lines, while genes characteristic of an epithelial phenotype are enriched in the clearance-incompetent cell lines. Interestingly, OVCA432, HEYC2 and OV2008 cells, which exhibited borderline clearance activity, expressed the weakest mesenchymal signature.

Protein expression of the epithelial marker, E-cadherin, and the mesenchymal marker, vimentin, were confirmed in the ovarian cancer cell lines by western blotting (Figure 4.1D). Consistent with the microarray data, average E-cadherin protein expression was lower in the clearance-competent cell lines compared to the clearance-incompetent cell lines (Figure 4.1E), whereas, average vimentin protein expression was higher in the clearance-competent cell lines compared to the clearance-incompetent cell lines (Figure 4.1F). Taken together, these data suggest that clearance-competent cell lines are enriched for mesenchymal markers, while clearance-incompetent cells are enriched for epithelial markers.

Over-expression of TWIST1, ZEB1 or SNAI1 Promotes Mesothelial Clearance:

To determine if mesenchymal gene programs functionally regulate mesothelial clearance, we modulated the expression of several EMT transcription factors in the ovarian cancer cell lines and measured the effects on clearance ability. First, we examined whether over-expression of the EMT transcription factors TWIST1, ZEB1, and SNAI1 in a clearance-incompetent cell line (MCAS) could promote clearance ability. TWIST1 and ZEB1 were chosen because their expression correlated significantly with clearance ability (Figure 4.1C). SNAI1 was chosen because it is known to be a strong inducer of EMT(28).

We were unable to establish stable lines of MCAS cells overexpressing TWIST1, ZEB1, and SNAI1, most likely because EMT-inducing transcription

factors can suppress proliferation when overexpressed in tumor cell lines(29-31); therefore, we inducibly over-expressed these genes in the clearance-incompetent MCAS cell line. Expression was induced for 7-14 days by supplementing the growth medium with 20nM 4-hydroxytamoxifen (OHT) (for the TWIST1 and SNAI1 vectors) or 1µg/ml Doxycycline (for the ZEB1 vector) every other day. Induction of SNAI1, ZEB1 or TWIST1 resulted in a 72-fold, 10-fold, or 3.6-fold increase in SNAI1, ZEB1 or TWIST1 mRNA, respectively (Figure 4.2A-C). The expression of several EMT markers was measured by qPCR in the SNAI1, ZEB1, and TWIST1-overexpressing cells. These markers were chosen because they were both differentially expressed in the clearance-competent and clearance-incompetent cell lines and part of Taube core EMT signature (Figure 4.1C). SNAI1 overexpression produced the most dramatic change in marker expression, inducing the mesenchymal markers TSHZ1, COL5A and FBN1 and suppressing the epithelial markers E-cadherin, MYO5C, KRT18, KRT8, ANXA3 and ST14 (Figure 4.2D). ZEB1 overexpression induced the expression of the mesenchymal markers TSHZ1 and FBN1, and decreased the expression of E-cadherin, while the expression of other epithelial markers was unchanged (Figure 4.2E). TWIST1 overexpression induced the expression of the mesenchymal marker N-cadherin and decreased the expression of the epithelial markers E-cadherin and keratin 8 (Figure 4.2F). Furthermore, phase-contrast imaging of attached cells showed that while control MCAS cells grouped in small clusters, TWIST1, ZEB1 and SNAI1 overexpressing MCAS cells were more discohesive. In addition, the SNAI1 overexpressing cells were elongated compared to control

FIGURE 4.2: Overexpression of EMT transcription factors increase mesothelial clearance ability. **A-C.** qRT-PCR measurements of mRNA levels of TWIST1(A), ZEB1(B) or SNAIL(C) in MCAS cells infected with the 'Control' WZL-empty vector, WZL-TWIST or WZL-SNAIL1 or MCAS rTTA cells infected with 'Control' FUW-LPT2 or FUW-LPT2 Zeb1. TWIST1 and SNAIL cells were treated with vehicle (un-induced) or 20nM tamoxifen (4-OHT) while ZEB1 cells treated with vehicle (un-induced) or 1µg/ml Doxycycline. **D-F.** qRT-PCR measurements of mRNA levels of EMT markers in TWIST1 (D), ZEB1 (E) or SNAIL (F) overexpressing cells. Measurements were normalized to RPLPO mRNA levels and expressed as fold changes compared to controls. Data are shown as the mean of three biological replicates for each condition. Each biological replicate was derived from an average of three technical replicates. **G.** Phase-contrast images of control, TWIST1, ZEB1 and SNAIL overexpressing MCAS cells induced with 20nM 4-OHT or 1µg/ml Doxycycline for 7-14 days. 10x magnification. **H-I.** Normalized average clearance area of ZT mesothelial monolayers 8 hours after co-culture with un-induced and 20nM 4-OHT or 1µg/ml Doxycycline induced MCAS spheroids carrying 'Control' WZL-empty vector, inducible WZL-TWIST, WZL-SNAIL, 'Control' FUW-LPT2, or FUW-LPT2 Zeb1 expression vectors. >20 spheroids averaged per condition. Error bars denote SEM. *, $p<0.05$ using Student's t-test.

Figure 4.2, cont'd.

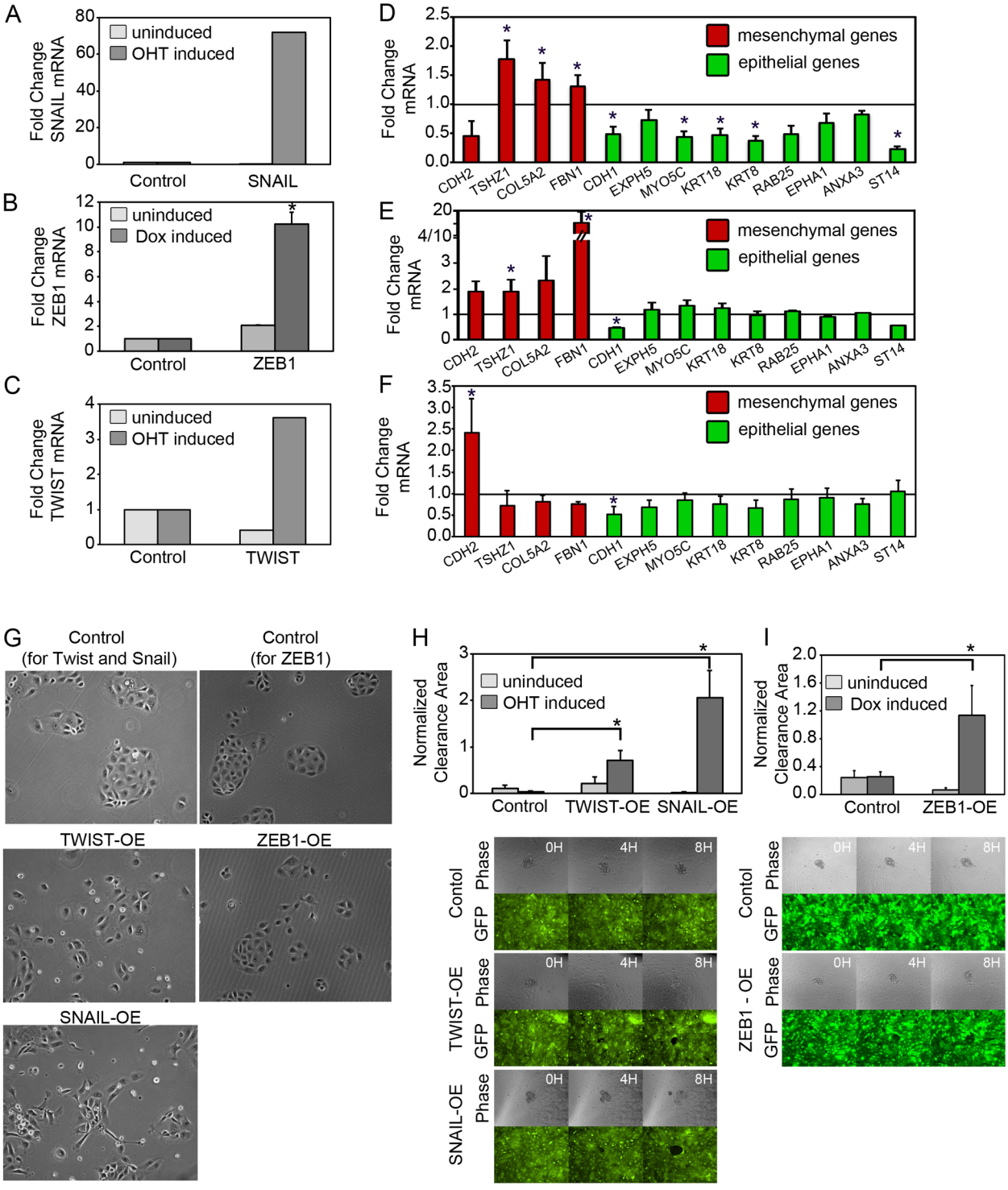

cells (FIGURE 4.2G). Failure to see a more dramatic switch in the TWIST1 and ZEB1 overexpressing cells (low fold change, only a small number of cells phenotypically different, Figure 4.2B,C and G) could reflect the fact that EMT transcription factor overexpression suppresses proliferation (32) suggesting that only a small number of cells in the population can sustain the EMT switch.

Mesothelial Clearance analysis revealed that SNAI1, ZEB1 or TWIST1 over-expression significantly increased the mesothelial clearance ability of MCAS spheroids compared to both un-transfected and un-induced controls (Figure 4.2H, 2I and Supplementary Figure 4.2) and the degree of increase in clearance ability correlated with the strength of epithelial and mesenchymal marker change (Figure 4.2D-F). Taken together, these results suggest that the over-expression of EMT transcription factors can increase mesothelial cell clearance ability. Interestingly, each transcription factor was associated with changes in a different set of mediators. This could suggest that several different mediators are involved or alternatively that mediators in addition to those assessed by QPCR are critical.

Knockdown of TWIST1 and ZEB1 Reduces Mesothelial Clearance:

To further evaluate the regulation of clearance by transcription factors that modulate EMT, we decreased the expression of EMT transcription factors in clearance-competent cell lines. Since TWIST1, ZEB1 and ZEB2 expression correlated significantly with clearance ability (Figure 4.1C), we knocked down the expression of TWIST and ZEB transcription factor family members in OVCA433 cells. Knockdown of ZEB1, TWIST1, ZEB2 and TWIST2 genes with siRNA

SMARTpools significantly decreased their respective mRNA expression levels as measured by qPCR 48 hours after treatment (Figure 4.3A-D). Western blot analysis revealed that E-cadherin protein expression was increased in both the TWIST1 and ZEB1 siRNA knockdown cells, while vimentin protein expression was unchanged (Figure 4.3I). qPCR analysis of other EMT markers revealed that ZEB1 knockdown produced the most dramatic effect, consistent with the strong level of E-cadherin protein expression; EXPH5, KRT18, KRT8 and ANXA3 mRNAs were significantly increased in the ZEB1 knockdown cells, while COL5A2 mRNA was significantly decreased (Figure 4.3E). The effects of TWIST 1 and ZEB2 knockdown on EMT marker gene expression were less significant (Figure 4.3F and G), and there was no significant marker expression change in TWIST2 knockdown cells (Figure 4.3H). The weak effects on gene expression, particularly the lack of decrease of vimentin and other mesenchymal markers, could reflect the need for a longer knockdown time to reverse the expression of the mesenchymal gene program (33, 34). Nevertheless, knockdown of TWIST1 and ZEB1 by siRNA in OVCA433 cells enhanced E-cadherin expression and several other epithelial markers; therefore we examined the effects of knockdown on mesothelial clearance.

The TWIST1, TWIST2 and ZEB1 siRNA SMARTpools significantly decreased mesothelial clearance while the ZEB2 SMARTpools did not (Figure 4.3J). To validate these findings, we tested the individual siRNAs that comprised the TWIST1, ZEB1, and TWIST2 SMARTpools for clearance inhibition; the reduction in clearance was consistent overall with the extent of knockdown for

Figure 4.3: Knockdown of EMT transcription factors or vimentin inhibit mesothelial clearance. **A-D.** qRT-PCR measurements of mRNA levels of ZEB1(A), TWIST1(B), ZEB2(C) and TWIST2(D) in OVCA433 cells transfected with siRNA SMARTpools targeting luciferase (Control), ZEB1, TWIST1, ZEB2 or TWIST2. **E-H.** qRT-PCR measurements of mRNA levels of EMT markers in ZEB1(E), TWIST1(F), ZEB2(G) or TWIST2(F) siRNA treated OVCA433 cells. Measurements were normalized to RPLPO mRNA levels and expressed as fold changes compared to controls. Data are shown as the mean of three biological replicates for each condition. Each biological replicate was derived from an average of three technical replicates. **I.** Western Blot analysis of E-cadherin and vimentin in OVCA433 cells transfected with siRNA SMARTpools targeting luciferase (Control), TWIST1 or ZEB1. **J.** Normalized average clearance area of ZT mesothelial monolayers at 8 hours after co-incubation with OVCA433 spheroids transfected with luciferase (Control), TWIST1, TWIST2, ZEB1 or ZEB2 siRNA SMARTpools. >60 positions scored per condition in three independent experiments. **K.** qRT-PCR measurements of mRNA levels of ZEB1 in OVCA433 cells transfected with empty vector control (LKO) or shRNAs targeting ZEB1 (1, 2, 4, 5). **L.** Western Blot analysis of E-cadherin and vimentin in OVCA433 cells transfected with empty vector control (LKO) or shRNAs targeting ZEB1 (1, 2, 4, 5). **M-P.** qRT-PCR measurements of mRNA levels of EMT markers in OVCA433 cells transfected with ZEB1 shRNA 1 (M), shRNA 2 (N), shRNA 4 (O), or shRNA 5 (P) normalized to control (LKO) marker expression. **Q.** Normalized average clearance area of ZT mesothelial monolayers at 8 hours after co-incubation with OVCA433 spheroids transfected with empty vector control (LKO) or shRNAs targeting ZEB1 (1, 2, 4, 5). >60 positions scored per condition in three independent experiments. **R.** Western Blot analysis of E-cadherin and vimentin in OVCA433 cells transfected with siRNA SMARTpools targeting luciferase (Control) or vimentin. **S.** Normalized average clearance area of ZT mesothelial monolayers at 8 hours after co-incubation with OVCA433 spheroids transfected with siRNA SMARTpools targeting luciferase (Control) or vimentin. >60 positions scored per condition in three independent experiments. Error bars denote SEM. *, $p<0.05$ using Student's t-test.

Figure 4.3, cont'd.

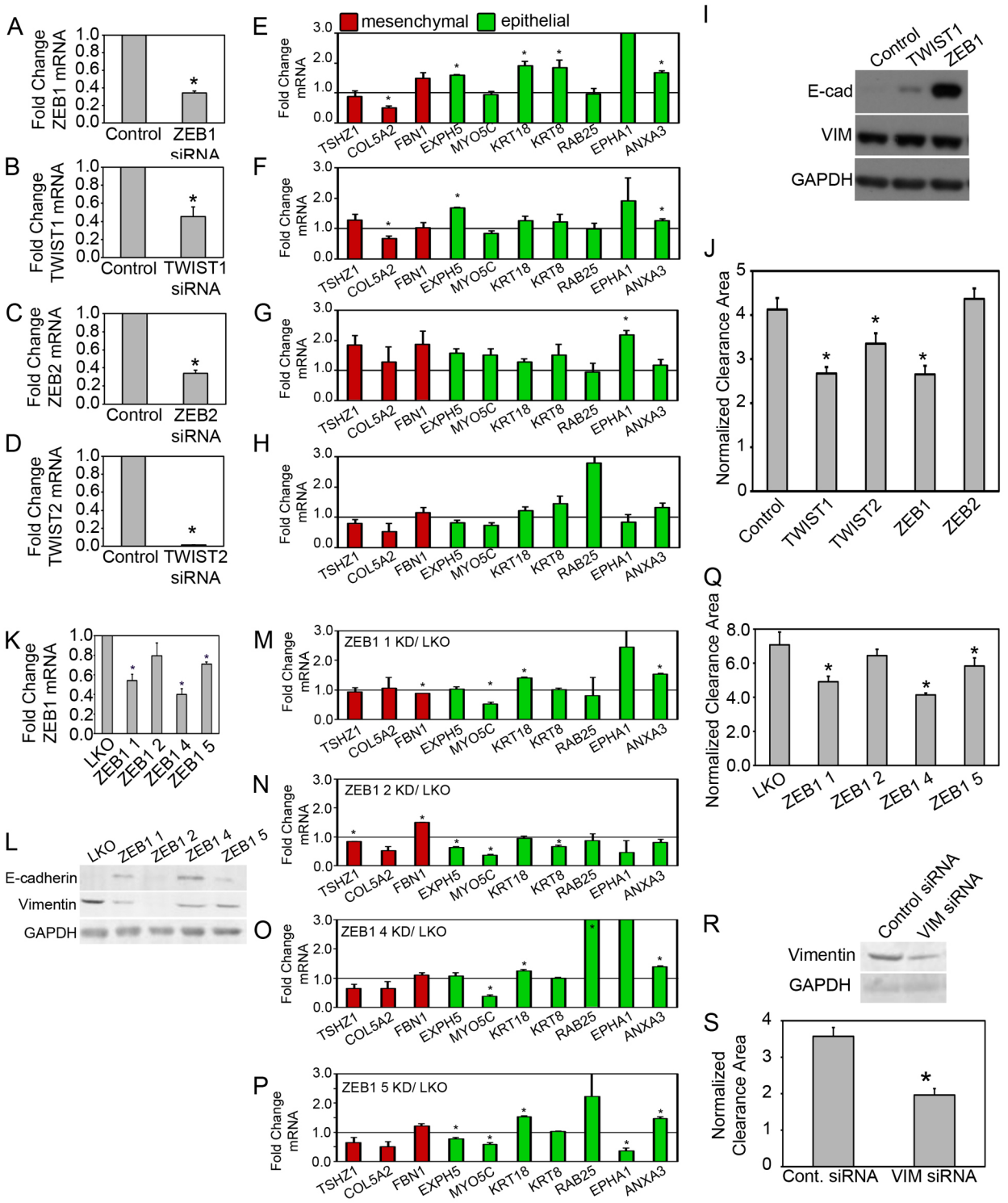

TWIST1 and ZEB1, but not TWIST 2 (Supplementary Figure 4.3). Finally, ZEB1 expression was knocked down using shRNA-expressing lentiviral vectors. Three of the four hairpins significantly decreased ZEB1 mRNA expression (Figure 4.3K). Western blot analysis revealed that E-cadherin expression was increased and vimentin expression was decreased in the cells with reduced ZEB1 expression (Figure 4.3L). While there was variation in the extent of up- or down-regulation of EMT markers, overall the expression of mesenchymal genes was decreased and the expression of epithelial genes were increased in the cells with significant ZEB1 down-regulation (Figure 4.3M-P). Consistent with the clearance results for the siRNA knockdown cells, ZEB1 down-regulation by shRNA significantly decreased mesothelial clearance (Figure 4.3Q). Knockdown of TWIST1 in OVCA433 cells using shRNA-expressing lentiviral vectors decreased mesothelial clearance and the expression of mesenchymal markers, and the decrease in clearance correlated with the extent of knockdown (Supplementary Figure 4.4). siRNA knockdown of TWIST1 and ZEB1 in a second cell line, OVCA432, also significantly decreased mesothelial clearance (Supplementary Figure 4.5). Taken together, these results suggest that TWIST1 and ZEB1 are required for efficient mesothelial clearance in OVCA433 and OVCA432 cell lines and that reduction in these transcription factors increases the epithelial phenotype of ovarian tumor cells lines.

Vimentin Regulates Mesothelial Clearance Ability:

Vimentin, an intermediate filament protein and downstream effector of EMT transcription factors (27) is enriched in the clearance-competent ovarian cancer cell lines (Figure 4.1). Because vimentin expression has been implicated in cell motility(35), we wanted to determine if vimentin could also regulate mesothelial clearance. Vimentin expression was reduced in OVCA433 cells using siRNA SMARTpools, causing a down-regulation of vimentin protein expression and significantly decreased mesothelial clearance. (Figure 4.3R and 3S, respectively). Furthermore, knockdown of vimentin using shRNA hairpins significantly decreased mesothelial clearance, as well (Supplementary Figure 4.6). In support of this data, vimentin knockdown in CP70 cells also decreased mesothelial clearance (Supplementary Figure 4.7).

Differential Clearance Ability in Primary Ovarian Cancer Cells from the Ascites Fluid of Ovarian Cancer Patients correlates with the Expression of E-cadherin and Vimentin:

To determine if similar correlations between clearance activity and epithelial or mesenchymal phenotypes could be observed in primary ovarian cancer cell samples, we examined mesothelial clearance activity of primary serous papillary ovarian tumor cells derived from ascites fluid of 21 patients with high-grade serous ovarian cancer (DF9, DF14, DF24, DF29, DF43, DF59, DF68, DF106, DF118, DF141, DF143, DF147, DF155, DF160, DF163, DF164, DF166, DF168, DF172, DF173, DF176). This was greatly facilitated by the development of WIT-

OC medium, which maintains the viability of primary tumor cells. Minimally processed frozen vials of primary ovarian cancer cells were plated on tissue culture plastic for 48 hours. The attached cells were trypsinized and divided into three aliquots. One aliquot was plated on untreated tissue culture plates for 24 hours and then lysed for Western Blot and Reverse Phase Protein Array (RPPA) analysis to measure the expression of epithelial and mesenchymal markers. A second aliquot was plated on poly-HEMA coated culture dishes and grown in suspension for 24 hours before being lysed for marker analysis. The third aliquot was plated, 100 cells per well, in 96-well poly-HEMA-coated culture dishes to form multicellular spheroids and after 16 hours in suspension the spheroids were analyzed for clearance activity (Figure 4.4A). After eight hours of co-culture in the Mesothelial Clearance assay, 14 of the primary cell lines were clearance-competent (normalized clearance area >1), while seven of the primary cell populations were clearance-incompetent (normalized clearance area <1)(Figure 4.4B, Supplementary Figure 4.8, Supplementary Movie 4.2). Cells from several representative clearance competent DF cell populations (DF143, 164, and 163) were stained for Pax8 (a mullerian marker expressed by serous papillary ovarian tumors (36-39)) after spreading on mesothelial monolayers or glass; all of these lines expressed nuclear Pax8, confirming the ovarian carcinoma origin of clearance-competent cells (Supplementary Figure 4.9). Quantification of the levels of expression of E-cadherin and vimentin from Western blot analyses revealed a significant enrichment of E-cadherin in the clearance-incompetent DF lines, while vimentin was enriched in the clearance-competent DF tumor cells

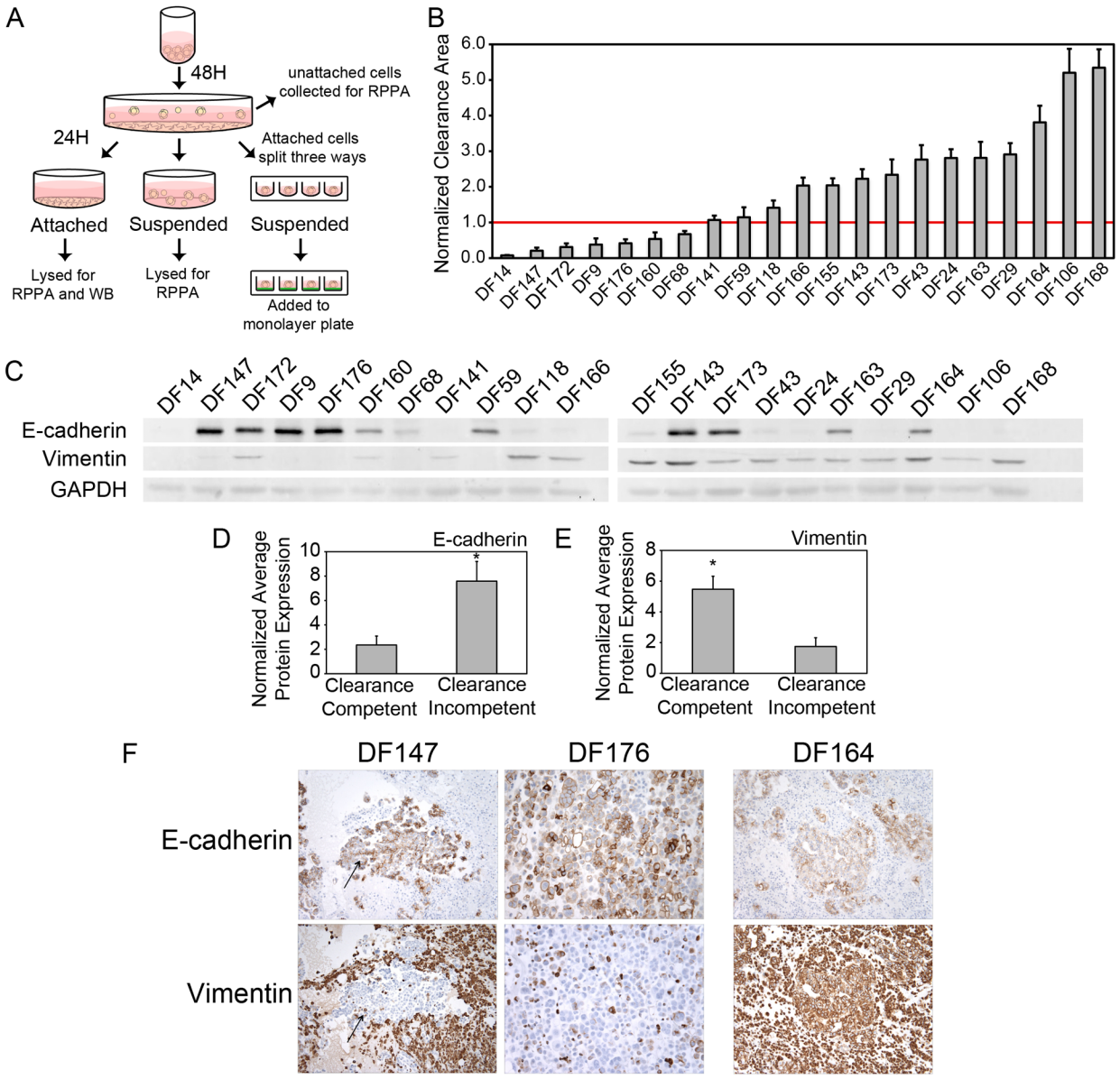

FIGURE 4.4: Spheroids from primary ovarian cancer cell lines display differential clearance ability that correlates with epithelial and mesenchymal marker expression. A. Schematic outlining the treatment of the DF primary cell populations. **B.** Normalized clearance area was measured in 21 primary ovarian cancer cell populations. Samples with an average normalized clearance area >1 were characterized as strong/ clearance-competent. Samples with an average normalized clearance area <1 were characterized as weak/ clearance-incompetent. >20 spheroids were analyzed per condition. **C.** Western blot analysis of E-cadherin and vimentin expression in 21 primary ovarian cancer cell lines. **D, E.** Average E-cadherin (D) or vimentin (E) protein expression levels in Clearance-competent and Clearance-incompetent cell lines measured by densiometry. **F.** Immunohistochemical analysis of sections from paraffin-embedded blocks of cells from the original ascitic fluid that the DF cell populations were derived from. Sections were stained with antibodies directed against E-cadherin or vimentin. Representative images from sections from weak (DF147 and DF176) and strong (DF164 and DF143) primary cells. The E-cadherin and vimentin images from DF147 and DF164 were from the same area of the tumor; however the tumor cells in the DF176 tumors were so discohesive that it wasn't feasible to find the same cells in both sections. All of the cell blocks were stained with Pax8 to confirm the Müllerian identity of the tumor cells (data not shown). Error bars denote SEM. *, $p<0.05$ using Student's t-test.

(Figure 4.4C, D and E). These results strongly support the findings from the established ovarian cancer cell lines.

We also examined the expression of E-cadherin and vimentin by immunofluorescent staining of sections from the cell blocks of the ascitic fluid from which the DF cell populations were derived. Figure 4.4F shows representative images of DF147, DF176, DF164 and DF143 tumor samples. Consistent with the western blot data, ovarian cancer cells from DF174 and DF176, two clearance-incompetent cell populations, were positive for E-cadherin, but not vimentin, while ovarian cancer cells from DF164, a clearance-competent line, strongly stain for vimentin and only weakly stain for E-cadherin. The stromal and hematopoietic cells in samples DF147 and DF164 express high levels of vimentin. These cells were likely cleared by the filtration step that was used for processing the ascitic fluid samples since there were low levels of vimentin in the cultured DF147 cells.

Protein Expression Profile of Clearance-Competent and Clearance-Incompetent Primary Ovarian Cancer Spheroids

To better characterize the primary tumor samples, the expression levels of 151 proteins and phosphoproteins representing major signaling pathways and some EMT marker proteins were measured in the 21 primary ovarian cancer cell populations using reverse phase protein arrays. To identify the proteins that are differentially expressed between primary cell populations with different levels of clearance activity, a multiple linear regression model was constructed using the

normalized clearance area data from the mesothelial clearance assay and the relative protein expression data from the RPPA analysis. In this analysis, only cell populations with a clearance-competent value >2.5 or a clearance-incompetent value <1.0 were used. Figure 4.5A shows a heatmap with the antibody probes that have a significant linear relationship ($p<0.05$) with normalized clearance area. Consistent with the above findings, epithelial proteins, including E-cadherin, claudin 7, and HER3 are enriched in the primary cell populations that display the weakest clearance activity. Mesenchymal markers are not well represented in the list of antibodies available for RPPA analysis, so the expression of mesenchymal proteins could not be evaluated in this analysis. Interestingly however, YAP, which induces EMT when over-expressed in mammary epithelial cells(40), is strongly correlated with clearance competent cell populations. eEF2 and eEEF2 kinase are also enriched in this population.

The RPPA data described above was derived from primary ovarian cancer cells that were able to initially attach to a cell culture dish 48 hours after thawing from a stock vial. For several of the primary cell populations, a proportion of the cells were unable to attach to the culture dish after 48 hours. These nonadherent cells did not display activity in the mesothelial clearance assay (data not shown). Interestingly, the protein expression profiles of the non-attached cell populations derived from the clearance-competent cell populations are strikingly similar to the protein expression profiles of the clearance-incompetent DF populations (being enriched for epithelial markers and other proteins in this signature), and clearly distinguished from the cell populations from the same tumor that initially attached

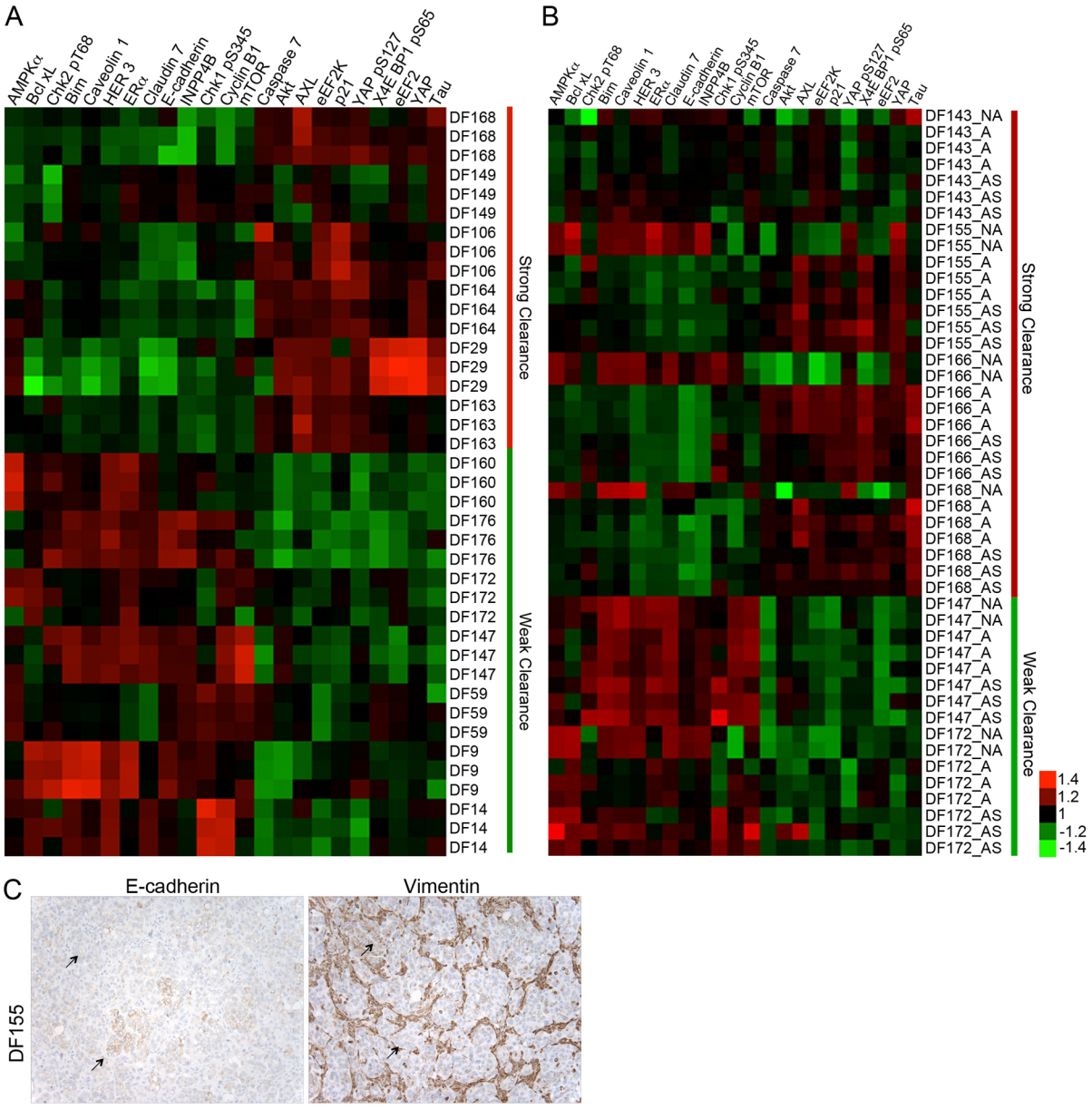

FIGURE 4.5: RPPA analysis reveals distinct populations of cells within some primary ovarian cancer cell lines. A. RPPA analysis of the DF ovarian tumor cell populations. Antibodies that distinguish clearance-competent (normalized clearance area >2.5) and clearance-incompetent lines (normalized clearance area < 1.0) are shown ($p<0.05$, Student's t-test). **B.** RPPA analysis of four clearance-competent and two clearance-incompetent ovarian cancer cell lines. Antibodies were chosen based on analysis in A. NA – population of cells that did not attach to the tissue culture dish 48 hours post thawing. A – population of cells that attached to the tissue culture dish 48 hours post thawing. AS – population of cells that attached to the tissue culture dish 48 hours post thawing followed by 24 hours of incubation in suspension in poly-HEMA coated culture dishes. **C.** Immunohistochemical analysis of sections from the primary tumor DF155. Tumor sections were stained with antibodies directed against E-cadherin or vimentin.

to tissue culture plates (Figure 4.5B). In contrast, for those tumors in which the attached cells were classified as clearance-incompetent, the protein expression pattern of the unattached population and attached population of the same cell line were indistinguishable (Figure 4.5B).

Figure 4.5C shows histology sections from the DF155 primary tumor (one of the tumors in which the ascites samples displayed heterogeneous cell populations with differential abilities to attach to culture plates) stained for both E-cadherin and vimentin. Both E-cadherin and vimentin were focally expressed in some, but not all, of the ovarian cancer cells. E-cadherin and vimentin expression was almost entirely mutually exclusive (see arrows), supporting the existence of two distinct tumor populations. Taken together, these results suggest that primary ovarian cancer effusions contain a heterogeneous population of cells with differential ability to clear monolayers and cells that exhibit mesenchymal markers display the strongest clearance activity.

Mesenchymal Gene Signature in Patients with Epithelial Ovarian Cancer

We compared the gene expression profiles of ovarian tumors in the Tothill data set to the EMT signature defined in Figure 4.1 and found that 21% (59/285) of the tumors expressed the EMT signature (Figure 4.6A). This group displayed significantly reduced overall and relapse-free survival compared to all other patients in this study (Figure 4.6B). This analysis indicates that there is a specific subtype of epithelial ovarian cancers that displays mesenchymal characteristics and mesenchymal characteristics correlate with reduced survival.

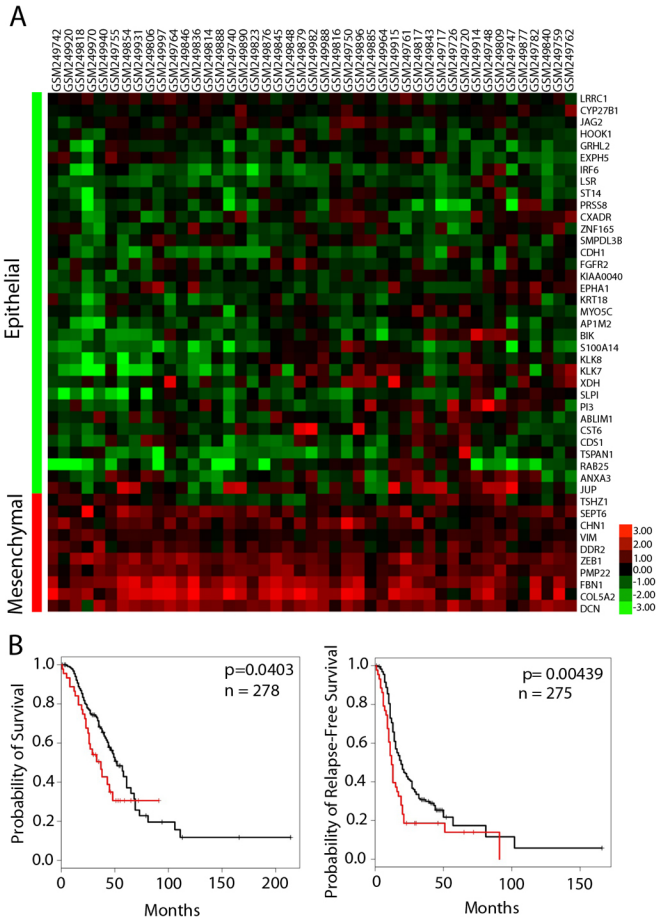

FIGURE 4.6: Mesenchymal gene signature in ovarian cancer data sets. A. Samples in the Tothill Ovarian Data Set that significantly overlap with the EMT signature in Figure 1. **B.** Probability of survival (left) and relapse-free survival (right) in EMT signature overlapping (red) versus non-overlapping (black) Tothill samples.

Discussion:

In this study, we conducted a comprehensive analysis of the gene and protein expression profiles of ovarian cancer spheroids with differential mesothelial clearance abilities. Using 20 ovarian tumor cell lines, we identified a gene expression profile that correlated with mesothelial clearance activity. The expression of genes in an EMT core signature was enriched in the cell lines that showed strong mesothelial clearance activity compared to those with weak or undetectable activity. This pattern was validated in primary tumor cell cultures using several EMT markers; vimentin (a mesenchymal marker) was expressed at higher levels in primary cells with high clearance activity, while E-cadherin, claudin 7, and HER3 (epithelial markers) expression was increased in primary cells with low clearance activity. These correlations were detected even in subpopulations within individual primary tumor cell samples. Thus, these studies provide insights into the molecular features that correlate with mesothelial invasive ability.

EMT is defined as a process in which apico-basal-polarized, immotile, epithelial cells that are attached together by cell-cell junctions are converted to planar-polarized, migratory, mesenchymal-like cells with weaker cell-cell adhesion. EMT occurs throughout development, most notably during gastrulation when cells in a single germ layer migrate to produce three germ layers and during vertebrate nervous system development when epithelial cells located near the dorsal midline of the neural tube are converted to mesenchymal cells that migrate to distinct regions within the embryo(41). It has been proposed that

cancer cells hijack EMT transcriptional programs to dissociate from the primary tumor, intravasate and extravasate through the blood or lymphatic systems to colonize distant sites(27). Ovarian cancer cells do not face these barriers to metastasize to the peritoneum; instead, they are displaced from primary tumors directly into the peritoneal cavity, where they can transit to other peritoneal tissues and then invade through the mesothelial lining to colonize new sites.

Our studies indicate that EMT transcription factors promote mesothelial invasion by ovarian cancer cells. Over-expression of SNAI1, ZEB1 or TWIST1 in clearance-incompetent cell lines significantly increased mesothelial clearance ability. Conversely, inhibition of TWIST1 and ZEB1 in clearance competent ovarian cancer cell lines significantly decreased mesothelial clearance. A recent study reported a correlation between expression of CD157, an ectoenzyme regulating leukocyte diapedesis, expression of mesenchymal markers, and enhanced mesothelial invasion in ovarian cancer cells(42). Previous reports have used Boyden chamber migration assays to examine the role of EMT transcription factors in modulating other phenotypic aspects of the invasive behavior of ovarian tumor cell lines. For example, down-regulation of SNAI1 or TWIST1 expression in ES2 or HEY cells, respectively, suppressed invasion through Matrigel(43, 44). Similar differences in invasive behavior caused by EMT transcription factor modulation have been described in many other tumor cell lineages (reviewed in(45, 46)).

Recently, Kwon et al. correlated the ability of ovarian cancer spheroids to remodel extracellular matrices with the expression of epithelial and mesenchymal

markers(47). They divided the cell lines into two groups: one that remodeled the ECM by degradation and one that remodeled the ECM by ROCK-mediated reorganization. The authors suggested that ovarian cancer cells could use two distinct strategies to remodel ECM during ovarian cancer metastasis. Interestingly, the cell lines that employed ROCK-mediated reorganization of the ECM expressed mesenchymal markers, including N-cadherin and vimentin, while the cell lines that remodeled the ECM via degradation expressed epithelial markers, including E-cadherin and pan-keratin. Our results suggest that only mesenchymal-like cells are able to clear the mesothelial monolayer and gain access to the underlying ECM. Therefore, in the context of metastasis, the ECM would be remodeled by ROCK-mediated reorganization by the mesenchymal-like cells. The ECM under the mesothelial monolayers would only be degraded via proteolysis if the invasive mesenchymal-like cells revert to an epithelial-like phenotype after implantation.

While we have shown that tumor cells that express genes associated with a mesenchymal program display more effective mesothelial clearance, *in vitro,* the contribution of these cells to ovarian cancer progression remains unclear. Studies have found that higher SNAI1 or TWIST expression in primary ovarian carcinomas, ovarian cancer effusions and metastases are associated with shorter overall and progression free survival(48-52). In addition, the expression of SNAI1 and TWIST1 are significantly higher in later stage (III and IV) compared to early stage ovarian tumors(48, 53). Consistently, increased expression of E-cadherin is associated with better survival, while loss of E-cadherin expression is

associated with poor survival in several studies(50, 54-56).

Tothill et al. used gene-expression profiling to characterize 285 well-annotated serous and endometrioid invasive ovarian, fallopian tube, and peritoneal cancers and defined six subgroups with distinct molecular and histopathologic characteristics(57). One subgroup expressed genes associated with mesenchymal development (including increased expression of homeobox genes, WNT/h-catenin pathway components, and N- and P-cadherin). Interestingly, this subgroup displayed poorer overall survival than four of the five other subgroups. When we compared the gene expression profiles of the ovarian tumors in the Tothill study to the clearance-associated EMT signature defined in Figure 4.1, we found that 21% (59/285) of the tumors expressed this EMT signature (Figure 4.6). This group displayed significantly reduced overall and relapse-free survival compared to all other patients in this study (Figure 4.6). The decreased survival in this tumor subgroup may be due, at least in part, to the increased ability of these cells to invade into the mesothelial lining of peritoneal cavity organs. However, given that ovarian tumors show intratumoral heterogeneity with respect to epithelial and mesenchymal markers (as detected in tumor DF155 in our study), analyses involving RNA or protein expression of the total population of cells may mask the existence of mesenchymal cells that could contribute to mesothelial clearance. It remains to be established whether inhibitors that block intercalation will be useful clinically to prevent new metastases, and their associated complications, following surgical debulking of peritoneal masses.

Our study provides insight into the molecular mechanisms that mediate mesothelial clearance by ovarian cancer multicellular spheroids. We have shown that ovarian cancer spheroids that display mesenchymal characteristics are more efficient at clearing a mesothelial monolayer. Furthermore, we found heterogeneity with respect to the expression of mesenchymal markers and competence for mesothelial clearance in primary tumor populations. These studies raise the possibility that inhibition of the mesenchymal program could reduce seeding of new metastatic lesions following surgical debulking.

Acknowledgements:

We would like to thank Yiling Lu and Doris Siwak (M.D. Anderson Cancer Center) for performing the RPPA studies; Jennifer Waters and the Nikon Imaging Center at Harvard Medical School for support on the microscopy studies; and Kong-Jie Kah and Robert Weinberg for kind donation of the ZEB1 overexpression construct. We also thank Ghassan Mouneimne for review of the manuscript and helpful discussions and Grace Gao for lab management. RPPA was performed at the MD Anderson RPPA Core Facility (supported by NIH grant CA016672). These studies were supported by the Dr. Miriam and Sheldon G. Adelson Medical Research Foundation (JB and RD), the Ovarian Cancer Research Fund (RD), the Honorable Tina Brozman Foundation (RD), the Robert and Debra First Fund (RD), the Gamel Family Ovarian Cancer Research Fund (RD), the Susan F. Smith Center for Women's Cancers at the Dana-Farber Cancer Institute (RD).

Methods:

Cell Culture:

Established Cell Lines.

All of the established ovarian cancer cell lines as well as the ZT mesothelial cells were cultured in a 1:1 ratio of medium MCDB 105 (Cell Applications, INC) and Medium 199 (GIBCO) supplemented with 10% FBS (GIBCO) and 5% pen-strep. The established ovarian cancer cell lines were a gift from Dr. Dennis Slamon (University of California, Los Angeles). ZT mesothelial cells were obtained from a benign pleural effusion. These cells were immortalized by ectopic expression of SV40 T antigen and over-expression of human telomerase (fused to GFP) as previously described. (58, 59).

Primary Tumor Cells.

With institutional review board approval, primary ovarian carcinoma cells (DF lines) were isolated directly from peritoneal paracentesis of patients with advanced-stage ovarian cancer at the time of initial cytoreductive surgery, as previously described(60, 61). Red blood cells were lysed as previously described(62). Only samples that were >80% pure tumor cells were used. In cases where there was more heterogeneity, the samples were enriched for tumor cells by filtration using a 40-μm nylon cell strainer (BD Falcon, San Jose, CA) to isolate tumor cell spheres. Tumor cells were frozen after isolation and aliquots were thawed and cultured in WIT-OC medium(63) as needed for the experiments described.

Mesothelial Clearance Assay:

Preparation of Spheroids and Mesothelial Monolayer. The mesothelial clearance assay was performed as previously described(25) with minor alterations. Briefly, to generate multicellular spheroids, ovarian cancer cells were dissociated by trypsinization, re-suspended in cell culture medium and counted. 100 cells per well were plated in poly-HEMA coated 96-well round bottom plates (Corning) and the plates were incubated at 37°C for 16 hours to promote spheroid formation. Concurrently, 5,000 ZT mesothelial cells per well were plated on fibronectin (5ug/ml, Sigma)-coated 384 well glass-bottom culture dishes (Corning). The mesothelial cells were incubated at 37°C for 16 hours to form confluent monolayers. After the 16-hour incubations, the ovarian cancer multicellular spheroids were transferred to the wells containing the mesothelial monolayers.

Live Cell Imaging.

Imaging was performed using a Nikon Ti-E Inverted Motorized Widefield Fluorescence Microscope with integrated Perfect Focus System and low (20x-0.75 NA) magnification/NA DIC optics, Nikon halogen trans illuminator with 0.52 NA LWD condenser, Nikon fast (<100ms switching time) excitation and emission filter wheels, Sutter fast transmitted and epi-fluorescence light path Smart shutters, Nikon linear-encoded motorized stage, Hamamatsu ORCA-AG cooled CCD camera, custom-built microscope incubation chamber with temperature and CO2 control, Nikon NIS Elements AR software v3 and TMC vibration-isolation table. Over 20 spheroids were imaged per condition. Phase and GFP images

were captured every 10 minutes for 8 hours.

Quantification of Mesothelial Clearance Area. The non-fluorescent area, created by the invading spheroid, in the GFP mesothelial monolayer images was measured at eight hours and divided by the initial area of the cancer spheroid at time zero. All measurements were taken using Nikon NIS Elements software.

Quantification of Percent Hole Formation. For each condition, after eight hours of co-incubation, the number of positions with a mesothelial clearance area >1 were counted, divided by the total number of positions, and multiplied by 100.

Microarray Analysis:

Microarray hybridizations were performed in the ovarian cell lines at baseline using the Agilent Human 44K array chip. Briefly, cells were grown to log phase and then RNA was extracted using the RNeasy Kit (Qiagen, Valencia, CA, USA). The purified RNA was eluted in 30-60 µl diethylpyrocarbonate (DEPC) water and the quantity of RNA was measured by spectral analysis using the Nanodrop Spectrophotometer (NanoDrop Products, Wilmington, DE, USA). RNA quality was determined by separation of the RNA via capillary electrophoresis using the Agilent 2000 Bioanalyzer (Agilent Technologies, Santa Clara, CA, USA). Characterization of individual ovarian cancer cell line transcripts was performed by comparison with a mixed reference cRNA pool consisting of equal amounts of RNA from 40 ovarian cancer cell lines and was conducted on a single slide in

which the cell line mixture RNA was labeled with cyanine-3 and RNA from the individual cell line was labeled with cyanine-5. Microarray slides were read using an Agilent Scanner and the Agilent Feature Extraction software version 7.5 was used to calculate gene expression values. Data was pre-filtered using a p-value threshold of $p<0.01$ in at least one cell line and differentially expressed genes were identified using the limma package of bioConductor R and a p-value threshold of 0.05.

Enrichment was assessed in two ways: 1) differentially expressed genes were assessed for enrichment of GeneGO categories using GeneGO software (http://www.genego.com). 2) The differentially expressed genes were merged to an EMT signature consisting of the Taube EMT core signature(26) and 6 additional transcription factors ('SNAI1','SNAI2','ZEB2','TWIST1','TWIST2','OVOL1'). The background population set was the 15,900 unique genes after pre-filtering the ovarian cell line data. Enrichment p-values were calculated with hypergeometric distribution implemented in the phyper function in R. Fold enrichment was defined as the observed frequency divided by the expected frequency. Hierarchical cluster diagrams were built using a Pearson uncentered distance measure under average linkage rules in Cluster (v.3.0) and visualized in Java Tree View (v1.1.0).

Survival Analysis:

The EMT signature was merged to the Tothill data downloaded from GEO (GSE9891)(57) using Affymetrix gene identifiers. In order to deal with multiple

probes per gene, the probe with the highest variance was selected. Patients were divided into two groups based on correlation or lack of correlation with the EMT signature; samples with the EMT signature were defined as Spearman ρ =>.295 ($p<0.05$). Kaplan-Meier curves were generated using the survival package in R. Log Rank p-values were computed with the survdiff function.

Western Blot Analysis:

Cells were lysed in RIPA buffer (50mM HEPES pH 7.4, 1% Triton X-100, 1% sodium deoxycholate, 0.1% SDS, 0.1M NaCl, 1mM sodium orthovanadate, 0.1M sodium pyrophosphate, 100mM NaF and 1mM PMSF). Lysates were clarified by centrifugation at 13,000g for 10 minutes at 4°C, protein concentration was quantified using the BCA assay (Pierce) and absorbance was read on a BioTEK Micro-Volume Spectrophotometer System (Epoch). 15ug lysates were boiled in 1x sample buffer (0.04M Tris-HCl pH 6.8, 1% SDS, 1% β-mercaptoethanol and 10% glycerol) for 10 minutes and resolved by SDS-PAGE. Proteins were transferred to Immobilon membranes (Whatman) and blocked with 5% BSA in PBS (140mM NaCl, 0.27mM KCl, 0.43mM Na_2HPO_4, 0.14mM KH_2PO_4 pH 7.3) for 30 minutes at room temperature. Membranes were incubated overnight at 4°C with one or more of the following antibodies: anti-E-cadherin monoclonal antibody (1:1000, BD), anti-vimentin polyclonal antibody (1:1000, Cell Signaling), anti-GAPDH polyclonal antibody (1:20000, Abcam), or anti-tubulin polyclonal antibody (1:20000, Abcam). Membranes were then probed with secondary antibodies linked to horseradish peroxidase (HRP, 1:5000, Santa Cruz) or

secondary antibodies linked to fluorophores (1:5000, LI-COR) Western Blot membranes incubated with HRP were developed using an enhanced chemiluminescent substrate (VWR) and visualized using a Kodak film developer and an Epson 3000 scanner. Fluorophore treated Western Blot membranes were visualized using the Odyssey Imaging System (LI-COR Biosciences). Protein expression levels were quantified from the Western Blot membranes visualized using the Odyssey imaging system by measuring the mean pixel density of the band in question, using Image J software, and dividing by the mean pixel density of the corresponding loading control band.

cDNA plasmids, siRNAs, shRNAs:

To ectopically express TWIST1 or SNAI1, the retroviral vector (pWZL Blast ER) encoding the genes for TWIST1 or SNAI1, were transfected into MCAS and RMG1 ovarian cancer cells (Addgene plasmids 18799 and 18798, respectively). Cells were selected in 50ug/ml Blasticidin and induced with 20nM 4-OHT for 7 day. siRNA SMARTpools against TWIST1, TWIST2, ZEB1, ZEB2, vimentin, and E-cadherin were used to attenuate the expression of the corresponding genes (Dharmacon). Lentiviruses lacking an shRNA sequence (pLKO) as a control, or plasmids containing TWIST1 hairpins (OpenBiosystems; G11 seq: 5'-CCGG-CGCCTTCTCGGTCTGGAGGAT-CTCGAG-ATCCTCCAGACCGAGAAGGCG-TTTTT-3', G12 seq: 5'-CCGG-TCCGCAGTCTTACGAGGAGCT-CTCGAG-AGCTCCTCGTAAGACTGCGGA-TTTTT-3') were used to attenuate the expression of TWIST1 in OVCA433 cells. Lentiviruses lacking an shRNA

sequence (pLKO) as a control, or plasmids containing vimentin hairpins (OpenBiosystems; A11 seq:5'-CCGG-GCTAACTACCAAGACACTATT-CTCGAG-AATAGTGTCTTGGTAGTTAGC-TTTTT-3', B1 seq: 5'-CCGG-GCAGGATGAGATTCAGAATAT-CTCGAG-ATATTCTGAATCTCATCCTGC-TTTTT-3', B2 seq: 5'-CCGG-CGCCATCAACACCGAGTTCAA-CTCGAG-TTGAACTCGGTGTTGATGGCG-TTTTT-3', B3 seq: 5'-CCGG-GACAGGTTATCAACGAAACTT-CTCGAG-AAGTTTCGTTGATAACCTGTC-TTTTT-3') were used to attenuate the expression of vimentin in OVCA433 cells. Lentiviruses lacking an shRNA sequence (pLKO) as a control, or plasmids containing ZEB1 hairpins (Arizona State University; 1 seq: CCGGGCAACAATACAAGAGGTTAAACTCGAGTTTAACCTCTTGTATTGTTGC TTTTT, 2 seq: CCGGGCTGCCAATAAGCAAACGATTCTCGAGAATCGTTTGCTTATTGGCAG CTTTTT, 3 seq: CCGGCCTCTCTGAAAGAACACATTACTCGAGTAATGTGTTCTTTCAGAGAGG TTTTT, 4 seq: CCGGGCTGTTGTTCTGCCAACAGTTCTCGAGAACTGTTGGCAGAACAACAG CTTTTT) were used to attenuate the expression of ZEB1 in OVCA433 cells. Lentivirus infected cells were selected in medium containing 1ug/ml puromycin (Dulbecco).

Quantitative Real Time PCR:

RNA was isolated from ovarian cancer cells using the Trizol reagent (Invitrogen) according to the manufacturers instructions. The RNA was reverse transcribed into cDNA using the qScript cDNA Synthesis Kit (Quanta) according to the manufacturers instructions. cDNA levels were quantitated by the SYBR green method on the T900HT (Life Technologies) in a 384-well format. Triplicate samples were quantified along with minus RT and minus template controls. Amplification was continued for 40 cycles as follows: 94 °C – 10 s, 55 °C – 15 s, 65 °C – 30 s. Relative expression was determined by normalizing to the PRLPO endogenous control.

Reverse Phase Protein Array:

A vial of primary ovarian cancer cells from each of the DF lines was thawed and plated on 10cm cell culture dishes. After 48 hours, the attached cells were trypsinized and split into 3 wells of a 6 well cell culture dish. Cells were allowed to re-attach over night to form confluent monolayers. RPPA analysis was performed as previously described(64). Briefly, cells were collected by washing with ice-cold PBS, scrapping and centrifugation at 900g at 4°C for 10 minutes. Pellets were resuspended in RPPA lysis buffer (1% Triton X-100, 50mM HEPES, pH 7.4, 150 mM NaCl, 1.5mM $MgCl_2$, 1mM EGTA, 100mM NaF, 10mM NaPPi, 10% glycerol, 1mM Na_3VO_4, and protease inhibitor (Roche) and incubated on ice with occasional shaking for 20 minutes. The lysates were centrifuged at 13,000g, 4°C for 10 minutes. Lysed proteins were denatured by adding 1% SDS and boiling for

5 minutes. Each sample was diluted in five 2-fold serial dilutions and printed onto nitrocellulose-coated glass slides (Grace Biolabs Bend Oregon) with an automated robotic Aushon arrayer (Aushon Biosystems Ballerica MA). Each slide was probed with a validated primary and secondary antibody, as described(64); 151 antibodies were used in total. Signal intensity was measured by scanning the slides with ImageQuant (Molecular Dynamics, Sunnyvale, CA) and quantified using the MicroVigene automated RPPA module (VigeneTech, Inc., North Billerica, MA). Relative protein levels were then determined for each sample. Signal intensity data were collected and analyzed using software specifically developed for RPPA analyses (http://www.VigeneTech.com). Log transformed intensity data were subjected to Students t-tests in bioConductor R. Significant antibody probes were defined as $p<0.05$. Log transformed and centered heatmaps were generated using Cluster 3.0 and Java TreeView 1.1.1.

Immunohistochemistry (IHC):

After institutional review board approval, sections of formalin-fixed, paraffin-embedded (FFPE) cell blocks (CBs) were obtained from the Cytology Division in the Department of Pathology at the Brigham and Women's Hospital (Boston, MA) to evaluate the expression of Vimentin and E-cadherin. The cell blocks corresponded to the ascites from the DF lines utilized in this study. Immunohistochemistry was performed using the Envision Plus/Horseradish Peroxidase system (Dako, Carpinteria, CA) and a polyclonal/monoclonal antibody to Vimentin (Dako, Clone 3B4, 1:400) and E-cadherin (Dako, Clone

NCH-38, 1:75) as previously described(37, 60). In brief, paraffin-embedded sections were incubated in hydrogen peroxidase and absolute alcohol for 30 minutes to block endogenous peroxidase activity. Antigen retrieval was performed using pressure cooker pretreatment in a citrate buffer (pH=6.0). Tissue sections were subsequently incubated with the primary antibody for 40 minutes at 25 degrees C. After tris-buffered saline rinses, the tissue was incubated using the Envision Plus secondary antibody for 30 minutes, followed by diaminobenzidine for 5 minutes. Slides were counterstained with Mayer hematoxylin.

Immunofluorescence (IF):

Cells were fixed with 4% formaldehyde, permeabilized with 0.1% Triton X-100, and blocked with blocking buffer (10% BSA and 1% Goat Serum in PBS) for 1 hour. Cells were then incubated with anti-Pax8 antibody (1:200, Proteintech) for 1 hour followed by anti- mouse Alexa Fluor 568 secondary antibody (1:300, Invitrogen) four 1 hour. Cells were counterstained with DAPI for 15 minutes to visualize nuclei. Imaging was performed using a Nikon Ti-E Inverted Motorized Widefield Fluorescence Microscope as described above.

References:

1. Jemal A, Siegel R, Ward E, Hao Y, Xu J, Thun MJ. Cancer statistics, 2009. CA Cancer J Clin. 2009;59:225-49.

2. Ries LG MD, Krapcho M, Stinchcomb DG, Howlader N, Horner MJ, Mariotto A, Miller BA, Feuer EJ, Altekruse SF, Lewis DR, Clegg L, Eisner MP, Reichman M, Edwards BK. SEER Cancer Statistics Review. http://seercancergov/csr/1975_2005: National Cancer Institute. Bethesda, MD; 2007.

3. Cannistra SA. Cancer of the ovary. New England Journal of Medicine. 2004;351:2519-29.

4. Shield K, Ackland ML, Ahmed N, Rice GE. Multicellular spheroids in ovarian cancer metastases: Biology and pathology. Gynecol Oncol. 2009;113:143-8.

5. Naora H, Montell DJ. Ovarian cancer metastasis: integrating insights from disparate model organisms. Nat Rev Cancer. 2005;5:355-66.

6. Sehouli J, Senyuva F, Fotopoulou C, Neumann U, Denkert C, Werner L, et al. Intra-abdominal tumor dissemination pattern and surgical outcome in 214 patients with primary ovarian cancer. J Surg Oncol. 2009;99:424-7.

7. Birbeck MS, Wheatley DN. An Electron Microscopic Study of the Invasion of Ascites Tumor Cells into the Abdominal Wall. Cancer Res. 1965;25:490-7.

8. Witz CA, Monotoya-Rodriguez IA, Schenken RS. Whole explants of peritoneum and endometrium: a novel model of the early endometriosis lesion. Fertil Steril. 1999;71:56-60.

9. Zhang XY, Pettengell R, Nasiri N, Kalia V, Dalgleish AG, Barton DP. Characteristics and growth patterns of human peritoneal mesothelial cells: comparison between advanced epithelial ovarian cancer and non-ovarian cancer sources. J Soc Gynecol Investig. 1999;6:333-40.

10. Burleson KM, Casey RC, Skubitz KM, Pambuccian SE, Oegema TR, Jr., Skubitz AP. Ovarian carcinoma ascites spheroids adhere to extracellular matrix components and mesothelial cell monolayers. Gynecol Oncol. 2004;93:170-81.

11. Kenny HA, Nieman KM, Mitra AK, Lengyel E. The First Line of Intra-abdominal Metastatic Attack: Breaching the Mesothelial Cell Layer. Cancer Discovery. 2011;1:100-2.

12. Niedbala MJ, Crickard K, Bernacki RJ. Interactions of human ovarian tumor cells with human mesothelial cells grown on extracellular matrix. An in vitro model system for studying tumor cell adhesion and invasion. Exp Cell Res. 1985;160:499-513.

13. Kenny HA, Dogan S, Zillhardt M, A KM, Yamada SD, Krausz T, et al. Organotypic models of metastasis: A three-dimensional culture mimicking the human peritoneum and omentum for the study of the early steps of ovarian cancer metastasis. Cancer Treat Res. 2009;149:335-51.

14. Burleson KM, Hansen LK, Skubitz AP. Ovarian carcinoma spheroids disaggregate on type I collagen and invade live human mesothelial cell monolayers. Clin Exp Metastasis. 2004;21:685-97.

15. Burleson KM, Boente MP, Pambuccian SE, Skubitz AP. Disaggregation and invasion of ovarian carcinoma ascites spheroids. J Transl Med. 2006;4:6.

16. Ahmed N, Riley C, Rice G, Quinn M. Role of integrin receptors for fibronectin, collagen and laminin in the regulation of ovarian carcinoma functions in response to a matrix microenvironment. Clin Exp Metastasis. 2005;22:391-402.

17. Lessan K, Aguiar DJ, Oegema T, Siebenson L, Skubitz AP. CD44 and beta1 integrin mediate ovarian carcinoma cell adhesion to peritoneal mesothelial cells. Am J Pathol. 1999;154:1525-37.

18. Strobel T, Cannistra SA. Beta1-integrins partly mediate binding of ovarian cancer cells to peritoneal mesothelium in vitro. Gynecol Oncol. 1999;73:362-7.

19. Heyman L, Kellouche S, Fernandes J, Dutoit S, Poulain L, Carreiras F. Vitronectin and its receptors partly mediate adhesion of ovarian cancer cells to peritoneal mesothelium in vitro. Tumour Biol. 2008;29:231-44.

20. Cannistra SA, Kansas GS, Niloff J, DeFranzo B, Kim Y, Ottensmeier C. Binding of ovarian cancer cells to peritoneal mesothelium in vitro is partly mediated by CD44H. Cancer Res. 1993;53:3830-8.

21. Shield K, Riley C, Quinn MA, Rice GE, Ackland ML, Ahmed N. Alpha2beta1 integrin affects metastatic potential of ovarian carcinoma spheroids by supporting disaggregation and proteolysis. J Carcinog. 2007;6:11.

22. Kenny HA, Krausz T, Yamada SD, Lengyel E. Use of a novel 3D culture model to elucidate the role of mesothelial cells, fibroblasts and extra-cellular matrices on adhesion and invasion of ovarian cancer cells to the omentum. Int J Cancer. 2007;121:1463-72.

23. Slack-Davis JK, Atkins KA, Harrer C, Hershey ED, Conaway M. Vascular cell adhesion molecule-1 is a regulator of ovarian cancer peritoneal metastasis. Cancer Res. 2009;69:1469-76.

24. Casey RC, Koch KA, Oegema TR, Jr., Skubitz KM, Pambuccian SE, Grindle SM, et al. Establishment of an in vitro assay to measure the invasion of ovarian carcinoma cells through mesothelial cell monolayers. Clin Exp Metastasis. 2003;20:343-56.

25. Iwanicki M, Davidowitz RA, Ng MR, Besser A, Muranen T, Merritt M, et al. Ovarian cancer spheroids use myosin-generated force to clear the mesothelium. Cancer Discovery. 2011;1:144-57.

26. Taube JH, Herschkowitz JI, Komurov K, Zhou AY, Gupta S, Yang J, et al. Core epithelial-to-mesenchymal transition interactome gene-expression signature is associated with claudin-low and metaplastic breast cancer subtypes. Proc Natl Acad Sci U S A. 2010;107:15449-54.

27. Kalluri R, Weinberg RA. The basics of epithelial-mesenchymal transition. J Clin Invest. 2009;119:1420-8.

28. Cano A, Perez-Moreno MA, Rodrigo I, Locascio A, Blanco MJ, del Barrio MG, et al. The transcription factor snail controls epithelial-mesenchymal transitions by repressing E-cadherin expression. Nat Cell Biol. 2000;2:76-83.

29. Vega S, Morales AV, Ocana OH, Valdes F, Fabregat I, Nieto MA. Snail blocks the cell cycle and confers resistance to cell death. Genes Dev. 2004;18:1131-43.

30. Mejlvang J, Kriajevska M, Vandewalle C, Chernova T, Sayan AE, Berx G, et al. Direct repression of cyclin D1 by SIP1 attenuates cell cycle progression in cells undergoing an epithelial mesenchymal transition. Mol Biol Cell. 2007;18:4615-24.

31. Evdokimova V, Tognon C, Ng T, Sorensen PH. Reduced proliferation and enhanced migration: two sides of the same coin? Molecular mechanisms of metastatic progression by YB-1. Cell Cycle. 2009;8:2901-6.

32. Tsai JH, Donaher JL, Murphy DA, Chau S, Yang J. Spatiotemporal Regulation of Epithelial-Mesenchymal Transition Is Essential for Squamous Cell Carcinoma Metastasis. Cancer Cell. 2012.

33. Casas E, Kim J, Bendesky A, Ohno-Machado L, Wolfe CJ, Yang J. Snail2 is an essential mediator of Twist1-induced epithelial mesenchymal transition and metastasis. Cancer Res. 2011;71:245-54.

34. Cieply B, Riley Pt, Pifer PM, Widmeyer J, Addison JB, Ivanov AV, et al. Suppression of the epithelial-mesenchymal transition by Grainyhead-like-2. Cancer Res. 2012;72:2440-53.

35. Mendez MG, Kojima S, Goldman RD. Vimentin induces changes in cell shape, motility, and adhesion during the epithelial to mesenchymal transition. FASEB J. 2010;24:1838-51.

36. Bowen NJ, Logani S, Dickerson EB, Kapa LB, Akhtar M, Benigno BB, et al. Emerging roles for PAX8 in ovarian cancer and endosalpingeal development. Gynecol Oncol. 2007;104:331-7.

37. Laury AR, Perets R, Piao H, Krane JF, Barletta JA, French C, et al. A comprehensive analysis of PAX8 expression in human epithelial tumors. Am J Surg Pathol. 2011;35:816-26.

38. Laury AR, Hornick JL, Perets R, Krane JF, Corson J, Drapkin R, et al. PAX8 reliably distinguishes ovarian serous tumors from malignant mesothelioma. Am J Surg Pathol. 2010;34:627-35.

39. Karst AM, Levanon K, Drapkin R. Modeling high-grade serous ovarian carcinogenesis from the fallopian tube. Proc Natl Acad Sci U S A. 2011;108:7547-52.

40. Overholtzer M, Zhang J, Smolen GA, Muir B, Li W, Sgroi DC, et al. Transforming properties of YAP, a candidate oncogene on the chromosome 11q22 amplicon. Proc Natl Acad Sci U S A. 2006;103:12405-10.

41. Acloque H, Adams MS, Fishwick K, Bronner-Fraser M, Nieto MA. Epithelial-mesenchymal transitions: the importance of changing cell state in development and disease. J Clin Invest. 2009;119:1438-49.

42. Morone S, Lo-Buono N, Parrotta R, Giacomino A, Nacci G, Brusco A, et al. Overexpression of CD157 contributes to epithelial ovarian cancer progression by promoting mesenchymal differentiation. PLoS One. 2012;7:e43649.

43. Elloul S, Vaksman O, Stavnes HT, Trope CG, Davidson B, Reich R. Mesenchymal-to-epithelial transition determinants as characteristics of ovarian carcinoma effusions. Clin Exp Metastasis. 2010;27:161-72.

44. Terauchi M, Kajiyama H, Yamashita M, Kato M, Tsukamoto H, Umezu T, et al. Possible involvement of TWIST in enhanced peritoneal metastasis of epithelial ovarian carcinoma. Clin Exp Metastasis. 2007;24:329-39.

45. Nieto MA. The ins and outs of the epithelial to mesenchymal transition in health and disease. Annu Rev Cell Dev Biol. 2011;27:347-76.

46. Lee JM, Dedhar S, Kalluri R, Thompson EW. The epithelial-mesenchymal transition: new insights in signaling, development, and disease. J Cell Biol. 2006;172:973-81.

47. Kwon Y, Cukierman E, Godwin AK. Differential expressions of adhesive molecules and proteases define mechanisms of ovarian tumor cell matrix penetration/invasion. PLoS One. 2011;6:e18872.

48. Yoshida J, Horiuchi A, Kikuchi N, Hayashi A, Osada R, Ohira S, et al. Changes in the expression of E-cadherin repressors, Snail, Slug, SIP1, and Twist, in the development and progression of ovarian carcinoma: the important role of Snail in ovarian tumorigenesis and progression. Med Mol Morphol. 2009;42:82-91.

49. Blechschmidt K, Sassen S, Schmalfeldt B, Schuster T, Hofler H, Becker KF. The E-cadherin repressor Snail is associated with lower overall survival of ovarian cancer patients. Br J Cancer. 2008;98:489-95.

50. Elloul S, Elstrand MB, Nesland JM, Trope CG, Kvalheim G, Goldberg I, et al. Snail, Slug, and Smad-interacting protein 1 as novel parameters of disease aggressiveness in metastatic ovarian and breast carcinoma. Cancer. 2005;103:1631-43.

51. Hosono S, Kajiyama H, Terauchi M, Shibata K, Ino K, Nawa A, et al. Expression of Twist increases the risk for recurrence and for poor survival in epithelial ovarian carcinoma patients. Br J Cancer. 2007;96:314-20.

52. Kajiyama H, Hosono S, Terauchi M, Shibata K, Ino K, Yamamoto E, et al. Twist expression predicts poor clinical outcome of patients with clear cell carcinoma of the ovary. Oncology. 2006;71:394-401.

53. Jin H, Yu Y, Zhang T, Zhou X, Zhou J, Jia L, et al. Snail is critical for tumor growth and metastasis of ovarian carcinoma. Int J Cancer. 2010;126:2102-11.

54. Quattrocchi L, Green AR, Martin S, Durrant L, Deen S. The cadherin switch in ovarian high-grade serous carcinoma is associated with disease progression. Virchows Arch. 2011;459:21-9.

55. Darai E, Scoazec JY, Walker-Combrouze F, Mlika-Cabanne N, Feldmann G, Madelenat P, et al. Expression of cadherins in benign, borderline, and

malignant ovarian epithelial tumors: a clinicopathologic study of 60 cases. Hum Pathol. 1997;28:922-8.

56. Faleiro-Rodrigues C, Macedo-Pinto I, Pereira D, Lopes CS. Prognostic value of E-cadherin immunoexpression in patients with primary ovarian carcinomas. Ann Oncol. 2004;15:1535-42.
57. Tothill RW, Tinker AV, George J, Brown R, Fox SB, Lade S, et al. Novel molecular subtypes of serous and endometrioid ovarian cancer linked to clinical outcome. Clin Cancer Res. 2008;14:5198-208.

58. Hahn WC, Counter CM, Lundberg AS, Beijersbergen RL, Brooks MW, Weinberg RA. Creation of human tumour cells with defined genetic elements. Nature. 1999;400:464-8.

59. Ince TA, Richardson AL, Bell GW, Saitoh M, Godar S, Karnoub AE, et al. Transformation of different human breast epithelial cell types leads to distinct tumor phenotypes. Cancer Cell. 2007;12:160-70.

60. Clauss A, Ng V, Liu J, Piao H, Russo M, Vena N, et al. Overexpression of elafin in ovarian carcinoma is driven by genomic gains and activation of the nuclear factor kappaB pathway and is associated with poor overall survival. Neoplasia. 2010;12:161-72.

61. Sheng Q, Liu X, Fleming E, Yuan K, Piao H, Chen J, et al. An activated ErbB3/NRG1 autocrine loop supports in vivo proliferation in ovarian cancer cells. Cancer Cell. 2010;17:298-310.

62. Barker SD, Casado E, Gomez-Navarro J, Xiang J, Arafat W, Mahasreshti P, et al. An immunomagnetic-based method for the purification of ovarian cancer cells from patient-derived ascites. Gynecol Oncol. 2001;82:57-63.

63. Agoston E, DeSousa A, Jones M, Krohn M, Selfors L, Liu W, et al. Characterization of novel ovarian tumor cell lines that retain the phenotype of primary tumors. Manuscript Submitted. 2012.

64. Tibes R, Qiu Y, Lu Y, Hennessy B, Andreeff M, Mills GB, et al. Reverse phase protein array: validation of a novel proteomic technology and utility for analysis of primary leukemia specimens and hematopoietic stem cells. Mol Cancer Ther. 2006;5:2512-21.

Chapter 5

Discussion

In this dissertation, I described investigations to elucidate the molecular mechanisms governing regulation of mesothelial clearance by ovarian cancer spheroids. Crucial to these investigations was the development of an *in vitro* assay that monitors intercalation of pre-clustered ovarian cancer spheroids into GFP-expressing mesothelial monolayers, thereby modeling the initial step of ovarian cancer metastasis. Time-lapse confocal microscopy revealed that ovarian cancer spheroids attach to, intercalate between, and protrude under the mesothelial cells in the monolayer, leading to mesothelial cell matrix adhesion disassembly and migration away from the invading spheroid. These findings represent the first detailed description of the cellular events that occur during invasion of mesothelial monolayers by ovarian cancer spheroids. While other groups have focused on the molecules that mediate the attachment of ovarian cancer spheroids to mesothelial monolayers, we delved deeper to describe the mechanisms that regulate invasion of spheroids through the mesothelial monolayer to the underlying matrix. We found that $\alpha5\beta1$ integrin, myosin IIA and talin I are all required for mesothelial clearance. These studies supported the hypothesis that actomyosin generated traction force exerted by $\alpha5\beta1$ integrin on the fibronectin matrix surrounding the mesothelial cells drives this clearance event.

To more systematically investigate the mechanisms regulating mesothelial clearance, we compared the clearance abilities of a large panel of both primary ovarian cancer cell samples and established ovarian cancer cell lines. We found that clearance ability was correlated with the expression of epithelial and mesenchymal genes and proteins; mesenchymal genes and proteins were enriched and epithelial genes and proteins were diminished in clearance-competent spheroids, while the opposite was observed in clearance-incompetent spheroids. Furthermore, we show that there is heterogeneity within the populations of tumor cells from individual patient samples; some samples have a mixture of both epithelial-like and mesenchymal-like cells and only the mesenchymal-like cells clear the mesothelial monolayer. This is the first study to correlate mesothelial clearance ability with a transcriptional EMT program in a large panel of ovarian cancer cell lines and primary ovarian cancer samples. Taken together, these studies provide insights into the mechanisms that may drive mesothelial clearance *in vivo*.

Advantage of Using Primary Cell Samples:

For several of our studies, as well as the studies performed by many other labs (1-6), established ovarian cancer cell lines were used. Established cell lines are convenient to use because they are immortalized, and therefore are able to be maintained in cell culture. However, the tumor cells that are able to survive and are propagated in culture may represent a small population of cells from the original tumor. Furthermore, the cells that do survive may have evolved in culture,

so it is unclear to what extent any of the established cell lines reflect the original tumor population.

A second concern about established ovarian cancer cell lines is that many of the cell lines we used were derived from multiple different subtypes of ovarian cancer (7-11)(Table 5.1). Distinct subtypes of ovarian cancers arise from different tissues; for example, serous ovarian cancers are proposed to arise from the fallopian tube fimbriae (12, 13), while endometrioid ovarian cancers arise from endometrial tissue (14). Differences in the cell-of-origin among the established tumor cell lines could mask detection of genes that distinguish clearance-competent versus clearance-incompetent tumor cells.

As shown in Table 5.1, the origin of some ovarian cancer cell lines have not been documented and interestingly, some established cell lines that have long been characterized as ovarian cancer display gene expression programs inconsistent with ovarian cancer, suggesting that cultures were mixed or mislabeled at some point. For example, the cell line SW626, which is characterized as ovarian, is most likely of colonic origin (15). While we didn't detect an enrichment of any tumor sub-type in the clearance-competent or incompetent cell lines, the mixed background of the cell lines employed in our study was a concern.

Cell Line	Clearance-Competent	Subtype
ES-2	Yes	Clear cell carcinoma
CP70	Yes	Unknown
OVCAR3	Yes	Serous papillary adenocarcinoma
OVCA433	Yes	Ovarian serous carcinoma
OV207	Yes	Clear cell adenocarcinoma
A2780	Yes	Ovarian adenocarcinoma
TOV112D	Yes	Endometrioid adenocarcinoma
DOV13	Yes	Ovarian serous carcinoma
OVCA432	Yes	Ovarian serous carcinoma
HEYC2	Yes	Papillary serous adenocarcinoma
OV2008	Yes	Poorly differentiated endometrioid adenocarcinoma
OVSAHO	No	Serous papillary adenocarcinoma
C13	No	Endometrioid carcinoma
OAW28	No	Unknown
PEO6	No	Well differentiated adenocarcinoma
CAOV3	No	Ovarian adenocarcinoma
OVCA429	No	Clear cell adenocarcinoma
EFO21	No	Ovarian serous cystadenocarcinoma
MCAS	No	Mucinous cystadenocarcinoma, papillary adenocarcinoma
RMG1	No	Ovarian clear cell

Table 5.1: Subtypes of Ovarian Cancer Cell Lines.

To circumvent these issues and more directly assess the relevance of our findings to human ovarian cancer, we chose to examine primary ovarian cancer cell samples that were all derived from patients with serous ovarian carcinoma. In agreement with the data from the established cell lines, we observed a wide range of clearance activity in the primary ovarian cancer cell samples, suggesting that differences in clearance ability was not due to the different origins of the established cell lines. We did not carry out genome-wide microarrays on the primary ovarian cancer tumor samples; however, in the future, it would be useful to perform RNA sequencing on these samples to further define the gene

programs that distinguish clearance-competent from clearance-incompetent tumor cells.

Unanswered Questions/ Future Studies:

Role of Force In Mesothelial Clearance:

In Chapter 3, we showed that actomyosin generated contractile force is required for mesothelial clearance. This finding raised several unanswered questions: Is the mechanical force exerted by ovarian cancer spheroids on the fibronectin surrounding the mesothelial cells sufficient to cause mesothelial clearance? Is force exerted by $\alpha 5\beta 1$ integrin the only mechanical stimulation involved in clearance of the mesothelial monolayer or does, for example, protrusive force generated by actin polymerization play a role? Finally, is mechanical force the only mechanism acting on the mesothelial cells to promote mesothelial clearance, or are there other molecules on the ovarian cancer cells that induce the retraction of the mesothelial monolayer?

To test the mechanical force hypothesis directly, magnetic tweezers, similar to the apparatus described in Kollmannsberger and Fabry(16), could be used to apply linear, nanonewton-scale forces to the mesothelial monolayers. Two types of force can be exerted on the mesothelial monolayer by the spreading ovarian cancer spheroids: [A] actomyosin contractility exerts force on integrin-based focal adhesions, which in turn exerts a pulling force on the ECM molecules surrounding the mesothelial cells or [B] ovarian cancer spheroid protrusion exerts a pushing force on the surrounding mesothelial cells via actin

polymerization against the ovarian cancer cell membrane(17-19). A pulling force can be applied to the ECM surrounding the mesothelial cells by using a magnetic bead coated with β1-integrin, to determine if pulling on the fibronectin surrounding mesothelial cells is sufficient to induce mesothelial clearance. On the other hand, an uncoated magnetic bead can be used to apply a pushing force, similar in magnitude to protrusive force, to the mesothelial cells to determine if a pushing force directly on the mesothelial cells is sufficient to induce mesothelial clearance.

Independently of whether or not mechanical force is sufficient to induce mesothelial clearance, it is possible that signaling molecules present on the ovarian cancer spheroids induce the mesothelial cells to retract away from the invading spheroid. It is unlikely that this is a soluble factor, since either incubating mesothelial monolayers with ovarian cancer spheroid conditioned media (data not shown) or with spheroids that are intact but unable to spread (due to α5β1 integrin, talin I or myosin II inhibition, Chapter 3) does not induce retraction of the mesothelial cells. Many cell membrane proteins have been implicated in cell-cell repulsion, including members of the ephrin and semaphorin families (20, 21). Interestingly, ephrins and semaphorins are up-regulated in some metastatic tumors (21, 22). These ligands and their receptors can be inhibited in the spheroids and mesothelial cells to determine if repulsion plays a role in mesothelial clearance.

Effect of Force on Ovarian Cancer Spheroid Behavior:

Thus far, our experiments have focused on the mechanisms by which invading ovarian cancer spheroids affect the behavior of the mesothelial monolayer. We have not, however, determined how the migratory properties of the mesothelial cells affect the behavior of the ovarian cancer spheroids. There is experimental evidence that force can promote the invasive behavior of cancer cells (23). Menon et al. applied a mechanical stimulus to the fibronectin surrounding cancer cells on a collagen I bed, by pulling on magnetic beads embedded in the collagen matrix. The authors found that human fibrosarcoma cells became more invasive when the force was applied, and fibronectin was required for this increased invasive capacity, suggesting that the cancers cells sensed and responded to the force exerted on the fibronectin in the collagen gel (23). The mesothelial cells in our clearance assay are not static; they are constantly moving within the monolayer (Chapter 3). It is likely that the mesothelial cells exert force on the stromal fibronectin, which is sensed by the invading ovarian cancer spheroids. It would be interesting to determine if the force exerted by the mesothelial cells promotes ovarian cancer spheroid invasion.

Epithelial and Mesenchymal Cell States in Ovarian Cancer:

In chapter 4, we found that some ovarian cancer cell lines express a mesenchymal-like gene signature while other ovarian cancer cell lines express an epithelial-like gene signature. Similarly, in primary ovarian cancer cell samples derived from patients with high-grade serous ovarian cancer, some samples

express vimentin, while others express E-cadherin. In addition, some tumors contained cells that express both markers, either in the same cells or in two adjacent populations. This degree of heterogeneity raises questions about the mechanisms responsible for the distinct differences in epithelial and mesenchymal markers in different patient tumors. Interestingly, the proposed 'cells of origin' of high-grade serous ovarian cancer are mesoepithelial cells that express both E-cadherin and vimentin [Figure 5.1, images adapted from images obtained from the Human Protein Atlas (www.proteinatlas.org) (24)]. This is in contrast to luminal epithelial cells of the breast and their progenitors that do not express vimentin [Figure 5.1, images adapted from images obtained from the Human Protein Atlas (www.proteinatlas.org) (24)]. Given the proposed mesoepithelial origin of high-grade serous ovarian cancer cells, these cells may be more plastic in shifting between predominantly epithelial or mesenchymal programs when adapting to different microenvironmental conditions. In contrast, since the cell-of-origin of most breast tumors are purely epithelial, conversion to a mesenchymal phenotype may involve distinct mechanisms relative to ovarian tumors.

Investigations from one laboratory provided evidence that ovarian cancer cells display more epithelial-like features in the ascites of ovarian cancer patients, and display more mesenchymal-like features in metastases. Elloul et al. measured the mRNA and protein expression of E-cadherin and SNAI1 in different stages of ovarian cancer progression. They found that E-cadherin expression was higher in tumor cells within ascites fluid compared to the primary

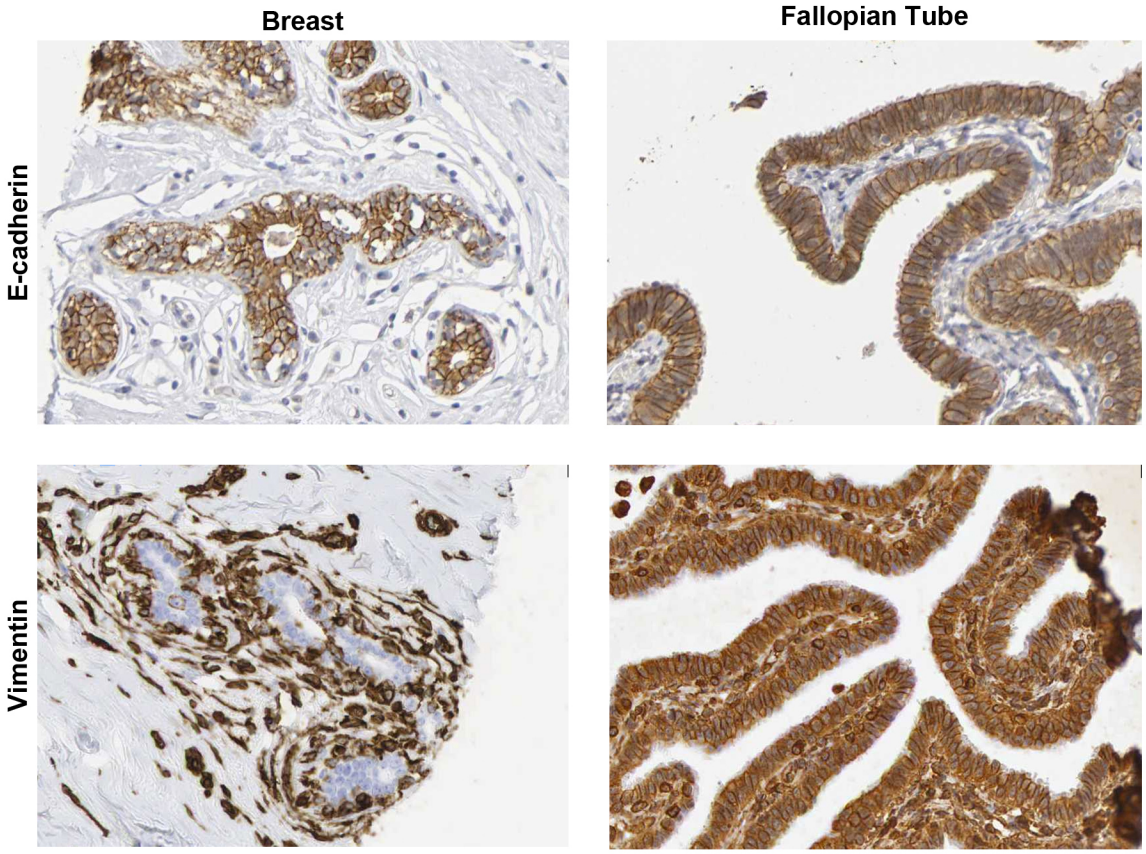

FIGURE 5.1: IHC of Normal Breast and Fallopian Tube Tissue. top panels are stained with an antibody directed against E-cadherin and the bottom panels are stained with an antibody directed against Vimentin. Images adapted from the Human Protein Atlas (20).

tumor and metastases. They also found that SNAI1 expression was lower in the ascites samples compared to the primary tumor and metastases (25). In a separate study, Elloul et al. found that TWIST1 and ZEB1 mRNA expression was higher in the metastases, compared to the primary tumor and ascites samples (26). It is difficult to draw conclusions about the processes responsible for mesenchymal and epithelial cell states in the primary, ascites and metastatic samples, however, because we cannot follow the fate of individual cells. The different microenvironments in the primary tumor, ascites, and metastatic site may select for cells that are either more mesenchymal or more epithelial, or EMT/MET switches may occur between the primary tumor, ascites, and metastatic sites.

To address this question, a transgenic mouse model can be developed that tags fallopian tube cells and follows their neoplastic progression. An rtTA-Pax8 mouse, tet-On-Cre mouse is commercially available (27) that can be used to express genes of interest, selectively, in the secretory cells of the fallopian tube, the cells of origin of serous ovarian cancer. These mice can be crossed with mice harboring constructs containing Lox-Stop-Lox plus genes that are commonly mutated in ovarian cancer and a fluorescent marker such as a GFP gene. A similar system has been used for stem cell lineage tracing (28). The correct combination of mutations expressed in the fallopian tube cells should create fallopian tube tumors that mimic ovarian cancer progression. Kim and colleagues created a mouse model of serous ovarian cancer by knocking out *Pten* and *Dicer* in fallopian tube cells (29). A fluorescent marker, such as GFP,

could be added where *Pten* or *Dicer* was knocked out to trace the lineage of carcinomas developed in these mice. The epithelial and mesenchymal states of the fluorescent cells can then be followed over time, to determine if there is a progressive switch between epithelial and mesenchymal cell states at different stages of ovarian cancer progression.

In vivo Relevance:

Is mesothelial clearance by mesenchymal-like ovarian cancer cells required for ovarian cancer metastasis in vivo?

We have shown that the expression of mesenchymal markers and the repression of epithelial markers are correlated with the mesothelial clearance ability of ovarian cancer spheroids *in vitro*. Furthermore, overexpression of EMT-inducing transcription factors promotes mesothelial clearance ability in ovarian cancer spheroids that were unable to clear a mesothelial monolayer. We did not, however, investigate the ability of EMT to regulate mesothelial clearance *in vivo*.

Shao and colleagues used a mouse xenograft model to investigate the role of EMT in ovarian cancer metastasis (30). They found that TG2 overexpression promotes EMT in OV90 ovarian cancer cells, while TG2 knockdown represses EMT in SKOV3 ovarian cancer cells. When control or TG2-knockdown SKOV3 cells were injected orthotopically under the ovarian bursa of nu/nu BALB/c nude mice, TG2 knockdown suppressed the formation of metastatic implants on the omentum, mesentery, and peritoneal surface of the abdominal cavity. (It is of note that the SKOV3 cells were serially passaged

through the mouse one time before they were able to produce metastasis from the ovarian bursa xenografts.) This data suggests EMT repression blocks ovarian metastasis formation in a mouse xenografts model.

An ovarian xenograft model such as the one described above could be used to address many questions regarding the relevance of EMT in ovarian cancer progression. First, mesothelial clearance-incompetent ovarian cancer cells could be injected into the ovarian bursa or within the peritoneal cavity fluid to determine if those cells produce peritoneal metastases. Furthermore, the ability of the ovarian cancer cells to clear the mesothelial layer *in vivo* could be monitored by excising the nodules attached to the peritoneal cavity organs (if any) and looking for the presence or absence of mesothelial cells under the attached nodules by IHC. In addition, the effect of EMT on mesothelial clearance *in vivo* can be tested by injecting clearance-incompetent cell lines that over-express an EMT-inducing transcription factor into mice. The ability to form metastasis and the presence or absence of mesothelial cells under metastatic nodules can then be compared between control and EMT transcription factor-overexpressing ovarian cancer cells to determine if EMT promotes metastasis and/ or mesothelial clearance *in vivo*.

This model system could also be used to determine if EMT/MET interconversion occurs during metastatic progression. The ovarian cancer cell line MCAS is epithelial-like and clearance-incompetent in our mesothelial clearance assay, yet it is able to form tumors after intraperitoneal injection in nude mice. It would be interesting to determine, first, if these cells are able to

clear the peritoneal mesothelial cells *in vivo*, and then, if an EMT event is required in order for mesothelial clearance/ and or seeding of metastatic nodules to occur. The expression of epithelial and mesenchymal markers can be compared between the MCAS cells in suspension in the peritoneal cavity and the MCAS cells that have attached to the peritoneal cavity organs at various time points after metastasis.

Do First-line Treatments Promote Metastasis?

Two interesting observations suggest that treatments that are used as a first-line defense against ovarian cancer may be detrimental to the patient by promoting ovarian cancer metastasis: Latifi et al. found that clinical samples, as well as the OVCA433 ovarian cancer cell line, upregulated mesenchymal markers such as Snail, Slug, Twist and vimentin and downregulated E-cadherin, when treated with the chemotherapeutic drug, cisplatin (31). Similarly, Slug was upregulated in mouse ovarian carcinoma xenografts treated with the chemotherapeutic drug, Paclitaxel (32). These data indicate that chemotherapeutic drugs either promote EMT in ovarian cancer cells, or kill only the epithelial-like ovarian cancer cells while allowing resistant mesenchymal-like cells to take over the population. This would complicate the analysis, described above, to determine when EMT and MET occur during ovarian cancer progression, since most ovarian cancer patients are treated with chemotherapeutics. A larger concern is that the therapeutics that are supposed to treat ovarian cancer may promote ovarian cancer metastasis. It is, therefore,

very important to perform an *in vivo* analysis where samples are collected from ovarian cancer patients before and after treatment with chemotherapeutic drugs when metastases recur. Mesenchymal and epithelial markers should be measured by IHC in those samples to determine if chemotherapeutic agents are promoting EMT in ovarian cancer cells.

EMT status and ability to debulk tumors *in vivo*:

Currently, the only treatment options for ovarian cancer are cytoreductive surgery followed by platinum/taxane-based chemotherapy (33-35). Improved survival directly correlates with the amount of tumor bulk that can be resected (36, 37). It would be interesting to determine if the extent of debulking correlates with the expression of epithelial or mesenchymal markers. To perform this analysis, the expression of epithelial and mesenchymal markers should be measured in samples that were collected during debulking under conditions where the surgeon measures the percentage of residual tumor after surgery. Our data suggests that mesenchymal-like cells are able to clear a mesothelial monolayer better than epithelial-like cells. This could indicate that mesenchymal-like cells are able to intercalate into peritoneal cavity organs better than epithelial-like cells, but it will have to be tested in mouse models (as described above) and by collecting ovarian cancer patient data.

Finally, since we have shown that mesenchymal-like cells more efficiently clear mesothelial monolayers, this raises the question of whether blocking the mesenchymal program in ovarian cancer cells within the ascites could prevent

re-seeding of tumors after debulking and chemotherapy? Several drugs, including metformin, TGF-β inhibitors, and other small molecules inhibitors have been show to reverse EMT in various contexts (38-40). Inhibitors such as these should be tested to evaluate their ability to reverse EMT in ovarian cancer cells. A drug, or combination of drugs, that can reverse EMT can then be tested in combination with current treatment methods to determine if tumor re-seeding can be reduced.

Assay Limitations:

The mesothelial clearance assay described in this dissertation uses a minimal number of components to model the interaction between two cell types, ovarian cancer spheroids and a mesothelial monolayer. But there are other components of the peritoneal organs that may play a role in metastasis. Below the mesothelial monolayer there is a basement membrane composed of ECM molecules including collagen types I and IV, laminin and fibronectin, and dispersed within the ECM are fibroblasts and macrophages. Our *in vitro* assay seeds the mesothelial cells directly on a glass-bottom cell culture plate coated with a thin layer of fibronectin. The stiffness of a glass substrate is much stiffer than the basement membrane underlying the mesothelial monolayers *in vivo (41)*, so it is possible that the ovarian cancer spheroids would behave differently on a more physiologically relevant substrate. To address this issue, we plated mesothelial monolayers on fibronectin-coated polyacrylamide gels with elastic moduli of 0.3 kPa or 10 kPa, similar substrate stiffness to connective tissue

(Chapter 3). OVCA433 spheroids were able to clear the mesothelial monolayers seeded on these physiologically relevant substrates, suggesting that mesothelial clearance is not an artifact of an artificially stiff substrate.

Kenny et al. developed a 3D *in vitro* model system (42, 43) that included more of the components of the peritoneal tissue than were included in our system. A bed of collagen I was deposited between the culture dish and the mesothelial monolayer, and fibroblasts were suspended within the collagen bed. A single cell suspension of ovarian cancer cells were added on top of the monolayers and allowed to invade. The authors found that the mesothelial monolayer dampened ovarian cancer cell invasion into the collagen bed compared to invasion into collagen that was not covered with a mesothelial monolayer. Interestingly, fibroblasts suspended in the collagen bed promoted adhesion and invasion compared to adhesion and invasion in wells where fibroblasts were left out of the collagen mix (43). However, the authors only monitored the invasion of single ovarian cancer cells in this model. It would be interesting to monitor the behavior of ovarian cancer multicellular spheroids in this model system to determine how the ovarian cancer spheroids behave in a more physiologically relevant context. Furthermore, it would be interesting to determine if the cutoff between the established and primary ovarian cancer spheroids that were clearance-competent versus clearance-incompetent would shift on the more compliant surface. It is possible that the cell lines that are able to clear, but are close to the cutoff (ex. HeyC2, OVCA432), would be unable to clear on the more compliant surface.

The model described by Kenny et al. does not include all of the components present in the peritoneal tissue. Below the mesothelial monolayer there is a dense layer of basement membrane that includes not only collagen and fibroblasts, but fibronectin, laminin and macrophages, as well (44, 45). A model system that incorporates all of these cell types would be more physiologically relevant than the ones described above.

Interestingly, *in vivo*, ovarian cancer spheroids preferentially home to the omentum, a soft pad of tissue in the peritoneum that has a thick layer of adipocytes directly under the mesothelial monolayer and basement membrane (46). Nieman and colleagues showed that Il-6 and Il-8, two cytokines that are secreted by the adipocytes, promote ovarian cancer cell homing to the omentum (46). It would be interesting to add a layer of adipocytes to the *in vitro* model to determine the effect of adipocytes homing and cytokine release on mesothelial clearance. It is possible that cell lines with different genetic backgrounds would respond differently to the addition of adipocytes.

Future Applications of Mesothelial Clearance Assay:

The mesothelial clearance assay can be easily adapted for drug screening by converting it to an automated, high-throughput assay. Robots can be used to automatically plate ovarian cancer cells in large quantities of 384-well low-adhesion culture plates to form spheroids and to coat 384-well plates with fibronectin and plate mesothelial cells in those wells. Robots can also be used to transfer the spheroids from the low adhesion culture plates to the monolayer

containing plates. The addition of different drugs or small molecules to each well of the 384 well assay plates can be similarly automated. Different libraries of drugs and small molecules can then be tested to determine their effects on mesothelial clearance. If certain drugs or small molecules can inhibit mesothelial clearance, they may be good candidates for new ovarian cancer metastasis treatments.

References:

1.Ahmed N, Riley C, Rice G, Quinn M. Role of integrin receptors for fibronectin, collagen and laminin in the regulation of ovarian carcinoma functions in response to a matrix microenvironment. Clin Exp Metastasis. 2005;22:391-402.

2.Shield K, Riley C, Quinn MA, Rice GE, Ackland ML, Ahmed N. Alpha2beta1 integrin affects metastatic potential of ovarian carcinoma spheroids by supporting disaggregation and proteolysis. J Carcinog. 2007;6:11.

3.Strobel T, Cannistra SA. Beta1-integrins partly mediate binding of ovarian cancer cells to peritoneal mesothelium in vitro. Gynecol Oncol. 1999;73:362-7.

4.Lessan K, Aguiar DJ, Oegema T, Siebenson L, Skubitz AP. CD44 and beta1 integrin mediate ovarian carcinoma cell adhesion to peritoneal mesothelial cells. Am J Pathol. 1999;154:1525-37.

5.Slack-Davis JK, Atkins KA, Harrer C, Hershey ED, Conaway M. Vascular cell adhesion molecule-1 is a regulator of ovarian cancer peritoneal metastasis. Cancer Res. 2009;69:1469-76.

6.Cannistra SA, Ottensmeier C, Niloff J, Orta B, DiCarlo J. Expression and function of beta 1 and alpha v beta 3 integrins in ovarian cancer. Gynecol Oncol. 1995;58:216-25.

7.Kidera Y, Yoshimura T, Ohkuma Y, Iwasaka T, Sugimori H. [Establishment and characterization of a cell line derived from mucinous cystadenocarcinoma of human ovary]. Nihon Sanka Fujinka Gakkai Zasshi. 1985;37:1820-4.

8.Langdon SP. Isolation and culture of ovarian cancer cell lines. Methods Mol Med. 2004;88:133-9.

9.Kim JH, Skates SJ, Uede T, Wong KK, Schorge JO, Feltmate CM, et al. Osteopontin as a potential diagnostic biomarker for ovarian cancer. JAMA. 2002;287:1671-9.

10.DeRycke MS, Andersen JD, Harrington KM, Pambuccian SE, Kalloger SE, Boylan KL, et al. S100A1 expression in ovarian and endometrial endometrioid carcinomas is a prognostic indicator of relapse-free survival. Am J Clin Pathol. 2009;132:846-56.

11.Yanagibashi T, Gorai I, Nakazawa T, Miyagi E, Hirahara F, Kitamura H, et al. Complexity of expression of the intermediate filaments of six new human ovarian carcinoma cell lines: new expression of cytokeratin 20. Br J Cancer. 1997;76:829-35.

12.Crum CP, Drapkin R, Miron A, Ince TA, Muto M, Kindelberger DW, et al. The distal fallopian tube: a new model for pelvic serous carcinogenesis. Curr Opin Obstet Gynecol. 2007;19:3-9.

13.Lee Y, Miron A, Drapkin R, Nucci MR, Medeiros F, Saleemuddin A, et al. A candidate precursor to serous carcinoma that originates in the distal fallopian tube. J Pathol. 2007;211:26-35.

14.Martin DC. Cancer and endometriosis: do we need to be concerned? Semin Reprod Endocrinol. 1997;15:319-24.

15.Furlong MT, Hough CD, Sherman-Baust CA, Pizer ES, Morin PJ. Evidence for the colonic origin of ovarian cancer cell line SW626. J Natl Cancer Inst. 1999;91:1327-8.

16.Kollmannsberger P, Fabry B. High-force magnetic tweezers with force feedback for biological applications. Rev Sci Instrum. 2007;78:114301.

17.Lauffenburger DA, Horwitz AF. Cell migration: a physically integrated molecular process. Cell. 1996;84:359-69.

18.Ingber DE. Cellular mechanotransduction: putting all the pieces together again. FASEB J. 2006;20:811-27.

19.Schwartz IM, Ehrenberg M, Bindschadler M, McGrath JL. The role of substrate curvature in actin-based pushing forces. Curr Biol. 2004;14:1094-8.

20.Tanaka M, Kamo T, Ota S, Sugimura H. Association of Dishevelled with Eph tyrosine kinase receptor and ephrin mediates cell repulsion. EMBO J. 2003;22:847-58.

21.Tamagnone L, Comoglio PM. To move or not to move? Semaphorin signalling in cell migration. EMBO Rep. 2004;5:356-61.

22.Surawska H, Ma PC, Salgia R. The role of ephrins and Eph receptors in cancer. Cytokine Growth Factor Rev. 2004;15:419-33.

23.Menon S, Beningo KA. Cancer cell invasion is enhanced by applied mechanical stimulation. PLoS One. 2011;6:e17277.

24.Uhlen M, Oksvold P, Fagerberg L, Lundberg E, Jonasson K, Forsberg M, et al. Towards a knowledge-based Human Protein Atlas. Nat Biotechnol. 2010;28:1248-50.

25.Elloul S, Silins I, Trope CG, Benshushan A, Davidson B, Reich R. Expression of E-cadherin transcriptional regulators in ovarian carcinoma. Virchows Arch. 2006;449:520-8.

26.Elloul S, Vaksman O, Stavnes HT, Trope CG, Davidson B, Reich R. Mesenchymal-to-epithelial transition determinants as characteristics of ovarian carcinoma effusions. Clin Exp Metastasis. 2010;27:161-72.

27.Traykova-Brauch M, Schonig K, Greiner O, Miloud T, Jauch A, Bode M, et al. An efficient and versatile system for acute and chronic modulation of renal tubular function in transgenic mice. Nat Med. 2008;14:979-84.

28.Fuchs E, Horsley V. Ferreting out stem cells from their niches. Nat Cell Biol. 2011;13:513-8.

29.Kim J, Coffey DM, Creighton CJ, Yu Z, Hawkins SM, Matzuk MM. High-grade serous ovarian cancer arises from fallopian tube in a mouse model. Proc Natl Acad Sci U S A. 2012;109:3921-6.

30.Shao M, Cao L, Shen C, Satpathy M, Chelladurai B, Bigsby RM, et al. Epithelial-to-mesenchymal transition and ovarian tumor progression induced by tissue transglutaminase. Cancer Res. 2009;69:9192-201.

31.Latifi A, Abubaker K, Castrechini N, Ward AC, Liongue C, Dobill F, et al. Cisplatin treatment of primary and metastatic epithelial ovarian carcinomas generates residual cells with mesenchymal stem cell-like profile. J Cell Biochem. 2011;112:2850-64.

32.Bani MR, Nicoletti MI, Alkharouf NW, Ghilardi C, Petersen D, Erba E, et al. Gene expression correlating with response to paclitaxel in ovarian carcinoma xenografts. Mol Cancer Ther. 2004;3:111-21.

33.Karst AM, Drapkin R. The new face of ovarian cancer modeling: better prospects for detection and treatment. F1000 Med Rep. 2011;3:22.

34.Armstrong DK, Bundy B, Wenzel L, Huang HQ, Baergen R, Lele S, et al. Intraperitoneal cisplatin and paclitaxel in ovarian cancer. N Engl J Med. 2006;354:34-43.

35.Vaughan S, Coward JI, Bast RC, Jr., Berchuck A, Berek JS, Brenton JD, et al. Rethinking ovarian cancer: recommendations for improving outcomes. Nat Rev Cancer. 2011;11:719-25.

36.Schorge JO, McCann C, Del Carmen MG. Surgical debulking of ovarian cancer: what difference does it make? Rev Obstet Gynecol. 2010;3:111-7.

37.Bristow RE, Tomacruz RS, Armstrong DK, Trimble EL, Montz FJ. Survival effect of maximal cytoreductive surgery for advanced ovarian carcinoma during the platinum era: a meta-analysis. J Clin Oncol. 2002;20:1248-59.

38.Gal A, Sjoblom T, Fedorova L, Imreh S, Beug H, Moustakas A. Sustained TGF beta exposure suppresses Smad and non-Smad signalling in

mammary epithelial cells, leading to EMT and inhibition of growth arrest and apoptosis. Oncogene. 2008;27:1218-30.

39.Rattan R, Ali Fehmi R, Munkarah A. Metformin: an emerging new therapeutic option for targeting cancer stem cells and metastasis. J Oncol. 2012;2012:928127.

40.Chua KN, Sim WJ, Racine V, Lee SY, Goh BC, Thiery JP. A cell-based small molecule screening method for identifying inhibitors of epithelial-mesenchymal transition in carcinoma. PLoS One. 2012;7:e33183.

41.Butcher DT, Alliston T, Weaver VM. A tense situation: forcing tumour progression. Nat Rev Cancer. 2009;9:108-22.

42.Kenny HA, Dogan S, Zillhardt M, A KM, Yamada SD, Krausz T, et al. Organotypic models of metastasis: A three-dimensional culture mimicking the human peritoneum and omentum for the study of the early steps of ovarian cancer metastasis. Cancer Treat Res. 2009;149:335-51.

43.Kenny HA, Krausz T, Yamada SD, Lengyel E. Use of a novel 3D culture model to elucidate the role of mesothelial cells, fibroblasts and extra-cellular matrices on adhesion and invasion of ovarian cancer cells to the omentum. Int J Cancer. 2007;121:1463-72.

44.Daya D, McCaughey WT. Pathology of the peritoneum: a review of selected topics. Semin Diagn Pathol. 1991;8:277-89.

45.Witz CA, Montoya-Rodriguez IA, Cho S, Centonze VE, Bonewald LF, Schenken RS. Composition of the extracellular matrix of the peritoneum. J Soc Gynecol Investig. 2001;8:299-304.

46.Nieman KM, Kenny HA, Penicka CV, Ladanyi A, Buell-Gutbrod R, Zillhardt MR, et al. Adipocytes promote ovarian cancer metastasis and provide energy for rapid tumor growth. Nat Med. 2011;17:1498-503.

Appendix

Supplementary Materials

Supplementary Materials for Chapter 2

SUPPLEMENTARY MOVIE 2.1: Video prepared for peer reviewed, PubMed-indexed video journal, JoVE.

Supplementary Materials for Chapter 3

SUPPLEMENTARY MOVIE 3.1: OVCA433 cancer spheroids clear the mesothelium. Cancer spheroids (red) were allowed to adhere to mesothelial monolayer. The interaction between the two cell populations was recorded over a 10 hour period. Movie shows a montage of phase image (top), red-labeled spheroid image, GFP-labeled mesothelium image and pseudo-colored overlay of spheroid and mesothelium image.

SUPPLEMENTARY MOVIE 3.2: Freshly isolated spheroids from peritoneal effusion of ovarian cancer patient were labeled (as described in methods) and allowed to interact with the mesothelial monolayer for a period longer than 10 hours. Movie shows montage of phase image (top), cancer spheroid (middle) and mesothelium (bottom).

SUPPLEMENTARY MOVIE 3.3: Side view reconstruction of mesothelial clearance by OVCA433 spheroids. 30 focal planes were reconstructed on x-z plane to observe cell interactions at the ventral and dorsal cell surfaces of mesothelial monolayer. Each plane is 1 um apart. Bar =100 μm.

SUPPLEMENTARY MOVIE 3.4: TIRFM of mesothelial cell (LP9) focal adhesions (green as labeled by GFP-Paxillin) in the presence of OVCA433 cancer spheroid membrane protrusions (red).

SUPPLEMENTARY MOVIE 3.5: TIRFM of mesothelial cell focal adhesions (labeled by GFP-Paxillin) in the absence of OVCA433 cancer spheroid.

SUPPLEMENTARY MOVIE 3.6: OVCA433 spheroids provoke migration of mesothelial cells away from spheroid attachment sites. Time lapse recording of GFP-Labeled mesothelial cells in the absence and presence of intercalating OVCA433 spheroid (red). Bar = 100 μm.

SUPPLEMENTARY MOVIE 3.7: Myosin II is required for cancer spheroid to induce mesothelial clearance. Time lapse recording of control RNAi and NMIIA/B RNAi treated OVCA433 (red) spheroids intercalating into mesothelial monolayer (green). Top recording represents DIC image. Bar = 100μm.

SUPPLEMENTARY MOVIE 3.8: Talin I is required for cancer spheroids to induce mesothelial clearance. Time-lapse recording of control RNAi and Talin I RNAi treated OVCA433 (red) spheroids intercalating into mesothelial monolayer (green). Top recording represent DIC image. Bar=100μm.

SUPPLEMENTARY MOVIE 3.9: Blocking α5β1 integrin in OVCA433 spheroids attenuates mesothelial clearance. OVCA433 spheroids were pretreated with IgG and ITGA5 function blocking antibody. Top recording shows DIC image and bottom recording shows clearance of mesothelial cells (green). Bar=100μm.

SUPPLEMENTARY MOVIE 3.10: Ectopic expression of ITGA5 in OVCAR5 spheroids is sufficient to promote mesothelial clearance. Top recordings represents DIC image series of OVCAR5 cells expressing either empty plasmid or plasmid encoding ITGA5. Bottom recordings represent florescent image series of GFP – labeled mesothelial cells. Bar = 100μm.

SUPPLEMENTARY MOVIE 3.11: Laser Scanning Confocal microscopy of intercalated OVCA433 spheroid (blue) into mesothelial monolayer (green) and fibronectin (red). There were 30 z planes acquired. Each plane was 1μm apart. Bar = 10μm.

SUPPLEMENTARY MOVIE 3.12: Spinning Disc Confocal Microscopy of intercalating OVCA433 spheroid (blue) into rhodamine-labeled fibronectin (red) covered mesothelium (green).

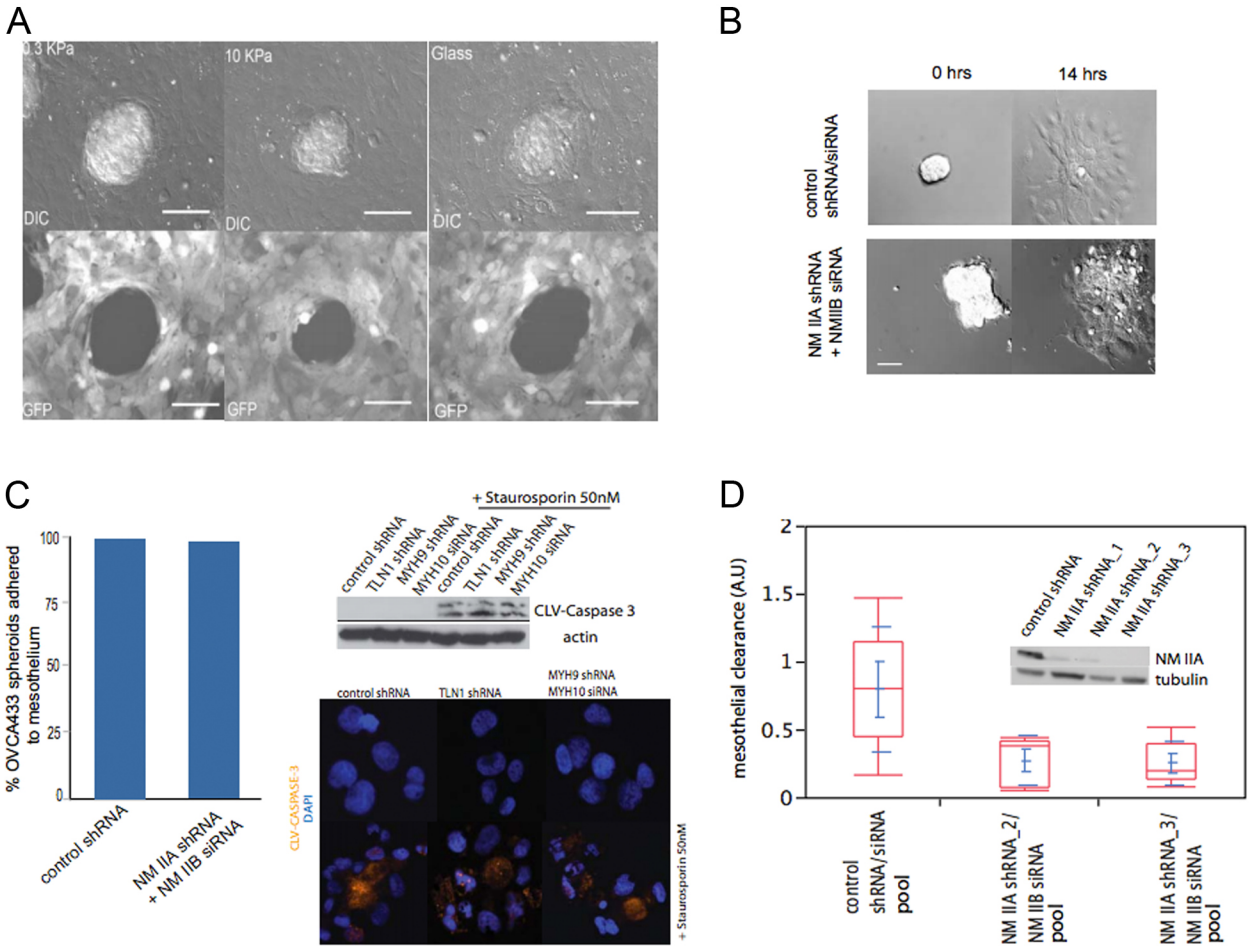

SUPPLEMENTARY FIGURE 3.1: A. GFP-expressing mesothelial cells were plated on either fibronectin-coated glass or fibronectin-coated polyacrylamide substrates with flexibility of 0.3KPa, 10KPa and glass. OVCA433 spheroids were applied on top of the monolayers and allowed to clear the mesothelium for 10 hours. Images represent the final frame of a 10 hours long time-lapse recording. Bar corresponds to 100 µm **B.** Control and myosin IIA shRNA/ myosin IIB siRNA OVCA433 spheroids were allowed to spread on fibronectin (5ug/ml) and collagen (5 ug/ml) coated glass surface for a period of 14 hours. DIC images represent frames corresponding to the 0 and 14 hour time points. **C.** Left panel: Adhesion of OVCA433 cells with attenuated expression of non-muscle myosin IIA/B to mesothelial monolayer. Upper right panel: Control, Talin 1 , Myosin II shRNA /siRNA expressing OVCA433 cells were cultured overnight in suspension in vehicle alone (DMSO) or 50nM staurosporin. Western blots show levels of cleaved caspase 3 and actin in OVCA433 spheroids treated with vehicle alone (DMSO) or staurosporin. Lower right panel: Laser scanning confocal images showing levels of cleaved caspase -3 (orange) in control, tailin 1 and myosin 9/10 shRNA expressing OVA433 spheroids. DAPI (blue) was used to mark nucleus. **D.** Quantification of mesothelial clearance. Two distinct myosin II-targeted shRNA sequences were individually combined with an siRNA pool targeting myosin IIB to validate myosin attenuation experiments from figure 3A. 8 independent regions were analyzed per condition. The inset shows the expression level of NM IIA in OVCA433 spheroids treated with various shRNA constructs targeting myosin IIA and myosin IIB by 4 pooled siRNA oligonulceotides.

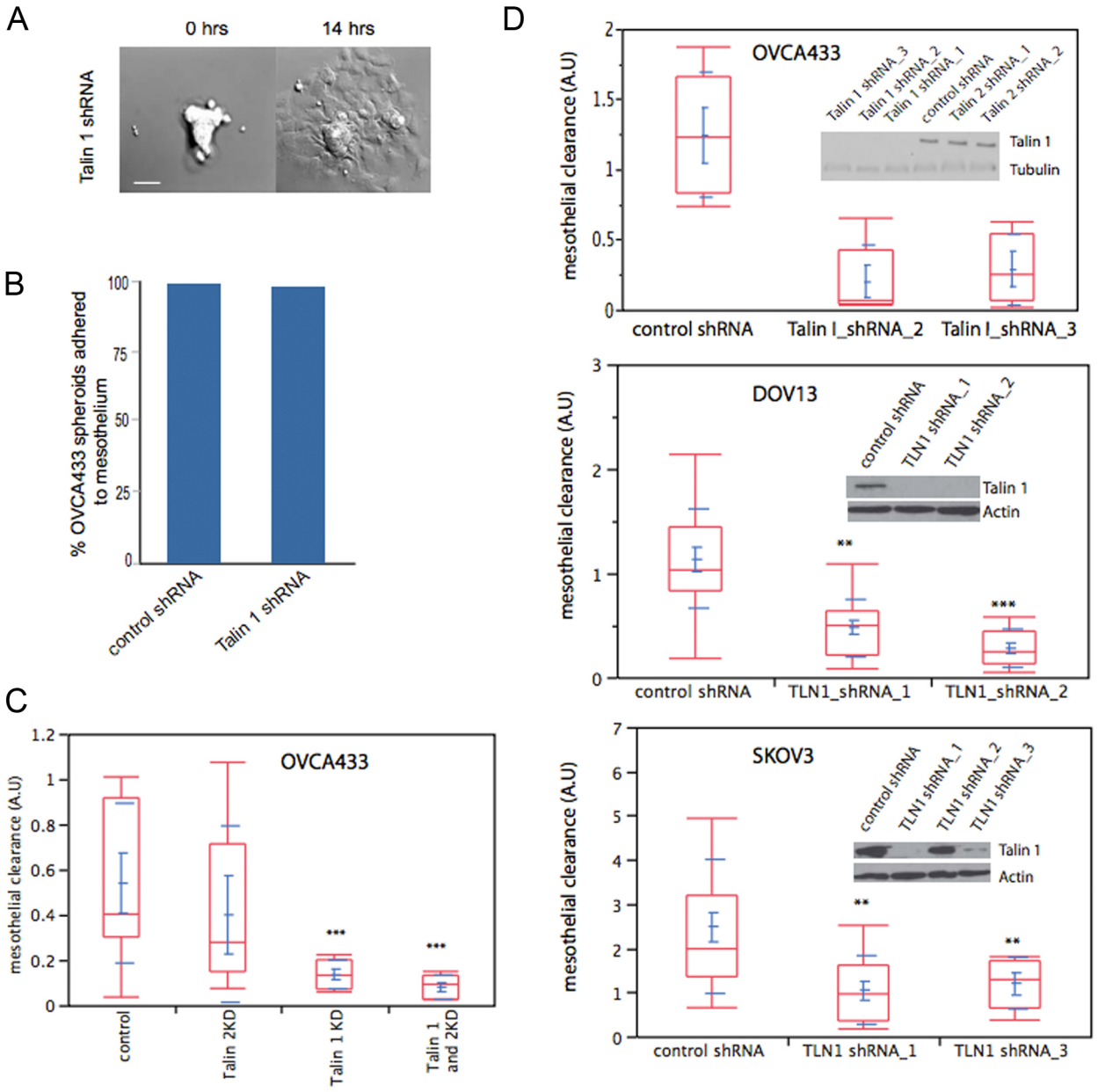

SUPPLEMENTARY FIGURE 3.2: A. Talin I shRNA expressing OVCA433 spheroids were allowed to spread on fibronectin- (5ug/ml) and collagen I- (5ug/ml) coated glass surfaces for a period of 14 hours. DIC images represent frames corresponding to 0 and 14 hour time points. **B.** Control and talin I shRNA expressing OVCA433 spheroids were allowed to adhere to the mesothelial monolayer for five hours. The graph represents the percent of spheroids adhered to the monolayer. **C.** Quantification of mesothelial clearance induced by control, talin II and talin I shRNA expressing OVCA433 spheroids. 12 distinct regions were analyzed per condition **D.** Quantification of mesothelial clearance. Distinct shRNA sequences directed against talin I were used to validate talin I attenuation experiments in OVCA433, DOV13 and SKOV3 ovarian cancer cell lines in. Between 8-15 independent regions were analyzed per condition. The insets show the expression level of talin 1 in OVCA433 spheroids treated with distinct shRNA lentiviral vectors targeting talin 1 and talin 2.

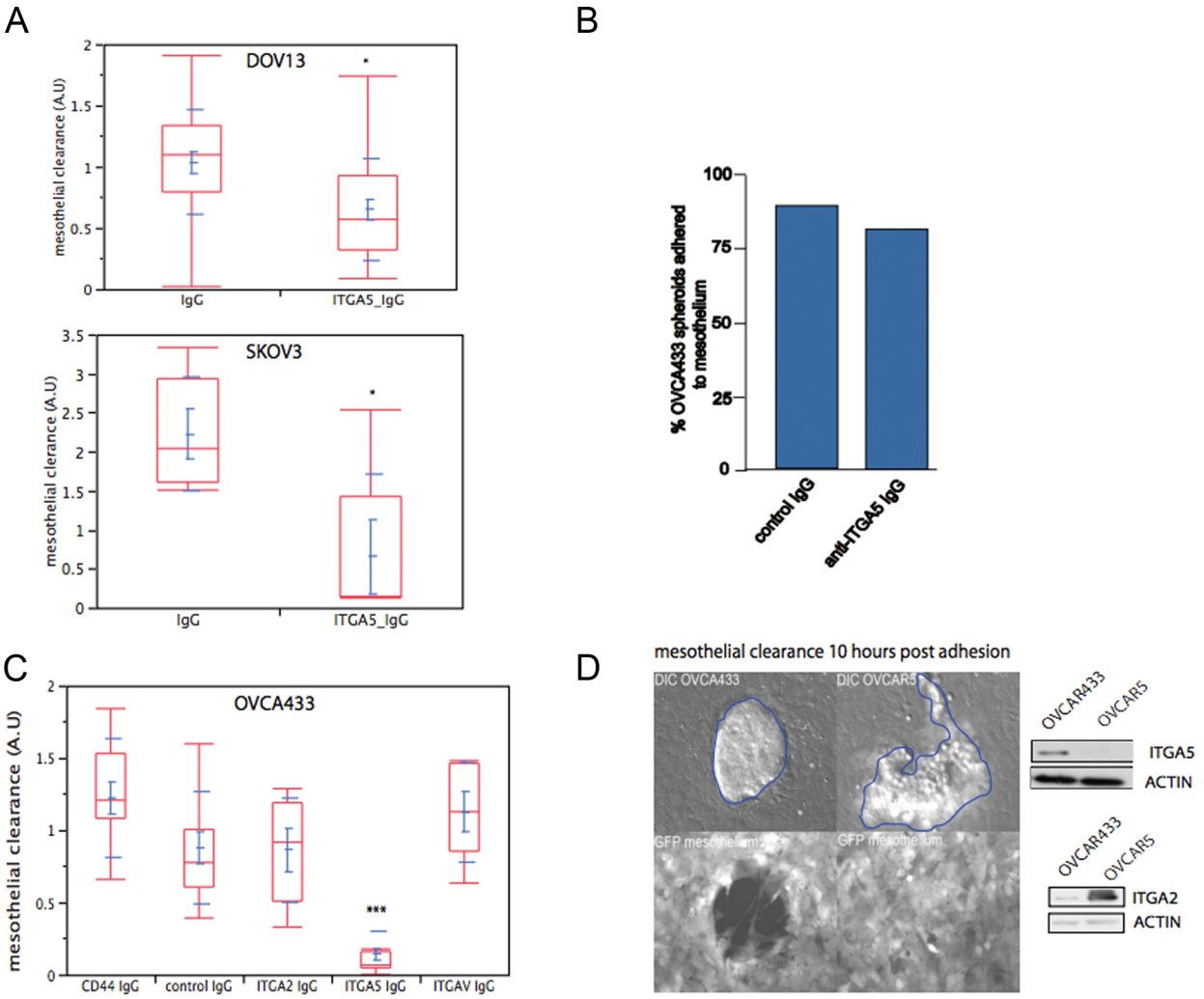

SUPPLEMENTARY FIGURE 3.3: A. Quantification of mesothelial clearance induced by DOV13 and SKOV3 spheroids treated with control IgG and integrin α5β1 IgG. 15 random regions were analyzed per condition **B.** Control or ITGA5 IgG treated OVCA433 spheroids were allowed to adhere to the mesothelial monolayer for 5 hours. The graph represents the percent of spheroids adhered to the mesothelial monolayer **C.** Quantification of mesothelial clearance by OVCA433 spheroids in the presence of various integrin inhibitory antibodies. 10 ramdomly chosen regions were measured. This experiment was repeated 3 times **D.** Right panels: Western blot analyses of the expression levels of ITGA5 and ITGA2 in OVCAR5 and OVCA433 spheroids. Left panels: Images showing representative examples of mesothelial clearance induced by OVCA433 or OVCAR 5 spheroids. Images show the final frame of a 10 hours time-lapse recording. Blue line outlines the spheroid in the phase image.

Supplementary Materials for Chapter 4

SUPPLEMENTARY MOVIE 4.1: Composite of representative movies of mesothelial clearance by ovarian cancer cell lines in order of clearance ability from left to right, top to bottom: ES2, CP70, OVCAR3, OVCA433, OV207, A2780, TOV112D, DOV13, OVCA432, HEYC2, OV2008, OVSAHO, C13, OAW28, PE06, CAOV3, OVCA429, EFO21, MCAS, RMG1.

SUPPLEMENTARY MOVIE 4.2: Composite of representative movies of mesothelial clearance by primary ovarian cancer cell samples in order of clearance ability from left to right, top to bottom: DF168, DF106, DF164, DF29, DF163, DF24, DF43, DF173, DF143, DF155, DF166, DF118, DF59, DF141, DF68, DF160, DF176, DF9, DF172, DF147, DF14.

SUPPLEMENTARY TABLE 4.1: Genes identified that distinguish the clearance-competent cell lines from the clearance-incompetent cell lines.

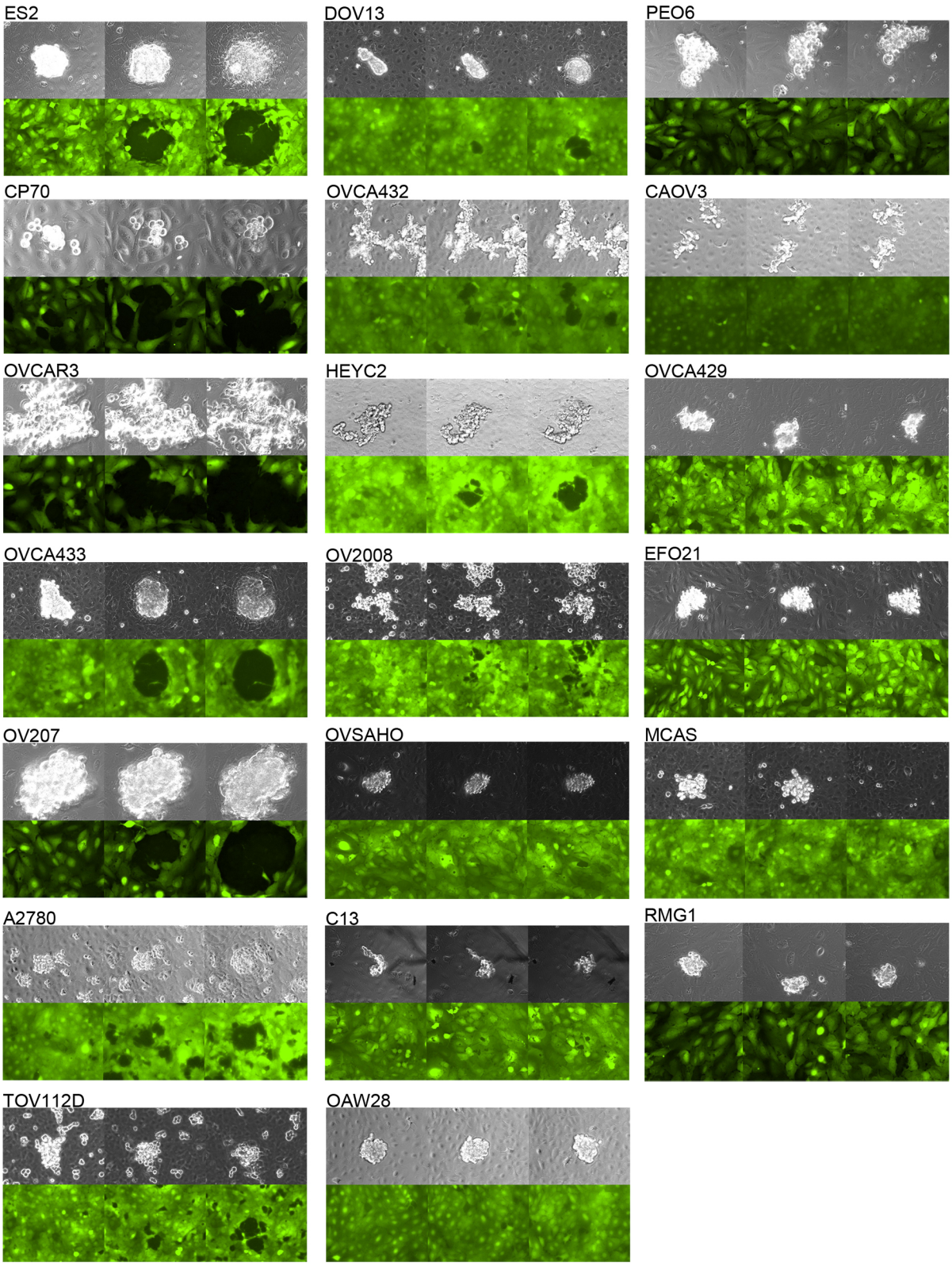

SUPPLEMENTARY FIGURE 4.1: Pre-clustered spheroids from 20 established ovarian cancer cell lines incubated with Mesothelial Monolayers. Images were taken 0, 4 and 8 hours after co-incubation. Phase-contrast images show ovarian cancer spheroids attached to mesothelial monolayers. GFP images of mesothelial monolayers (green) were used to measure clearance area at 8 hours post co-culture.

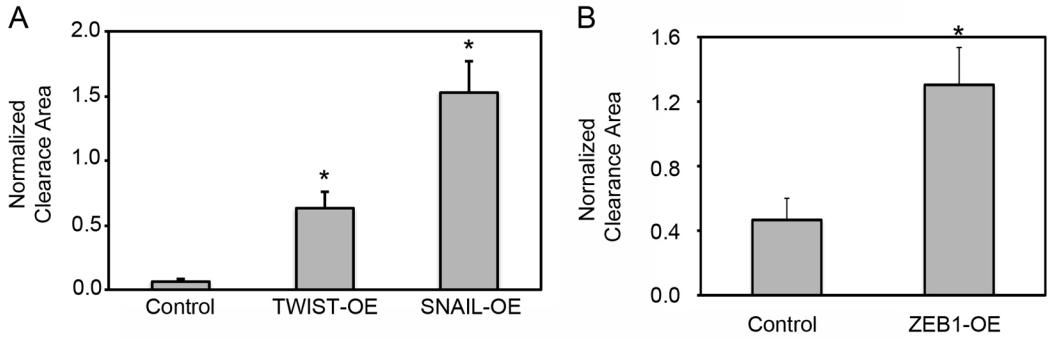

SUPPLEMENTARY FIGURE 4.2: Over-expression of EMT transcription tactors in OVCA433 cells promote mesothelial clearance – Average of 3 experiments. A. Normalized average clearance area of ZT mesothelial monolayers 8 hours after co-culture with 20nM 4-OHT-induced MCAS spheroids carrying control empty vector, inducible WZL-TWIST or WZL-SNAIL expression vectors. **B.** Normalized average clearance area of ZT mesothelial monolayers 8 hours after co-culture with 1µg/ml Doxycycline -induced MCAS spheroids carrying control empty vector, inducible FUW-LPT2 Zeb1 expression vectors. >60 spheroids averaged per condition. Results are shown as averages from three replicate experiments in which triplicate samples were analyzed. Error bars denote SEM. *, $p<0.05$ using Student's t-test.

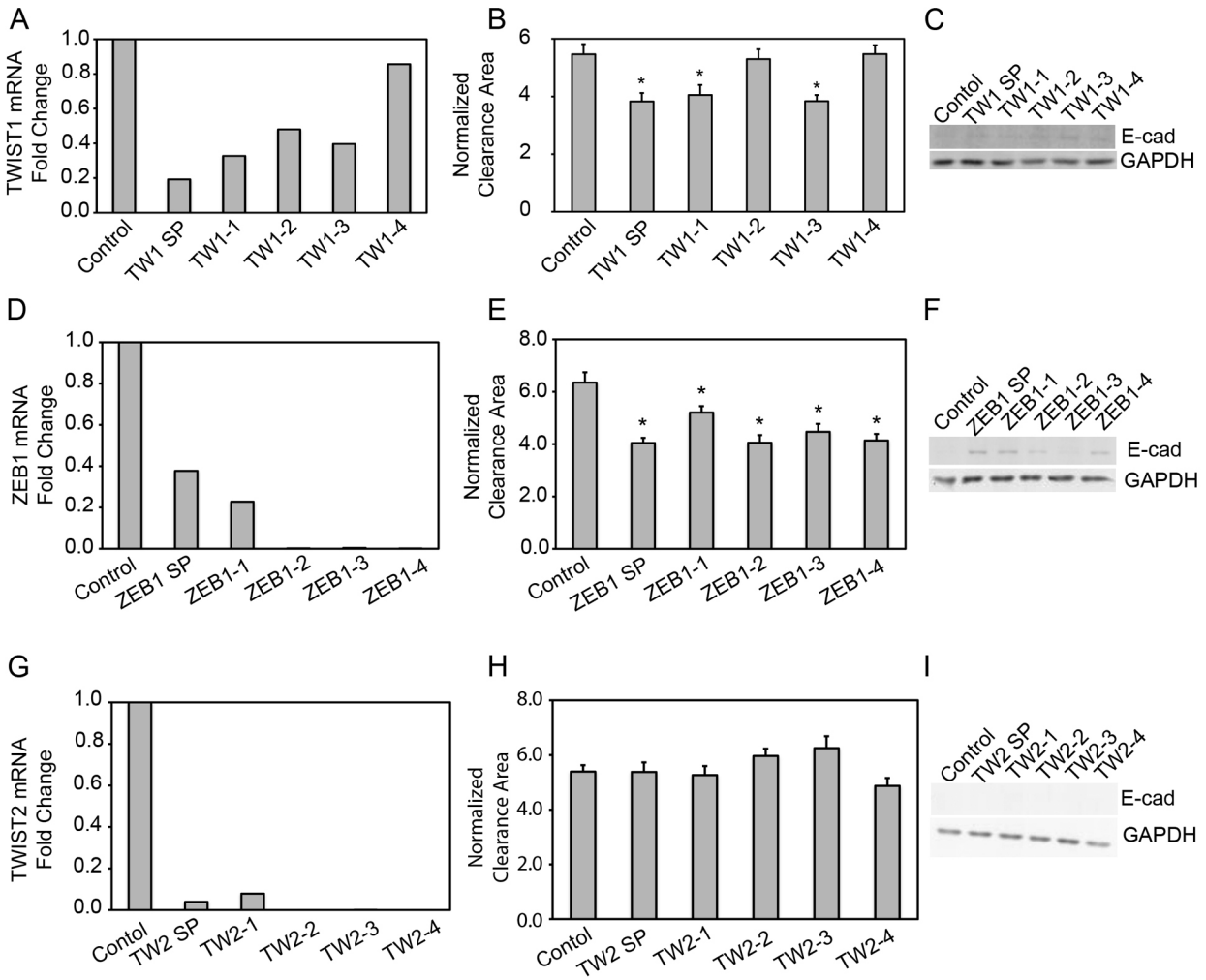

SUPPLEMENTARY FIGURE 4.3: TWIST1, TWIST2, and ZEB1 siRNA deconvolution. A. qRT-PCR measurements of mRNA levels of TWIST1 in OVCA433 cells treated with control (luciferase), TWIST1 SMARTpool, and four individual siRNA hairpins that comprise the SMARTpool. **B.** Normalized average clearance area of ZT mesothelial monolayers 8 hours after co-culture with OVCA433 ovarian cancer spheroids treated with control (luciferase), TWIST1 SMARTpool, and four individual siRNA hairpins that comprise the SMARTpool. **C.** E-cadherin expression in OVCA433 ovarian cancer spheroids treated with control (luciferase), TWIST1 SMARTpool, and four individual siRNA hairpins that comprise the SMARTpool by Western Blot. **D.** qRT-PCR measurements of mRNA levels of TWIST1 in OVCA433 cells treated with control (luciferase), ZEB1 SMARTpool, and four individual siRNA hairpins that comprise the SMARTpool. **E.** Normalized average clearance area of ZT mesothelial monolayers 8 hours after co-culture with OVCA433 ovarian cancer spheroids treated with control (luciferase), ZEB11 SMARTpool, and four individual siRNA hairpins that comprise the SMARTpool. **F.** E-cadherin expression in OVCA433 ovarian cancer spheroids treated with control (luciferase), ZEB11 SMARTpool, and four individual siRNA hairpins that comprise the SMARTpool by Western Blot. **G.** qRT-PCR measurements of mRNA levels of TWIST1 in OVCA433 cells treated with control (luciferase), TWIST2 SMARTpool, and four individual siRNA hairpins that comprise the SMARTpool. **H.** Normalized average clearance area of ZT mesothelial monolayers 8 hours after co-culture with OVCA433 ovarian cancer spheroids treated with control (luciferase), TWIST2 SMARTpool, and four individual siRNA hairpins that comprise the SMARTpool. **I.** E-cadherin expression in OVCA433 ovarian cancer spheroids treated with control (luciferase), TWIST2 SMARTpool, and four individual siRNA hairpins that comprise the SMARTpool. >60 spheroids averaged per condition over three independent experiments in mesothelial clearance experiments. Error bars denote SEM. *, $p<0.05$ using Student's t-test.

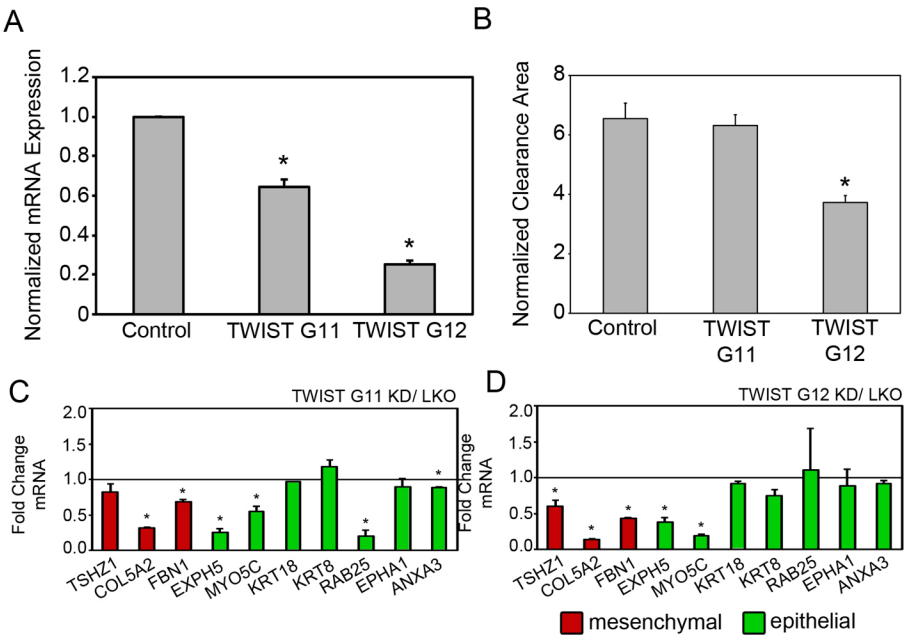

SUPPLEMENTARY FIGURE 4.4: Knockdown of TWIST1 and ZEB1 in OVCA433 ovarian cancer spheroids using shRNA hairpins attenuates mesothelial clearance. A. qRT-PCR measurements of mRNA levels of TWIST1 in OVCA433 cells infected with 'Control' LKO empty vector, LKO-TWIST1 shRNA G11, and LKO-TWIST1 shRNA G12. **B.** Normalized average clearance area of ZT mesothelial monolayers 8 hours after co-culture with OVCA433 spheroids carrying 'Control' LKO empty vector, LKO-TWIST1 shRNA G11 and LKO-TWIST1 shRNA G12. >60 spheroids averaged per condition in three independent experiments. **C-D.** qRT-PCR measurements of mRNA levels of EMT markers in TWIST1 G11(C) or TWIST1 G12(D) shRNA carrying OVCA433 cells. Measurements were normalized to RPLPO mRNA levels and expressed as fold changes compared to controls. Data are shown as the mean of three biological replicates for each condition. Each biological replicate was derived from an average of three technical replicates. Error bars denote SEM. *, $p<0.05$ using Student's t-test.

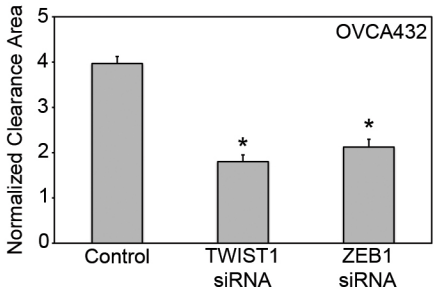

SUPPLEMENTARY FIGURE 4.5: Knockdown of TWIST1 and ZEB1 in OVCA432 ovarian cancer spheroids using siRNA SMARTpools attenuates mesothelial clearance. Normalized average clearance area of ZT mesothelial monolayers 8 hours after co-culture with OVCA432 ovarian cancer spheroids transfected with siRNA SMARTpools targeting luciferase (control), TWIST1, and ZEB1. >60 spheroids averaged per condition in three independent experiments. Error bars denote SEM. *, $p<0.05$ using Student's t-test.

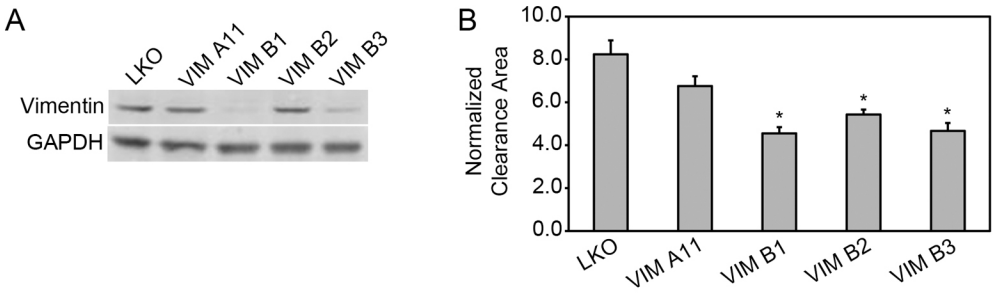

SUPPLEMENTARY FIGURE 4.6: Knockdown of vimentin in OVCA433 ovarian cancer spheroids using shRNA hairpins attenuates mesothelial clearance. A. Western Blot analysis of vimentin in OVCA433 cells carrying 'Control' LKO empty vector, LKO-Vimetin AII, B1, B2 or B3. **B.** Normalized average clearance area of ZT mesothelial monolayers 8 hours after co-culture with OVCA433 spheroids carrying 'Control' LKO empty vector, LKO-Vimetin AII, B1, B2 or B3. >60 spheroids averaged per condition in three independent experiments. Error bars denote SEM. *, $p<0.05$ using Student's t-test.

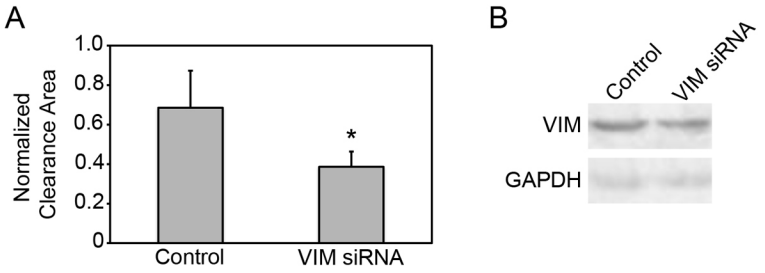

SUPPLEMENTARY FIGURE 4.7: Knockdown of vimentin in CP70 ovarian cancer spheroids using siRNA SMARTpools attenuates mesothelial clearance. **A.** Normalized average clearance area of ZT mesothelial monolayers 8 hours after co-culture with CP70 ovarian cancer spheroids transfected with siRNA SMARTpools targeting luciferase and vimentin. >60 positions averaged per condition over three independent experiments. **B.** Western Blot analysis of vimentin expression in control and vimentin siRNA SMARTpool treated CP70 cells. Error bars denote SEM. *, $p<0.05$ using Student's t-test.

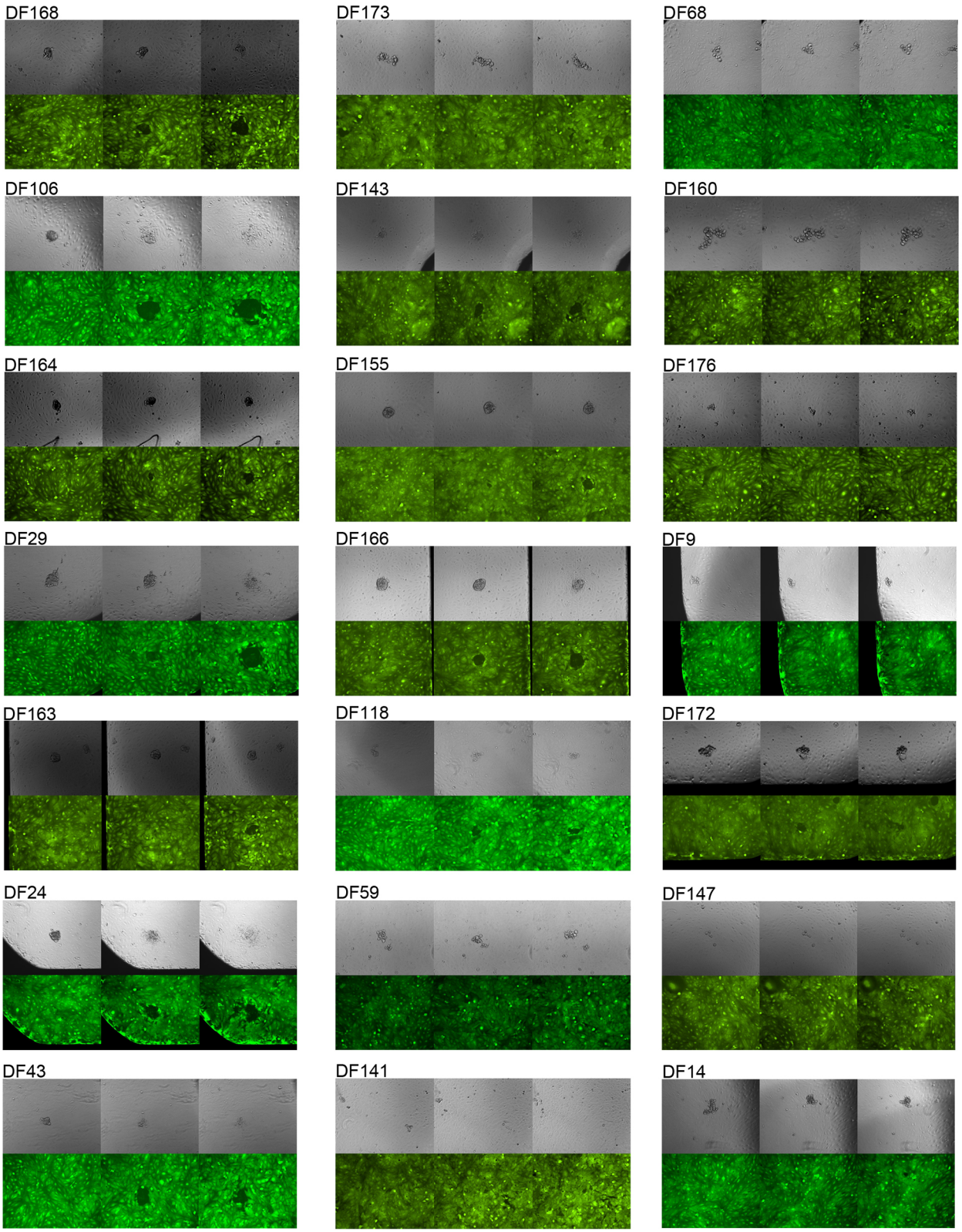

SUPPLEMENTARY FIGURE 4.8: Pre-clustered spheroids from 21 primary ovarian cancer cell lines incubated with mesothelial monolayers. Images were taken 0, 4 and 8 hours after co-incubation. Phase-contrast images show ovarian cancer spheroids attached to mesothelial monolayers. GFP images of mesothelial monolayers (green) were used to measure clearance area at 8 hours post co-culture.

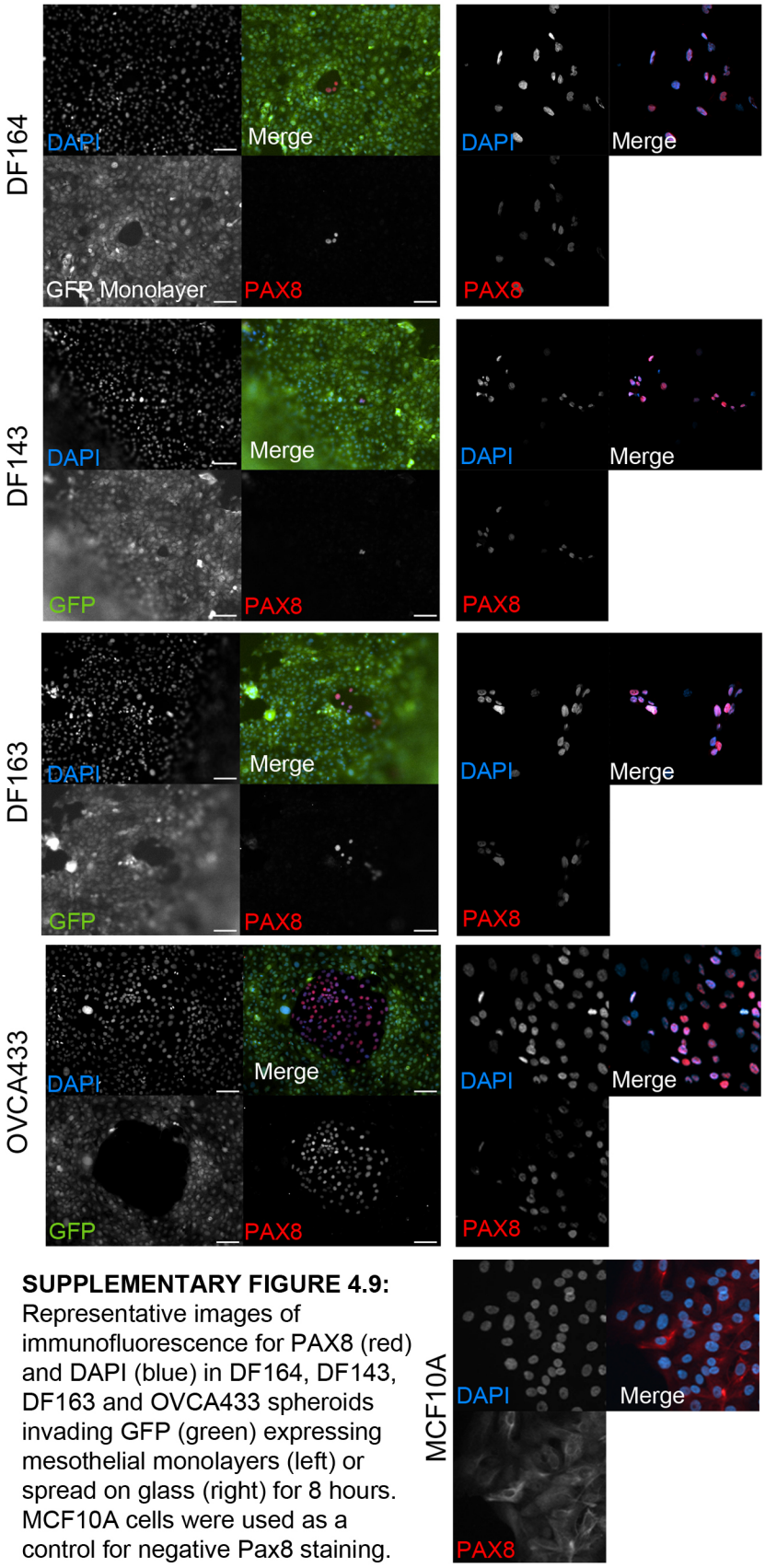

SUPPLEMENTARY FIGURE 4.9: Representative images of immunofluorescence for PAX8 (red) and DAPI (blue) in DF164, DF143, DF163 and OVCA433 spheroids invading GFP (green) expressing mesothelial monolayers (left) or spread on glass (right) for 8 hours. MCF10A cells were used as a control for negative Pax8 staining.